Effects of Bacterial-induced Prostatic Inflammation on Vascular Remodeling and Collagen Deposition

By

Letitia L. Wong

A dissertation submitted in partial fulfillment of

the requirements for the degree of

Doctor of Philosophy

(Molecular and Environmental Toxicology)

at the

UNIVERSITY OF WISCONSIN-MADISON

2014

Date of final oral examination: June 2, 2014

The dissertation is approved by the following members of the Final Oral Committee:

Wade A. Bushman, Professor, Urology
Patricia J. Keely, Professor, Cell and Regenerative Biology
Paul C. Marker, Associate Professor, Pharmaceutical Sciences
William A. Ricke, Associate Professor, Urology
Chad M. Vezina, Assistant Professor, Comparative Biosciences

ACKNOWLEDGEMENTS

The achievement of my graduate degree and the work presented here would not have been fulfilled without the unconditional support from my family, friends, and peers. Throughout these years, my parents and brother have provided me the best caring and support (of the best food, of course) and given me the opportunity to strive for this almost unendurable yet honored path. I hope that after all this effort, my family will find this thesis as their little pride and recognition of their success in raising and educating me.

My passion for learning came from my grandfather. Although he was a principal at a secondary school in Hong Kong, he never forced me to study hard. Instead, he taught me to learn outside the books in a more fun and creative way. He showed me how to do math using Legos and poker, Chinese and English by going to the playgrounds and catching birds and butterflies, and art without using any art supplies. While my parents and relatives were disappointed that I always failed my classes in primary school, my grandfather wholeheartedly believed in my intelligence and creativity as if he saw a different side of me that no one knew except him. One day, I showed him my homework with a grade of F because I painted the sheep and elephant in pink. Thinking that I would probably get yelled at, surprisingly he looked at it and said encouragingly, “With the world this big, just because we have not seen it yet doesn’t mean they don’t exist. Imagination and creativity drive the impossible to be possible.” His teaching, encouragement,

patience, and confidence have profoundly gained my respect and directed me along the way. I wish that we could share this achievement one day in heaven.

I am very grateful for the opportunity to pursue my graduate education provided by my advisor Wade Bushman in his laboratory. While I am probably one of his most stubborn and frustrated graduate students, he has continued to support me, explore my strengths and passions in science and offer the best scientific mentoring/training, as well as hold high expectations for me. Things I have learned throughout these years from him are priceless and I am very appreciative of all the support he has given me. I am also very thankful for the fortunate opportunity to be supported by the METC program, one of the best graduate programs on campus. I enjoyed the METC outreach activities and from which, I have overcome my feeling that teaching kids about science is actually not that scary. Furthermore, the opportunities to work with our distinguished collaborators motivated me to come to work everyday. One of my most cherished experiences in graduate school was to interact and share interesting scientific or random thoughts with them that will surely be missed.

In these years, whenever I felt frustrated of the research, my friends and new friends I made in METC and in labs were always there to support and listen to me. They brought me my favorite food, told me the best jokes, said the sweetest and lovable things to put a smile on my face, sent me wishes and cards, and

most important, grabbed me to go somewhere to leave the lab (ha) – basically anything to cheer me up and help me to get through interference. Their tolerance of my craziness, weird dance, random jokes and cat meowing has allowed me to express myself. In return, I give my deepest blessing, love and support to them forever.

I want to express my highest appreciation to the following: My committee including Patricia Keely, Paul Marker, Will Ricke, and Chad Vezina for their support and scientific criticisms; Paul Hutson, Jerry Gipp, Chris Bradfield, David Beebe, Lian Yu, Mara Domenech, Ashleigh Theberge, Daniel Shi, Travis Jerde, Sara Colopy, Min Yu, Sanghee Lee, Monica Montano, Bayli Boehm, Rob Lipinski, Walt Hopkins, Molly Benck, Jason Carr, Cris Loftus, Josh Everson, Bill (William) Mulligan, Vince Yang, Vatsal Mehta, Mark Marohl, Barb Lewis, Eileen Stevens, Kristen Uchtmann, Emily Ricke, Tristan Nicholson, Dagna Sheerar, Lance Rodenkirch, Gail Pearsall, Shana Peterson, Dan Marsman, Don Bjerke, Laura Babcock, Denise Gutshall

Equally important to be acknowledged here, the support, love, and understanding from my best fluffy friend, Miao Miao The Cat who was always there when I was happy, sad, frustrated and needed someone to cuddle, dance or talk with.

Finally, although the combined endeavors of the work contributed by individuals here likely represent the edge of the universal knowledge in science, we must remain hopeful that this work, together with others would advance urologic research with significant impact in public health.

ABSTRACT

Benign prostatic hyperplasia (BPH) and its associated lower urinary tract symptoms (LUTS) is a common disorder among elderly men. Prostatic inflammation is considered to be a major etiologic factor of this disease due to its strong association with the symptom severity and disease progression. However, the exact mechanisms are still poorly understood and are a major focus of urologic research. In addition to its effect on epithelial and stromal hyperplasia, emerging evidence supports the hypothesis that prostatic inflammation contributes to BPH/LUTS by a variety of mechanisms, including disruption of vascular remodeling and homeostasis, and excessive extracellular matrix deposition. Here, we used our previously established mouse model of bacterial-induced prostatic inflammation to study the vascular and fibrotic responses to inflammation. We demonstrated that prostatic inflammation induces angiogenesis characterized by increased endothelial proliferation and vessel density but decreased mRNA expression of the classic pro-angiogenic factors. We also found that prostatic inflammation induces collagen deposition. This fibrotic change is associated with increased collagen synthesis, increased mRNA expression of collagen remodeling-associated genes, and an accumulation of collagen producing fibrocytes. Finally, using a broad-spectrum antibiotic enrofloxacin to resolve bacterial infection and prostatic inflammation, we demonstrated that prostatic fibrosis is a reversible inflammatory process. Further characterization of the cellular and molecular mechanisms of these

vascular and fibrotic changes in inflammation as well as the effects of these histological changes in tissue function and voiding pattern using the mouse model described here is anticipated to provide significant insight into the underlying etiology of this common aging disease.

TABLE OF CONTENTS

ABBREVIATIONS

αSMA	alpha-smooth muscle actin
ρ	Spearman's rank correlation coefficient
$t_{½}$	half-life
Angpt	Angiopoietin
AP	Anterior prostate
AUASS	American urological association symptoms score
BPH	Benign prostatic hyperplasia
BrdU	5-bromo-2-deoxyuridine
C. muridarum	*Chlamydia muridarum*
CCL	Chemokine (C-C motif) ligand
CCl_4	Carbon tetrachloride
CCR	Chemokine (C-C motif) receptor
CFU	Colony-forming unit
Col	Collagen
COX	Cyclooxygenase
CXCL	Chemokine (C-X-C motif) ligand
CXCR	Chemokine (C-X-C motif) receptor
DLP	Dorsolateral prostate
E. coli	*Escherichia coli*
ECM	Extracellular matrix
FACS	Fluorescence Activated Cell Sorting

Fgf	Fibroblast growth factor
Figf	C-fos induced growth factor
FMOC-Cl	Fluorenylmethyloxycarbonyl chloride
H&E	Hematoxylin and eosin
HGF	Hepatocyte growth factor
HPLC	High-performance liquid chromatography
HYP	Hydroxyproline
IFN	Interferon
IHC	Immunohistochemistry
IL	Interleukin
IL-1R	Interleukin 1 receptor
IP	Intraperitoneal
IPSS	International prostate symptom score
Lox	Lysyl oxidase
LUTS	Lower urinary tract symptoms
Mmp	Matrix metalloproteinase
MTOPS	Medical therapy of prostatic symptoms
MVD	Mean vessel density
NSAIDS	Non-steroidal ant-inflammatory drugs
OPA	*o*-phthalaldehyde
P4H	Prolyl 4-hydroxylase
P. acnes	*Propionibacterium acnes*

PCR	Polymerase chain reaction
Pdgf	Platelet-derived growth factor
Pecam	Platelet endothelial cell adhesion molecule
PID	Post instillation day
REDUCE	REduction by DUtasteride of prostate Cancer Events
RNA	Ribonucleic acid
RT-PCR	Real-time polymerase chain reaction
SEM	Standard error of the mean
Tek	Endothelial tyrosine kinase
TGFβ	Transforming growth factor beta
Tie1	Tyrosine kinase with immunoglobulin-like and EGF-like domains 1
Timp	Tissue inhibitor of metalloproteinase
TNF	Tumor necrosis factor
TURP	Transurethral resection of the prostate
UGS	Urogenital sinus
Vegf	Vascular endothelial growth factor
VIM	Vimentin
VP	Ventral prostate
WT	Wild type

CHAPTER ONE

INTRODUCTION

A. The Natural History of Benign Prostatic Hyperplasia and Associated Lower Urinary Tract Symptoms

Benign prostatic hyperplasia (BPH) is a common and worldwide urological disorder affecting 50% to 90% of aging men. The prevalence of BPH increases with age, starting at age of 40 years and reaching approximately 90% at age of 80 [1-3]. BPH is histologically characterized by progressive prostate enlargement resulting from hyperplastic growth of the epithelial and stromal component predominately in the periurethral transition zone of the human prostate [1,3]. McNeal's studies have described that the hyperplasic process of BPH is multi-focal and gives rise to stromal and glandular nodules [4]. During the initial phase of BPH development as early as the fourth decade in men, the disease is characterized by a diffuse growth of the prostate and a gradual increase in the number of small stromal and glandular nodules. A second phase of BPH then follows, generally by the age of 70, in which there is a substantial increase in size of glandular nodules.

The histopathological conditions of BPH are often associated with lower urinary tract symptoms (LUTS) that require medical or surgical treatment. The prevalence of LUTS also increases with age [5]. LUTS are categorized into two types: Irritative symptoms and obstructive symptoms. Irritative symptoms consist

of urgency, frequency, nocturia, and urge incontinence. Obstructive symptoms consist of hesitancy, weak stream, straining, prolonged micturition, urinary retention, overflow incontinence and possible postvoid dribbling [2]. Although not life threatening, LUTS can significantly reduce quality of life in men [6,7] and when left untreated may be complicated by recurrent urinary tract infections, acute urinary retention and bladder muscle dysfunction.

BPH and LUTS are historically interrelated. It is presumably that the enlarged prostate resulting from BPH mechanically compresses the prostatic urethra that leads to bladder outlet obstruction, ultimately manifesting clinically as LUTS [1,8]. However, there is increasing evidence to suggest that this simplistic causal relationship among prostate enlargement, bladder outlet obstruction and LUTS is not always applicable to predict the natural history and disease progression. Several community-based studies of men with no history of prostate cancer or prostate surgery have reported a significant but very weak correlation of the IPSS with prostate volume, peak flow rate and post-void residual urine volume [9,10]. Clinical studies in men with BPH/LUTS also have demonstrated that the symptom score correlated poorly with prostate size, urinary flow rate and post-void residual urine volume [11-13]. Furthermore, the prevalence of bladder outlet obstruction is only between 34% and 80% in men with BPH/LUTS documented in numerous pressure-flow urodynamic studies [14-17]. A weak but significant positive correlation among the degree of urodynamic obstruction and prostate

volume was found in BPH/LUTS patients [14]; however, there is a lack of relationship between the severity of obstruction and LUTS [16-19]. Specifically, there was no statistically significant difference in the mean total IPSS, obstructive, or irritative scores between patients with and without obstruction [16-18]. Therefore, it is apparent that prostate enlargement and bladder outlet obstruction are not the sole determinant of LUTS in elderly men with BPH and is plausible that there are other factors for BPH/LUTS etiology that have yet to be identified.

Despite extensive research over many years, the mechanisms underlying development and progression of BPH/LUTS are still poorly understood. Evidence for the incomplete correlation of prostate volume, LUTS severity, and bladder outlet obstruction suggests that bladder outlet obstruction due to prostate enlargement is not the only factor that contributes to LUTS. Indeed, accumulating evidence suggests that BPH/LUTS is a multifactorial disease. Epidemiological studies have shown a high prevalence of erectile dysfunction, type II diabetes, cardiovascular disease, hypertension, autonomic nervous system overactivity and metabolic syndrome among patients with BPH/LUTS [20-25]. The comorbid conditions in BPH/LUTS suggest that more than one contributing factor exist in the pathophysiology of BPH/LUTS. In fact, aging, prostatic inflammation, lifestyle modifiable factors, sex steroid hormones, and genetics are all considered to play a role in BPH/LUTS [5]. Taken together, the

pathophysiology of BPH associated LUTS may be more complex than previously proposed. There is a major need to reevaluate the contribution of prostate enlargement and obstruction to BPH/LUTS and to elucidate the role of the each individual factor in the pathogenesis of BPH and LUTS for gaining new insight into therapeutic treatment and prevention.

B. Prostatic Inflammation in Benign Prostatic Hyperplasia/Lower Urinary Tract Symptoms

Prostatic inflammation is common histologic finding in aging men and is now considered one of the major contributors to development and progression of BPH/LUTS. Previous studies have shown that prostatic inflammation is extremely common in men with BPH. Acute and chronic inflammation are both seen but chronic inflammation is more frequent [26]. Histological analysis of prostatic specimens in 80 men diagnosed with BPH who underwent transurethral resection of the prostate (TURP) showed evidence of inflammatory infiltrates in all patients [27]. In a subsequent study that characterized the inflammatory infiltrates on tissue microarrays obtained from 282 BPH patients treated with TURP or open prostatectomy, 81% of cases had T-lymphocytes, 52% had B-lymphocytes, and 82% had macrophages [28]. This was further confirmed by an analysis of baseline data from 8224 elderly men in the REduction by DUtasteride of prostate Cancer Events (REDUCE) study that found 15.4% cases had acute inflammation based on histological evidence of neutrophils and 77.6% cases had

chronic inflammation as evidenced by the presence of lymphocytes, plasma cells and macrophages [26]. Moreover, a variety of inflammatory cytokines including IFN-γ, IL-1, IL-2, IL-4, IL-6, IL-7, IL-8, IL-13, IL-15, IL-17, IL-23, and COX-2 was significantly expressed in BPH specimens, further suggesting a possible role of inflammatory pathways in BPH/LUTS [29,30].

Follow up studies have demonstrated that the severity of inflammation in BPH/LUTS was associated with the severity of urinary symptoms and disease progression. The REDUCE study reported that the total IPSS score, irritative subscore and obstructive subscore were all significantly higher in men with histological chronic inflammation at baseline as compared to those without chronic inflammation [26]. There were weak but statistically significant correlations between the degree of chronic inflammation and the total IPSS score, and the IPSS subscores. Similarly, in the subgroup analysis of 1197 randomly selected BPH patients in the Medical Therapy of Prostatic Symptoms (MTOPS) study, patients with chronic inflammation at baseline were more likely to experience symptomatic progression and acute urinary retention, and to require BPH-related surgery than those with no inflammation [6]. Additionally, population based studies and clinical trial studies have demonstrated that regular use of non-steroidal anti-inflammatory drugs (NSAIDS) may have protective effects for patients with BPH/LUTS. Men who used NSAIDS daily had a significantly reduced risk of developing moderate-to-severe LUTS, decreased

peak urinary flow rate, increased prostate volume and need for medical or surgical treatment for BPH later in life [31,32]. Taken together, these findings suggest that inflammation may play a substantial role in the development and progression of BPH/LUTS.

The cause of prostatic inflammation in BPH/LUTS has been a subject of speculation and is likely multifactorial. Bacterial infection appears to be common in BPH specimens. Sexual transmission and urine reflux into the prostatic ducts have been suggested as the possible routes of infection for uropathogenic organisms [33,34]. Previous studies have indicated that a positive polymerase chain reaction (PCR) detection of bacterial 16S ribosomal RNA gene in the human prostate was strongly associated with the presence of prostatic inflammation [35]. Bedalov and colleagues have demonstrated that 63.6% of BPH specimens obtained by prostatectomy had bacterial growth [36] while Nickel and colleagues have reported that 44% of 80 BPH biopsies showed positive result in bacterial culture [27]. The strains of bacteria that are known to induce infection and inflammation in the prostate appears to be heterogeneous including a variety of different gram positive and negative organisms [27,34,36]. Among all, uropathogenic *Escherichia coli* (*E. coli*) is one of the most frequent isolates derived from bacterial prostatitis [33,37-39]. Other possible causes of prostatic inflammation that have previously been proposed include autoimmunity, viral

infection, dietary and environmental factors, and age-dependent changes in estrogen and androgen levels [30,34].

The mechanisms by which inflammation contributes to development and progression of BPH/LUTS have yet to be fully elucidated. It is postulated that prostatic inflammation induces proliferation of epithelial and stromal cells, disrupts vascular homeostasis, induces fibrosis and sensitizes afferent fibers. These concepts are being tested in several rodent models of bacterial-induced prostatic inflammation. Elkahwaji and colleagues have reported a mouse model of prostatic inflammation induced by a single transurethral instillation of uropathogenic *E. coli* 1677 isolated from the urine of a patient with lower urinary tract infection into adult C3H/HeOuJ male mice [40]. Prostatic tissues of day 5 following bacterial infection showed evidence of acute inflammation characterized by increased infiltration of neutrophils into the periglandular stroma, interstitial edema, focal hemorrhage and shedding of epithelium into the glandular lumen. At 12 weeks post-bacterial inoculation, infected mouse prostates exhibited characteristics of chronic inflammation including dense lymphocytic infiltration in the periglandular stroma accompanied by varying degrees of atypical hyperplasia and dysplasia in prostatic glandular epithelium, increased epithelial proliferation and oxidative stress. Using the same strain of uropathgenic *E. coli* to induce acute bacterial infection in the mouse prostates, Boehm and colleagues performed a comprehensive characterization of the acute

inflammatory response throughout the acute phase of infection in the prostates of adult C57BL/6J male mice [41]. The inflammatory response to bacterial infection was characterized by a primarily neutrophilic infiltrate on the first two day post-inoculation followed by a lymphocytic infiltrate 3-5 days following infection, which was similar to the leukocytic composition observed in human prostatic inflammation in BPH [28]. Quantitative histological measurements showed that the degrees of epithelial hyperplasia and proliferation, inflammatory infiltrate, hemorrhage and tissue damage were more severe between day 2 and 5 post-inoculation and had largely resolved on day 7 following infection. Increases in expression of a variety of cytokines, including *Il-1α, Il-1β, Il-6, Il-8, Il-18, Cox-2, Tnfa, Il-1ra* and Il-10 were also observed in the *E. coli* infected mouse prostates. A similar cytokine expression profile was observed in human BPH as well [29,30]. Rudick et al. have described another *E. coli* infection model of prostatic inflammation using a strain of uropathogenic *E. coli* (CP1) isolated from the prostate of a patient with chronic prostatitis/chronic pelvic pain syndrome [42]. This study has showed that transurethral inoculation of uropathogenic *E. coli* CP1 in adult NOD male mice not only resulted in prostatic infection and inflammation but also appeared to induce chronic pelvic pain.

Several other models of bacterial-induced prostatic inflammation utilize bacteria other than *E. coli*. Mackern-Oberti et al. have showed that transurethral inoculation of *Chlamydia muridarum* (*C. muridarum*) for 3 consecutive days

resulted in chronic prostatic infection and inflammation in two strains of animals genetically susceptible to experimental autoimmune prostatitis, Wistar rats and NOD mice [43]. Histological examination of the infected prostates revealed the presence of mononuclear and polymorphonuclear infiltrates that were mostly composed of CD3+ cells. The marked inflammatory infiltration in *C. muridarum* infected prostates was accompanied by high serum levels of antibodies against different prostate antigens in both infected adult Wistar rats and NOD mice, suggesting a possible role of *Chlamydia*-induced prostatic inflammation in stimulating autoimmune reactions in genetically susceptible hosts. Shinohara and colleagues have also established a mouse model of prostatic inflammation induced by a single transurethral instillation of a radical prostatectomy-derived strain of *Propionibacterium acnes* (PA2 *P. acnes*) [44]. Histological analysis demonstrated that *P. acnes* infection induced acute and chronic inflammation that persisted for at least 8 weeks post-inoculation in the prostates of adult C57BL/6J male mice. In addition, *P. acnes* induced prostatic inflammation was accompanied by increased epithelial proliferation, decreased expression of Nkx3.1 and androgen receptor in the epithelium of the inflamed glands, which were similar to the cellular and molecular features of the human prostate associated with inflammation [45,46].

In summary, these studies show that bacterial-induced prostatic inflammation can recapitulate certain histopathologic, cellular and molecular characteristics of

the inflamed human prostate. Studies are currently underway in several laboratories to determine the effects of prostatic inflammation on voiding behavior, fibrosis, extracellular matrix deposition and neurovascular physiology that are believed to be highly relevant in BPH/LUTS development.

C. Prostatic Vasculature in Development, Inflammation, Benign Prostatic Hyperplasia/Lower Urinary Tract Symptoms

The prostatic vasculature provides nutrients and oxygen to the organ that is necessary for its normal development, growth and function. Previous studies of the adult rat prostatic vasculature highlighted its importance in androgen-mediated prostatic growth homeostasis. Castration induced a rapid reduction in blood flow to the prostate accompanied with vasoconstriction, increased vascular permeability, increased apoptosis and decreased proliferation of endothelial cells in 12-24 hours after castration [47-53]. This response preceded the onset of prostatic epithelial cell apoptosis and tissue regression that occurred 24-72 hours post-castration [48-50]. Subsequent testosterone replenishment of the castrated animals rapidly restored the prostatic vasculature through increasing endothelial proliferation and blood flow preceding epithelial proliferation in the prostate [50]. Follow up studies in rats and rabbits have demonstrated that reduction in prostatic blood flow through impairment of iliac arterial supply created an ischemic condition in the prostate that induced epithelial cell apoptosis, and functional and structural alterations of the prostatic tissues [54,55]. Taken

together, these observations suggest that the vasculature might play a more important role in supporting the normal prostatic growth and function than previously recognized.

Vascular remodeling and angiogenesis is a critical feature of the response to injury, inflammation and wound healing. The initial response to injury is hemostasis and is characterized by platelet adhesion and aggregation, development of a fibrin clot and coagulation. This is followed by vasodilation, increased vascular permeability and blood flow at the site of injury facilitating the infiltration of inflammatory cells through the endothelium into the injured tissue. These vascular changes are tightly regulated by vascular mediators released mainly from platelets and inflammatory cells, including platelet-derived growth factor, platelet-activating factor, prostaglandin, leukotriene, histamine and clotting factors [56,57]. At the later phase of wound healing, inflammatory cells, epithelial cells, fibroblasts and endothelial cells near the wound area secrete a variety of angiogenic factors to promote angiogenesis for new blood vessel growth from preexisting vessels in the wound tissue. These classical angiogenic factors primarily include vascular endothelial growth factors, angiopoietins, and fibroblast growth factors [56,57]. In summary, the vascular response to inflammation contributes significantly to the process of tissue repairing and is predominantly mediated by the actions of angiogenic factors on the vasculature.

Studies in animal models of tissue injury and inflammation have characterized the vascular response to inflammation and the role of angiogenic factors in this process in various organ systems; however, this study has never been conducted in the prostate. In a swine skin excision model of tissue injury, ultrasound serial images of the wound area revealed the formation of a highly vascularized granulation tissue at the injured site [58]. Local treatment with neutralizing VEGFA antibody significantly reduced vessel density and inhibited wound granulation tissue formation compared with animals treated with a control IgG. Previous studies have also demonstrated that mustard oil-induced inflammation resulted in increased vascular permeability in the mouse skin ear as evidenced by the leakage of Evan blue dye from the ear vasculature after injecting the dye into the femoral vein [59,60]. Importantly, this vascular response to inflammation was inhibited in transgenic mice overexpressing *Angpt1* whereas the effect was increased in transgenic mice overexpressing *Vegfa* [60]. Studies in rodents infected with the respiratory pathogen *Mycoplasma pulmonis* have showed that bacterial-induced airway inflammation was accompanied by vascular changes that preceded tissue remodeling [61]. The vascular remodeling in the trachea in response to bacterial infection involved increased endothelial cell proliferation, enhanced angiogenesis, increased vessel density, increased vessel permeability, enlargement of vessel diameter, and vascular reorganization in a non-uniform pattern [61-65]. Similarly, respiratory infection with herpes virus in mice induced endothelial cell proliferation and

vessel thickening in the lung [66]. Previous studies have further suggested that these vascular changes were at least in part mediated by Angiopoietin/Tek receptor signaling [67,68]. Overexpression of *Angpt1* in pathogen-free mice induced the vascular remodeling similar to as in *Mycoplasma pulmonis* infected animals while blocking its effect by injection of soluble Tek receptor in infected animals inhibited the vascular response to inflammation [68].

Experimental and clinical studies have consistently suggested that vascular pathogenesis is a potential contributor to the etiology of BPH/LUTS. Previous studies in spontaneously hypertensive rats have shown that this rat strain exhibited hyperactive urinary voiding and developed benign adenomatous hyperplasia in the aging prostate, suggesting a possible pathogenic link between vascular diseases and BPH/LUTS [69,70]. Studies in aging men have further revealed that atherosclerotic diseases, such as coronary heart disease, hypertension, diabetes mellitus, are a risk factor for BPH/LUTS and are associated with the prevalence or symptom severity of BPH/LUTS [22-24,71-74]. Several studies indicated that reduced prostatic blood flow and increased vascular resistance in the transition zone in patients with BPH/LUTS compared to control healthy group [72,75]. It also appears that BPH/LUTS patients with vascular disorders had a greater reduction of prostatic blood flow and a greater severity of BPH symptoms than men without vascular disorders [23,72]. Despite there is accumulating evidence to suggest that vascular diseases are likely a risk

factor for BPH/LUTS, the causal relationship between these two pathological conditions has yet to be elucidated. Given that prostatic inflammation and vascular pathology are associated with BPH/LUTS and vascular response is essential during inflammation for tissue repair, the mechanisms underlying the vascular changes in response to inflammation in the prostate are postulated to contribute to the etiology of BPH/LUTS.

D. Prostatic Fibrosis in Inflammation and Benign Prostatic Hyperplasia/Lower Urinary Tract Symptoms

Emerging evidence suggests that increased collagen accumulation in the prostate is a contributing factor to the pathogenesis of BPH/LUTS. An epidemiological study of BPH patients with LUTS has revealed that the amount of prostatic fibrosis was significantly inversely correlated with urine flow rate, implicating that increased fibrous tissue in the prostate may compromise urinary functions [76]. A recent study has further demonstrated that the periurethral prostatic tissues from men with LUTS had a higher collagen amount that was positively correlated with the tissue stiffness as compared with those without LUTS [77]. More importantly, the mechanical stiffness of the tissues was directly associated with the severity of LUTS. Taken together, these studies support an idea that prostatic tissue stiffening attributed to high collagen content and fibrosis impairs urethral function and compliance. To date, the mechanisms leading to increased collagen deposition in BPH/LUTS have not yet been investigated.

Many studies have suggested that immune regulation is the key player in the establishment and progression of excessive collagen deposition in various diseases [78-80]. Collagen remodeling and deposition is a predominant feature of tissue inflammation for normal wound healing [81,82]. However, when inflammation fails to resolve a pathological state of chronic wound healing response occurs and results in development of fibrosis. Considering that prostatic inflammation and fibrosis are characteristics in BPH/LUTS and that increased collagen deposition occurs in response to chronic inflammation/injury for tissue repair, we postulate that prostatic inflammation contributes to development and progression of BPH/LUTS by inducing fibrosis. This concept is supported by a recent prospective study showing a significantly higher collagen content in the periurethral prostatic tissues with histological evidence of inflammation as compared to those without inflammation [83].

E. Summary

BPH/LUTS is one of the most common diseases in aging men. Due to the associated bothersome clinical symptoms and the high prevalence and incidence of BPH/LUTS in the aging population, this disease has been a subject of interest in research and clinical studies for many years. According to the current literature, it is evident that prostatic inflammation is commonly noted in BPH/LUTS and has been suggested as one of the factors contributing to BPH/LUTS. However, as of today the mechanisms of prostatic inflammation

underlying the pathogenesis of BPH/LUTS is still unclear. Additionally, there is increasing evidence suggesting that vascular pathology and prostatic fibrosis might contribute to LUTS in aging men. We used our previously described mouse model of bacterial-induced inflammation [40,41,84] to examine the effect of inflammation on the vascular system and extracellular matrix of the prostate. The work presented here addresses three specific aims:

Aim 1: To examine the effects of bacterial-induced prostatic inflammation on endothelial proliferation in the prostate

Aim 2: To examine the effects of bacterial-induced prostatic inflammation on collagen deposition in the prostate

Aim 3: To examine whether the changes in collagen deposition induced by bacterial prostatic inflammation is reversible

The results of these aims are described in the following chapters. They are believed to serve as a useful resource for future studies in understanding the roles of angiogenesis and fibrosis associated with prostatic inflammation in the complex pathobiology of BPH/LUTS.

REFERENCES

1. Roehrborn CG (2008) Pathology of benign prostatic hyperplasia. Int J Impot Res 20 Suppl 3: S11-18.

2. Paolone DR (2010) Benign prostatic hyperplasia. Clin Geriatr Med 26: 223-239.

3. Bushman W (2009) Etiology, epidemiology, and natural history of benign prostatic hyperplasia. Urol Clin North Am 36: 403-415, v.

4. McNeal J (1990) Pathology of benign prostatic hyperplasia. Insight into etiology. Urol Clin North Am 17: 477-486.

5. Parsons JK (2010) Benign Prostatic Hyperplasia and Male Lower Urinary Tract Symptoms: Epidemiology and Risk Factors. Curr Bladder Dysfunct Rep 5: 212-218.

6. Roehrborn CG (2006) Definition of at-risk patients: baseline variables. BJU Int 97 Suppl 2: 7-11; discussion 21-12.

7. Girman CJ, Epstein RS, Jacobsen SJ, Guess HA, Panser LA, et al. (1994) Natural history of prostatism: impact of urinary symptoms on quality of life in 2115 randomly selected community men. Urology 44: 825-831.

8. Lepor H (2005) Pathophysiology of lower urinary tract symptoms in the aging male population. Rev Urol 7 Suppl 7: S3-S11.

9. Bosch JL, Hop WC, Kirkels WJ, Schroder FH (1995) The International Prostate Symptom Score in a community-based sample of men between 55 and 74 years of age: prevalence and correlation of symptoms with age,

prostate volume, flow rate and residual urine volume. Br J Urol 75: 622-630.

10. Girman CJ, Jacobsen SJ, Guess HA, Oesterling JE, Chute CG, et al. (1995) Natural history of prostatism: relationship among symptoms, prostate volume and peak urinary flow rate. J Urol 153: 1510-1515.
11. Vesely S, Knutson T, Damber JE, Dicuio M, Dahlstrand C (2003) Relationship between age, prostate volume, prostate-specific antigen, symptom score and uroflowmetry in men with lower urinary tract symptoms. Scand J Urol Nephrol 37: 322-328.
12. Barry MJ, Cockett AT, Holtgrewe HL, McConnell JD, Sihelnik SA, et al. (1993) Relationship of symptoms of prostatism to commonly used physiological and anatomical measures of the severity of benign prostatic hyperplasia. J Urol 150: 351-358.
13. Ezz el Din K, Kiemeney LA, de Wildt MJ, Debruyne FM, de la Rosette JJ (1996) Correlation between uroflowmetry, prostate volume, postvoid residue, and lower urinary tract symptoms as measured by the International Prostate Symptom Score. Urology 48: 393-397.
14. Eckhardt MD, van Venrooij GE, Boon TA (2001) Interactions between prostate volume, filling cystometric estimated parameters, and data from pressure-flow studies in 565 men with lower urinary tract symptoms suggestive of benign prostatic hyperplasia. Neurourol Urodyn 20: 579-590.

15. Reynard JM, Yang Q, Donovan JL, Peters TJ, Schafer W, et al. (1998) The ICS-'BPH' Study: uroflowmetry, lower urinary tract symptoms and bladder outlet obstruction. Br J Urol 82: 619-623.

16. Nitti VW, Kim Y, Combs AJ (1994) Correlation of the AUA symptom index with urodynamics in patients with suspected benign prostatic hyperplasia. Neurourol Urodyn 13: 521-527; discussion 527-529.

17. Yalla SV, Sullivan MP, Lecamwasam HS, DuBeau CE, Vickers MA, et al. (1995) Correlation of American Urological Association symptom index with obstructive and nonobstructive prostatism. J Urol 153: 674-679; discussion 679-680.

18. Ko DS, Fenster HN, Chambers K, Sullivan LD, Jens M, et al. (1995) The correlation of multichannel urodynamic pressure-flow studies and American Urological Association symptom index in the evaluation of benign prostatic hyperplasia. J Urol 154: 396-398.

19. de la Rosette JJ, Witjes WP, Schafer W, Abrams P, Donovan JL, et al. (1998) Relationships between lower urinary tract symptoms and bladder outlet obstruction: results from the ICS-"BPH" study. Neurourol Urodyn 17: 99-108.

20. Rosen RC, Giuliano F, Carson CC (2005) Sexual dysfunction and lower urinary tract symptoms (LUTS) associated with benign prostatic hyperplasia (BPH). Eur Urol 47: 824-837.

21. McVary KT, Rademaker A, Lloyd GL, Gann P (2005) Autonomic nervous system overactivity in men with lower urinary tract symptoms secondary to benign prostatic hyperplasia. J Urol 174: 1327-1433.

22. Bourke JB, Griffin JP (1966) Hypertension, diabetes mellitus, and blood groups in benign prostatic hypertrophy. Br J Urol 38: 18-23.

23. Michel MC, Mehlburger L, Schumacher H, Bressel HU, Goepel M (2000) Effect of diabetes on lower urinary tract symptoms in patients with benign prostatic hyperplasia. J Urol 163: 1725-1729.

24. Berger AP, Bartsch G, Deibl M, Alber H, Pachinger O, et al. (2006) Atherosclerosis as a risk factor for benign prostatic hyperplasia. BJU Int 98: 1038-1042.

25. Kupelian V, McVary KT, Kaplan SA, Hall SA, Link CL, et al. (2009) Association of lower urinary tract symptoms and the metabolic syndrome: results from the Boston Area Community Health Survey. J Urol 182: 616-624; discussion 624-615.

26. Nickel JC, Roehrborn CG, O'Leary MP, Bostwick DG, Somerville MC, et al. (2008) The relationship between prostate inflammation and lower urinary tract symptoms: examination of baseline data from the REDUCE trial. Eur Urol 54: 1379-1384.

27. Nickel JC, Downey J, Young I, Boag S (1999) Asymptomatic inflammation and/or infection in benign prostatic hyperplasia. BJU Int 84: 976-981.

28. Robert G, Descazeaud A, Nicolaiew N, Terry S, Sirab N, et al. (2009) Inflammation in benign prostatic hyperplasia: a 282 patients' immunohistochemical analysis. Prostate 69: 1774-1780.

29. Kramer G, Steiner GE, Handisurya A, Stix U, Haitel A, et al. (2002) Increased expression of lymphocyte-derived cytokines in benign hyperplastic prostate tissue, identification of the producing cell types, and effect of differentially expressed cytokines on stromal cell proliferation. Prostate 52: 43-58.

30. Kramer G, Mitteregger D, Marberger M (2007) Is benign prostatic hyperplasia (BPH) an immune inflammatory disease? Eur Urol 51: 1202-1216.

31. St Sauver JL, Jacobson DJ, McGree ME, Lieber MM, Jacobsen SJ (2006) Protective association between nonsteroidal antiinflammatory drug use and measures of benign prostatic hyperplasia. Am J Epidemiol 164: 760-768.

32. Kahokehr A, Vather R, Nixon A, Hill AG (2013) Non-steroidal anti-inflammatory drugs for lower urinary tract symptoms in benign prostatic hyperplasia: systematic review and meta-analysis of randomized controlled trials. BJU Int 111: 304-311.

33. Kirby RS, Lowe D, Bultitude MI, Shuttleworth KE (1982) Intra-prostatic urinary reflux: an aetiological factor in abacterial prostatitis. Br J Urol 54: 729-731.

34. De Marzo AM, Platz EA, Sutcliffe S, Xu J, Gronberg H, et al. (2007) Inflammation in prostate carcinogenesis. Nat Rev Cancer 7: 256-269.

35. Hochreiter WW, Duncan JL, Schaeffer AJ (2000) Evaluation of the bacterial flora of the prostate using a 16S rRNA gene based polymerase chain reaction. J Urol 163: 127-130.

36. Bedalov G, Vuckovic I, Fridrih S, Bruk M, Puskar D, et al. (1994) Prostatitis in benign prostatic hyperplasia: a histological, bacteriological and clinical study. Acta Med Croatica 48: 105-109.

37. Alexeyev O, Bergh J, Marklund I, Thellenberg-Karlsson C, Wiklund F, et al. (2006) Association between the presence of bacterial 16S RNA in prostate specimens taken during transurethral resection of prostate and subsequent risk of prostate cancer (Sweden). Cancer Causes Control 17: 1127-1133.

38. Mitsumori K, Terai A, Yamamoto S, Ishitoya S, Yoshida O (1999) Virulence characteristics of Escherichia coli in acute bacterial prostatitis. J Infect Dis 180: 1378-1381.

39. Lipsky BA (1989) Urinary tract infections in men. Epidemiology, pathophysiology, diagnosis, and treatment. Ann Intern Med 110: 138-150.

40. Elkahwaji JE, Zhong W, Hopkins WJ, Bushman W (2007) Chronic bacterial infection and inflammation incite reactive hyperplasia in a mouse model of chronic prostatitis. Prostate 67: 14-21.

41. Boehm BJ, Colopy SA, Jerde TJ, Loftus CJ, Bushman W (2012) Acute bacterial inflammation of the mouse prostate. Prostate 72: 307-317.

42. Rudick CN, Berry RE, Johnson JR, Johnston B, Klumpp DJ, et al. (2011) Uropathogenic Escherichia coli induces chronic pelvic pain. Infect Immun 79: 628-635.

43. Mackern-Oberti JP, Motrich RD, Breser ML, Cejas H, Cuffini C, et al. (2011) Male rodent genital tract infection with Chlamydia muridarum: persistence in the prostate gland that triggers self-immune reactions in genetically susceptible hosts. J Urol 186: 1100-1106.

44. Shinohara DB, Vaghasia AM, Yu SH, Mak TN, Bruggemann H, et al. (2013) A mouse model of chronic prostatic inflammation using a human prostate cancer-derived isolate of Propionibacterium acnes. Prostate 73: 1007-1015.

45. Bethel CR, Faith D, Li X, Guan B, Hicks JL, et al. (2006) Decreased NKX3.1 protein expression in focal prostatic atrophy, prostatic intraepithelial neoplasia, and adenocarcinoma: association with gleason score and chromosome 8p deletion. Cancer Res 66: 10683-10690.

46. De Marzo AM, Marchi VL, Epstein JI, Nelson WG (1999) Proliferative inflammatory atrophy of the prostate: implications for prostatic carcinogenesis. Am J Pathol 155: 1985-1992.

47. Shabsigh A, Chang DT, Heitjan DF, Kiss A, Olsson CA, et al. (1998) Rapid reduction in blood flow to the rat ventral prostate gland after castration:

preliminary evidence that androgens influence prostate size by regulating blood flow to the prostate gland and prostatic endothelial cell survival. Prostate 36: 201-206.

48. Shabisgh A, Tanji N, D'Agati V, Burchardt M, Rubin M, et al. (1999) Early effects of castration on the vascular system of the rat ventral prostate gland. Endocrinology 140: 1920-1926.

49. Lekas E, Johansson M, Widmark A, Bergh A, Damber JE (1997) Decrement of blood flow precedes the involution of the ventral prostate in the rat after castration. Urol Res 25: 309-314.

50. Franck-Lissbrant I, Haggstrom S, Damber JE, Bergh A (1998) Testosterone stimulates angiogenesis and vascular regrowth in the ventral prostate in castrated adult rats. Endocrinology 139: 451-456.

51. Hayek OR, Shabsigh A, Kaplan SA, Kiss AJ, Chen MW, et al. (1999) Castration induces acute vasoconstriction of blood vessels in the rat prostate concomitant with a reduction of prostatic nitric oxide synthase activity. J Urol 162: 1527-1531.

52. Shibata Y, Kashiwagi B, Arai S, Fukabori Y, Suzuki K, et al. (2004) Direct regulation of prostate blood flow by vascular endothelial growth factor and its participation in the androgenic regulation of prostate blood flow in vivo. Endocrinology 145: 4507-4512.

53. Shibata Y, Kashiwagi B, Ono Y, Fukabori Y, Suzuki K, et al. (2004) The evaluation of rat prostate blood flow using a laser speckle flowmetry: a

comparative study using the microsphere method in castrated and androgen-replenished rats. Urol Res 32: 44-48.

54. Lekas E, Engstrand C, Bergh A, Damber JE (1999) Transient ischemia induces apoptosis in the ventral prostate of the rat. Urol Res 27: 174-179.

55. Kozlowski R, Kershen RT, Siroky MB, Krane RJ, Azadzoi KM (2001) Chronic ischemia alters prostate structure and reactivity in rabbits. J Urol 165: 1019-1026.

56. Li J, Chen J, Kirsner R (2007) Pathophysiology of acute wound healing. Clin Dermatol 25: 9-18.

57. Davis C, Fischer J, Ley K, Sarembock IJ (2003) The role of inflammation in vascular injury and repair. J Thromb Haemost 1: 1699-1709.

58. Howdieshell TR, Callaway D, Webb WL, Gaines MD, Procter CD, Jr., et al. (2001) Antibody neutralization of vascular endothelial growth factor inhibits wound granulation tissue formation. J Surg Res 96: 173-182.

59. Inoue H, Asaka T, Nagata N, Koshihara Y (1997) Mechanism of mustard oil-induced skin inflammation in mice. Eur J Pharmacol 333: 231-240.

60. Thurston G, Suri C, Smith K, McClain J, Sato TN, et al. (1999) Leakage-resistant blood vessels in mice transgenically overexpressing angiopoietin-1. Science 286: 2511-2514.

61. Ezaki T, Baluk P, Thurston G, La Barbara A, Woo C, et al. (2001) Time course of endothelial cell proliferation and microvascular remodeling in chronic inflammation. Am J Pathol 158: 2043-2055.

62. Dahlqvist K, Umemoto EY, Brokaw JJ, Dupuis M, McDonald DM (1999) Tissue macrophages associated with angiogenesis in chronic airway inflammation in rats. Am J Respir Cell Mol Biol 20: 237-247.

63. Aurora AB, Baluk P, Zhang D, Sidhu SS, Dolganov GM, et al. (2005) Immune complex-dependent remodeling of the airway vasculature in response to a chronic bacterial infection. J Immunol 175: 6319-6326.

64. Baluk P, Yao LC, Feng J, Romano T, Jung SS, et al. (2009) TNF-alpha drives remodeling of blood vessels and lymphatics in sustained airway inflammation in mice. J Clin Invest 119: 2954-2964.

65. Kwan ML, Gomez AD, Baluk P, Hashizume H, McDonald DM (2001) Airway vasculature after mycoplasma infection: chronic leakiness and selective hypersensitivity to substance P. Am J Physiol Lung Cell Mol Physiol 280: L286-297.

66. Calabrese F, Kipar A, Lunardi F, Balestro E, Perissinotto E, et al. (2013) Herpes virus infection is associated with vascular remodeling and pulmonary hypertension in idiopathic pulmonary fibrosis. PLoS One 8: e55715.

67. Tabruyn SP, Colton K, Morisada T, Fuxe J, Wiegand SJ, et al. (2010) Angiopoietin-2-driven vascular remodeling in airway inflammation. Am J Pathol 177: 3233-3243.

68. Fuxe J, Lashnits E, O'Brien S, Baluk P, Tabruyn SP, et al. (2010) Angiopoietin/Tie2 signaling transforms capillaries into venules primed for leukocyte trafficking in airway inflammation. Am J Pathol 176: 2009-2018.

69. Golomb E, Rosenzweig N, Eilam R, Abramovici A (2000) Spontaneous hyperplasia of the ventral lobe of the prostate in aging genetically hypertensive rats. J Androl 21: 58-64.

70. Clemow DB, McCarty R, Steers WD, Tuttle JB (1997) Efferent and afferent neuronal hypertrophy associated with micturition pathways in spontaneously hypertensive rats. Neurourol Urodyn 16: 293-303.

71. Berger AP, Deibl M, Halpern EJ, Lechleitner M, Bektic J, et al. (2005) Vascular damage induced by type 2 diabetes mellitus as a risk factor for benign prostatic hyperplasia. Diabetologia 48: 784-789.

72. Berger AP, Deibl M, Leonhartsberger N, Bektic J, Horninger W, et al. (2005) Vascular damage as a risk factor for benign prostatic hyperplasia and erectile dysfunction. BJU Int 96: 1073-1078.

73. Weisman KM, Larijani GE, Goldstein MR, Goldberg ME (2000) Relationship between benign prostatic hyperplasia and history of coronary artery disease in elderly men. Pharmacotherapy 20: 383-386.

74. Meigs JB, Mohr B, Barry MJ, Collins MM, McKinlay JB (2001) Risk factors for clinical benign prostatic hyperplasia in a community-based population of healthy aging men. J Clin Epidemiol 54: 935-944.

75. Berger AP, Horninger W, Bektic J, Pelzer A, Spranger R, et al. (2006) Vascular resistance in the prostate evaluated by colour Doppler ultrasonography: is benign prostatic hyperplasia a vascular disease? BJU Int 98: 587-590.

76. Bercovich E, Barabino G, Pirozzi-Farina F, Deriu M (1999) A multivariate analysis of lower urinary tract ageing and urinary symptoms: the role of fibrosis. Arch Ital Urol Androl 71: 287-292.

77. Ma J, Gharaee-Kermani M, Kunju L, Hollingsworth JM, Adler J, et al. (2012) Prostatic fibrosis is associated with lower urinary tract symptoms. J Urol 188: 1375-1381.

78. Borthwick LA, Wynn TA, Fisher AJ (2013) Cytokine mediated tissue fibrosis. Biochim Biophys Acta 1832: 1049-1060.

79. Atamas SP (2002) Complex cytokine regulation of tissue fibrosis. Life Sci 72: 631-643.

80. Ueha S, Shand FH, Matsushima K (2012) Cellular and molecular mechanisms of chronic inflammation-associated organ fibrosis. Front Immunol 3: 71.

81. Broughton G, 2nd, Janis JE, Attinger CE (2006) The basic science of wound healing. Plast Reconstr Surg 117: 12S-34S.

82. Frantz C, Stewart KM, Weaver VM (2010) The extracellular matrix at a glance. J Cell Sci 123: 4195-4200.

83. Cantiello F, Cicione A, Salonia A, Autorino R, Tucci L, et al. (2013) Periurethral fibrosis secondary to prostatic inflammation causing lower urinary tract symptoms: a prospective cohort study. Urology 81: 1018-1023.

84. Elkahwaji JE, Hauke RJ, Brawner CM (2009) Chronic bacterial inflammation induces prostatic intraepithelial neoplasia in mouse prostate. Br J Cancer 101: 1740-1748.

CHAPTER TWO

This manuscript was published in *The Prostate* 2014;74(4):345-58.

Contributions of authors: L.W. performed transurethral instillation experiments and prepared the manuscript. J.G. performed India ink perfusion, RT-PCR and immunohistochemical analyses in prostate development and infection experiments and assisted in manuscript preparation. J.C. and C.J.L. assisted in RT-PCR and immunohistochemical analyses. M.B. designed and drew schematic illustrations. S.L. performed vascular density analysis and assisted in India ink perfusion. V.M. and C.M.V. performed India ink perfusion and immunohistochemical analysis in prostate development and assisted in manuscript preparation. W.B. supervised studies and assisted in manuscript preparation.

Prostate angiogenesis in development and inflammation

Letitia Wong, Jerry Gipp, Jason Carr, Christopher J. Loftus, Molly Benck, Sanghee Lee, Vatsal Mehta, Chad M. Vezina, Wade Bushman

ABSTRACT

BACKGROUND. Prostatic inflammation is an important factor in development and progression of BPH/LUTS. This study was performed to characterize the normal development and vascular anatomy of the mouse prostate and then examine, for the first time, the effects of prostatic inflammation on the prostate vasculature.

METHODS. Adult mice were perfused with India ink to visualize the prostatic vascular anatomy. Immunostaining was performed on the E16.5 UGS and the P5, P20 and adult prostate to characterize vascular development. Uropathogenic *E. coli* 1677 was instilled transurethrally into adult male mice to induce prostate inflammation. RT-PCR and BrdU labeling was performed to assay anigogenic factor expression and endothelial proliferation, respectively.

RESULTS. An artery on the ventral surface of the bladder trifurcates near the bladder neck to supply the prostate lobes and seminal vesicle. Development of the prostatic vascular system is associated with endothelial proliferation and robust expression of pro-angiogenic factors *Pecam1, Tie1, Tek, Angpt1, Angpt2, Fgf2, Vegfa, Vegfc,* and *Figf*. Bacterial-induced prostatic inflammation induced endothelial cell proliferation and increased vascular density but surprisingly

decreased pro-angiogenic factor expression.

CONCLUSIONS. The striking decrease in pro-angiogenic factor mRNA expression associated with endothelial proliferation and increased vascular density during inflammation suggests that endothelial response to injury is not a recapitulation of normal development and may be initiated and regulated by different regulatory mechanisms.

INTRODUCTION

The prostate is an androgen-dependent male accessory sex organ that is composed of the epithelial ductal glands surrounded by the stromal components, including the vasculature. In addition to androgen stimulation, the prostate requires nutrients and oxygen supplied by the vasculature for normal development, growth and function. Studies of the adult rat prostatic gland have consistently emphasized the importance of the prostatic vascular system in growth homeostasis, yet its aspect in prostate biology is still understudied. In response to androgen deprivation, there was an early and rapid reduction in blood flow to the adult rat ventral prostate after castration accompanied with vasoconstriction, increased vascular permeability, increased apoptosis and decreased proliferation of endothelial cells that occurred prior to the onset of prostatic epithelial cell apoptosis and tissue regression [1-3]. Androgen supplements rapidly restored the prostatic vasculature after castration that was required for the subsequent epithelial regeneration [1,2,4]. Studies in human

prostates have further revealed vascular changes in prostate cancer and benign prostatic hyperplasia (BPH) including increased vessels with tiny lumens and irregular shapes, increased vessel density, and reduced blood flow, suggesting changes in vascular architecture or anatomy may have a potential role in prostate diseases [8-11]. To date, there has been only one published study to describe the vascular anatomy in the rat ventral prostate [12]. The arterial supply to the ventral lobe of the adult rat prostate was shown to derive in common or individually from the inferior vesical artery. The arterioles and venules traveled along the periphery of the glandular lobules while thin walled capillaries predominated immediately adjacent to the basement membranes of the glands as well as within the stroma surrounding the ducts. As of yet, the vascular anatomy of the adult mouse prostate and the development of the mouse prostatic vascular system have never been studied.

Vascular remodeling is a critical feature during inflammation after tissue injury and is mediated by angiogenic factors [4-6]. Studies in rodents infected with the respiratory pathogen *Mycoplasma pulmonis* have showed that bacterial infection induced airway inflammation was accompanied by numerous early vascular responses that preceded the tissue remodeling and was persistent as the infection continued toward chronic conditions [16]. The vascular remodeling in the trachea in response to bacterial infection involved increased endothelial cell proliferation, enhanced angiogenesis, increased vessel density, increased vessel

permeability, enlargement of vessel diameter, and vascular reorganization in a non-uniform pattern [16-20]. Similarly, respiratory infection with herpes virus in mice induced endothelial cell proliferation and vessel thickening in the lung [21]. Previous studies have further suggested that these vascular changes were at least in part mediated by Angiopoietin/Tek receptor signaling. Overexpression of Angpt1 in pathogen-free mice induced the vascular remodeling similar to as in *Mycoplasma pulmonis* infected animals while blocking its effect by injection of soluble Tek receptor in infected animals inhibited the vascular responses to inflammation [22].

Prostatic inflammation is a common feature in aging men and is considered to be one of the major factors in the development and progression of BPH and its associated lower urinary tract symptoms (LUTS) as previous studies have demonstrated a strong association between the presence of prostatic inflammation and the increased incidence of BPH/LUTS [7-10]**.** In spite of this connection, the underlying mechanisms of how prostatic inflammation contributes to BPH/LUTS, has yet to be elucidated. There is increasing evidence suggesting that the vascular pathogenesis is a potential contributor to the etiology of BPH/LUTS. Studies in aging men have revealed that atherosclerotic diseases, such as coronary heart disease, hypertension, diabetes mellitus, are a risk factor for BPH/LUTS and are associated with the prevalence or symptom severity of BPH/LUTS [11-17]. Subsequent studies on BPH have indicated that reduced

prostatic blood flow and increased vascular resistance in the transition zone of the prostate were observed in patients with BPH/LUTS compared to control healthy group [12,18]. It also appears that BPH/LUTS patients with vascular disorders had a greater reduction of prostatic blood flow and a greater severity of BPH symptoms than men without vascular disorders [12,14]. Given that prostatic inflammation and vascular pathology are associated with BPH/LUTS and vascular response is essential during inflammation for tissue repair, the mechanisms underlying the vascular changes in response to inflammation in the prostate are postulated to contribute to the etiology of BPH/LUTS. Therefore, it is tempting to investigate the effect of inflammation on vascular changes in the prostate.

In this study, the vascular development and its response to inflammation in the mouse prostate were described. We began the study by describing the vascular anatomy of the mouse prostate at the macroscopic level. We also evaluated the relationship of prostate vasculature with the epithelium, endothelial proliferation and mRNA expression of the major angiogenic factors in the developing and the mature adult mouse prostates. Finally exploiting our previously described mouse model of bacterial-induced prostatic inflammation [19], we characterized the vascular response to acute inflammation by measuring endothelial proliferation, vessel density and changes in the mRNA expression of the major angiogenic factors in the adult mouse prostate. The findings of this study are to serve as a

fundamental resource for future research aimed at elucidating the role of vascular mechanisms in prostate development as well as the pathogenesis of inflammation associated prostatic diseases.

MATERIALS AND METHODS

Visualization of the Vascular System by Intra-cardiac Perfusion of India Ink

Adult C57BL6/J (Jackson Laboratory) or CD-1 WT (Charles River) male mice were used in these studies. To visualize the vascular anatomy of the mouse prostate, anesthetized mice were perfused with 25% India ink in sterile PBS through the left ventricle. India ink is commonly used in research for visualization of the blood vessels [20,21]. After the ink is completely distributed to all vessels in the entire body, the urogenital tracts were removed immediately from the animals and were fixed in 10% neutral buffered formalin overnight at 4^{o}C. The next day the tissues are rinsed in PBS and then incubated in PBS+ 1% KOH for 2 days at 4^{o}C followed by serial steps with graded increasing concentration of glycerol in PBS + 1% KOH starting at 25-50%, 75% and finally 100% for 2 days each with final storage in glycerol, all incubations done at 4°C. Note that as the concentration of glycerol goes up the concentration of the PBS/KOH goes down, starting with 1% KOH in PBS. The vasculature of the prostate was visualized under the dissecting light microscope and images were obtained using a digital SPOT camera.

Transurethral Instillation

Transurethral instillation was performed as previously described [19]. Briefly, 8- to 10-week old CD-1 (Charles River) or C57BL6/J (Jackson Laboratory) WT male mice were anesthetized with isoflurane and a lubricated sterile polyethylene catheter was inserted into the mouse urethra. Uropathogenic *E. coli* 1677 (2 x10^6 CFU/ml) or sterile PBS in a volume of 200µl was instilled transurethrally into the adult male mice.

Animals were sacrificed 1, 2, 3, 5, and 7 days post-instillation. Naïve animals not undergoing instillation procedures were also sacrificed to control for vascular changes associated with catherization or transurethral instillation. In the study of the effect of prostatic inflammation on endothelial proliferation, animals were intraperitoneally injected with BrdU 2 hr prior to sacrifice and the prostate was collected from each animal for histology and immunohistochemistry. In the study of the effect of prostatic inflammation on gene expression of the angiogenic factors, the prostatic lobes were collected from each animal for RNA isolation. Four to seven mice per time point and per treatment were used. Ten animals without any treatment were sacrificed as naïve.

Vascular Development

CD-1 WT pregnant females and 8-week old male mice were purchased from Charles River. For study in quantitation of endothelial proliferation, animals were

sacrificed at postnatal Day 15 (n = 6) and 8-week (n = 6). Prostatic tissues were harvested and processed as described below for histology and immunohistochemistry. For study of angiogenic factor expressions, the male urogenital sinus (UGS) at embryonic Day 16 (n = 4), the prostate at postnatal Day 5 (n = 4) and the prostatic lobes at 8-week old animals (n = 5) were collected for RNA isolation.

Immunohistochemical staining

Co-staining for Brdu and PECAM was used to assess the proliferation in endothelial cells. Tissue was removed from the animals and fixed in 4% PFA overnight at 4^{o}C. PFA was replaced with 20% sucrose and incubated at 4^{o}C for 3 days after which sucrose was replaced with OCT for 3 hr prior to embedding in fresh OCT. Samples were stored at -80^{o}C until sectioned. Serially sections were cut at 10 µm and slides stored at -80^{o}C until staining. To begin staining tissue sections were washed in 0.01M PBS (pH 7.4) with 0.1% triton x100 (3x 5min). Incubate in 1N HCl for 10 min on ice followed by 2N HCl for 10 min at room temp and transfer to 37^{o}C for another 20 min. Immediately place in 0.1M borate buffer (pH 9) for 12 min at room temperature. Slides were then washed in PBS + 0.1% Triton x100, three times 5 min each at room temperature. IHC blocking was with PBS (pH 7.4) + 0.1% Triton x100 + Glycine (1M) + 5% normal donkey serum for 1hr at room temperature. Following blocking primary antibody in blocking solution was added, BrdU (Abcam 1893) at 1:50 dilution and PECAM (BD 550274) at

1:200 dilution. Primary antibodies were incubated at room temperature overnight followed by three 5 min washes with PBS + 0.1% Triton x100. Secondary staining was done with fluorescence antibodies from Invitrogen, (A21209, Alexa594 for PECAM, A11015, Alexa488 for BrdU) at 1:200 dilution in block buffer for 1hr at room temperature. Wash three times as above for primary antibody. To stain nuclei add Hoechst 33258 at 4µg/ml in PBS for 10 min at room temperature. Wash three times, 5 min each in PBS, coverslip and image.

Co-staining for CDH1 and KDR was used to assess the relationship of the endothelial cells with the epithelial cells in the mouse UGS and prostate at different stages of development. Male urogenital sinus from E16.5, and prostates from P5, P20 and adult C57BL/6J mouse tissues were fixed in 4% paraformaldehyde, dehydrated in methanol, infiltrated with paraffin, and cut into 5-µm sections. After deparaffinization, hydration, and antigen unmasking in boiling 1mM Tris-EDTA buffer (pH 9), tissues were blocked for 1 hr in TBSTw containing 1% Blocking Reagent (Roche Diagnostics, Indianapolis, IN), 5% normal goat sera, and 1% bovine serum albumin fraction 5 (RGBTw). Tissues were incubated overnight at 4°C with primary antibodies diluted in RGBTw as follows: 1:250 mouse anti-CDH1 (61081, BD Transduction Laboratories, Franklin Lakes, NJ) and 1:600 rabbit anti-KDR (2479S, Cell Signaling Technology). Secondary antibodies were diluted as follows: 1:250 Dylight 488-conjugated anti-mouse IgG (115-487-003, Jackson Immunoresearch, West Grove, PA), 1:250

Alexa Fluor 594 Goat Anti-Rabbit IgG (A11012, Life Technologies, Grand Island, NY). Immunofluorecent labeled tissues were counterstained with 4′,6-diamidino-2-phenylindole, dilactate, and mounted in anti-fade media (phosphate-buffered saline containing 80% glycerol and 0.2% n-propyl gallate).

Mean Blood Vessel Density (MVD)

Eight to twelve-week old C57BL6/J WT male mice (Jackson Laboratory) were instilled transurethrally with uropathogenic *E. coli* or sterile saline as described above. Prostatic tissues at Day 3 (n = 4 saline, n = 3 *E. coli)* and 7 (n = 4 saline, n = 4 *E. coli)* post-instillation were harvested, fixed in 10% formalin, embedded in paraffin and serially sectioned at 6μm. Standard H&E staining were performed for histology. The severity of inflammation was graded based on our previously established grading system [19]. The identification of blood vessels in the H&E images was consulted with a pathologist. The number of blood vessels in the stromal area per 10X field were counted and used to determine MVD for the DLP. The data are presented as the mean ± SEM.

Endothelial Proliferation

Immunohistochemical staining for BrdU and PECAM were performed on frozen sections as described above. 20X field images were obtained using an Olympus fluorescent microscope and a digital SPOT camera. Double positive BrdU/PECAM (+/+) cells representing endothelial proliferation were counted. For

developmental experiments comparisons were made between animals at P15 and 8-week old. Comparisons between saline and 3, 5, 7-day *E. coli* post-instillation were used to assess proliferation during inflammation. In addition, H&E staining for histology was performed to confirm prostatic inflammation in the *E. coli* infected animals. The data are presented as the mean ± SEM.

RNA isolation and cDNA

UGS tissues and prostatic lobes from animals were collected in 1.6 ml microcentrifuge tubes and snap frozen in liquid nitrogen immediately. RNA from the tissues was extracted using RNeasy Micro Kit (Qiagen, Inc.) and following the manufacture's protocol and RNA yield was measured and purity determined by 260 / 280 nm ratio on a Nanodrop 1000 spectrophotometer (Thermo Scientific Inc.). RNA was converted to cDNA by reverse transcription as previously described [19].

Semi-Quantitative Real-Time PCR

Semi-quantitative RT-PCR was performed with cDNA samples to quantitate gene expression levels of the angiogenic factors. The forward and reverse primers of each angiogenic factor *Pecam, Pdgfa, Tie1, Tek, Angpt1, Angpt2, Angpt4, Fgf2, Vegfa, Vegfb, Vegfc*, and *Figf* were designed using the NCBI mouse nucleotide database, the mouse genomic BLAST database and the Primer-3 program. The sequences of the primers used are shown in Table I. RT-PCR cycle reactions

were detected with SYBR green (Roche) and run on a BioRad Real-Time CFX with run conditions of 95°C for 10 min, followed by 50 cycles of 95°C for 15 sec and 60°C for 1 min. Gene expression levels were normalized to the housekeeping gene *Gapdh*.

Statistical Analysis

Gene expression between different time periods was compared using ANOVA (analysis of variance), followed by a Fisher's LSD (Least Significant Difference) test for pair-wise comparisons of different time periods. Prior to ANOVA, Levene's test was used to verify the homoscedasticity assumption and a non-parametric procedure was used for non-conforming data. All analysis was conducted using SAS 9.2 (SAS Institute, Cary NC) software. A P-value < 0.05 was considered statistically significant in two-tailed statistical tests.

To explore the relationship between mean vessel density and inflammation score for different prostatic lobes, Spearman's rank correlation coefficient (ρ) was calculated together with its test statistic. Commonly the strength of the correlation ranges from -1 to 1, with values closer to 1 indicating very strong correlation and to 0 representing very weak correlation. The sign (+ or -) of the correlation coefficient defines the direction of the relationship. Further, a comparison was performed on the inflammation score between WT and *E. coli* for different prostatic lobes on Day 3 and 7 using a two-sample t-test. All analysis was

conducted using SAS 9.2 (SAS Institute, Cary NC) software. A P-value < 0.05 was considered statistically significant in two-tailed statistical tests.

RESULTS

Vascular Anatomy of the Adult Mouse Prostate

We investigated the vascular anatomy of the adult mouse prostate vasculature by intra-cardiac injection of India ink and light microscopy (Fig. 1 A and B). The India ink angiograms revealed one main artery on each side of the ventral aspect of the bladder supplying the prostate/seminal vesicle complex. This artery branches into three vessels near the neck of the bladder to supply the bladder, prostate, seminal vesicle and the urethra. The central branch bifurcates - giving off one vessel that runs along the anterior prostate to supply the anterior prostatic ducts and parts of the adjacent seminal vesicle and another vessel that directly supplies the anterior prostate. The dorsal branch supplies the dorsolateral prostate while the ventral branch supplies the ventral surface of the bladder and the ventral prostate. Vessels supplying the ventral and dorsolateral prostate lobes enter near the junction of the main prostate ducts with the urethra and arborize as they extend distally (Fig. 1C and D). Schematic illustrations of the vascular anatomy of the adult male mouse urogenital tract are shown in Figure 1E and F.

Architecture of Vascular Development

To visualize the relationship between microvessels and prostate ducts during their initial outgrowth (E16.5), branching morphogenesis (P5), glandularization (P20), and upon maturation (P50), we conducted double immunofluorescent staining for vascular endothelial growth factor receptor 2 (VEGFR2 also known as KDR, marks endothelium) and cadherin 1 (CDH1, marks prostatic epithelium). We observed a distinct vascular network in the stroma along the entire cranial-caudal axis of the urethra of the male UGS at E16.5 (Fig. 2A). This network was also detected in the stroma of the seminal vesicle and ejaculatory duct epithelium, similar to the observations made by Abler et al., 2011 [36]. Importantly, a discernible vascular network circumscribed nascent ducts from the very beginning of their development, suggesting a coordinated mechanism of pattern formation (Fig. 2A). A similar spatial relationship was observed at P5, when microvessels enveloped newly formed prostatic branch tips (Fig. 2B). Vessels were oriented along the proximodistal duct axis at P20 (Fig. 2C) and P50 (Fig. 2D), again suggesting coordination in patterning of prostatic ducts and the prostatic vascular supply.

Angiogenic Factor Expression in Mouse Prostate Development

We analyzed mRNA expression pattern of angiogenic factors in the male E16 UGS, P5 prostate and the individual lobes of the adult prostate (Fig. 3). Expression of *Pecam1, Tie1, Tek, Angpt1, Angpt2, Fgf2, Vegfc, and Figf* was

higher at E16 than at the adult stage. A subset of these genes (*Tie1, Tek, Angpt1, Fgf2, Vegfc,* and *Figf)* as well as *Vegfa,* were expressed more abundantly at P5 as well. Several genes, including *Angpt2, Angpt4* and *Vegfb*, did not exhibit increased expression at either E16 or P5 and actually seemed to be expressed more abundantly in the adult. In contrast, *Pdgfa* showed no significant differences in expression at any of the time points examined. All of the angiogenic factors examined have been shown to have important functions associated with angiogenesis. However, their angiogenic effects are highly dependent on the presence of each other and the interaction with specific receptors [37, 38]. Further, many of these angiogenic factors have multiple isoforms with variable potency and activity [37, 38]. It is therefore difficult to directly correlate the temporal patterns of mRNA expression for any factor with a specific angiogenic process in either the developing or adult prostate. However, our finding that a majority of angiogenic factors are expressed more abundantly in the perinatal period is clearly consistent with generally robust angiogenic activity required for vascularization of the growing prostate.

Vascular Response to Acute Inflammation in the Mouse Prostate

To assess the response of vasculature in bacterial-induced injury and inflammation we measured the mean blood vessel density, endothelial cell proliferation and the expression profiles of angiogenic genes in the DLP following bacterial infection. The DLP was selected for analysis since our previous work

has shown that the DLP exhibits the most consistent and robust inflammatory response to bacterial inoculation [33]. Analysis of H&E stained sections showed a significant increase of inflammatory degree and mean blood vessel density in the stromal area of the DLP of the *E. coli* infected mice at Day 3 and 7 post-instillation (Fig. 4A and B). Correlation analysis revealed a strong positive relationship between the severity of inflammation and the mean blood vessel density (Fig. 4C and D). To determine whether increased mean vessel density is associated with an increase in endothelial proliferation, mice were injected IP with BrdU 2 hr before sacrifice. Proliferating endothelial cells were identified by co-immunostaining for BrdU and the endothelial marker (PECAM). The number of double positive PECAM/BrdU (+/+) cells was 16-fold higher on Day 3 post-infection as compared to saline control. Endothelial proliferation returned to baseline by Day 5 post-infection (Fig. 5A-D, G). There was no difference in endothelial BrdU labeling index between naïve and saline controls (data not shown), demonstrating that the instillation procedure itself had no effect on endothelial proliferation. To ascertain the relative magnitude of the proliferative response induced by inflammation of the adult prostate, we compared the endothelial labeling index in adult and P15 mice. P15 is a period of robust ductal morphogenesis and growth of the prostate ductal network is at its peak. This revealed that endothelial proliferation was six-fold higher at P15 than in the adult (Fig. 5E-F, H). These data show that there is a rapid vascular response to

bacterial-induced inflammation that is characterized by a very robust increase in endothelial proliferation.

Angiogenic Factor Expression in the Bacterial-Inflamed Prostate

We analyzed mRNA expression pattern of angiogenic factors in the DLP (Fig. 6) of the adult mice at Day 1, 2, 3, 5, and 7 post-instillation. Expression of *Pecam, Pdgfa, Tie1, Tek, Angpt1, Angpt2, Angpt4, Fgf2, Vegfb, Vegfc*, and *Figf* decreased significantly in the first 3 days following bacterial infection. By Day 5 and 7 post-infection, expression of most of these genes (*Pdgfa, Tie1, Tek, Angpt1, Angpt2, Angpt4, Fgf2, Vegfb,* and *Vegfc*) returned to baseline while *Pecam* and *Figf* exhibited a rebound expression significantly higher than baseline. Expression of *Vegfa* showed no significant changes at any time point.

DISCUSSION

We used intra-cardiac injection of India ink to visualize the mouse prostatic vasculature. Injection into the beating heart allowed the ink to distribute through the arterial system. We observed a single main artery on the ventral aspect of each side of the bladder running laterally onto the side of the prostatic urethra and trifurcating near the bladder neck. The ventral branch supplies the bladder and the ventral prostate; the central branch supplies the seminal vesicle and the anterior prostate; the dorsal branch supplies the dorsolateral prostate.

Immunonstaining for VEGFR2 in the UGS demonstrated an abundant microvessel network circumscribing the newly formed prostatic bud. This network enveloped the elongating ducts and duct tips postnatally and generated the microvascular network of the adult prostate. These observations complement a detailed electron-microscopy study of the microvascular network in the adult rat previously published by Buttyan and colleagues [12]. Formation of this vascular network during prostate development was accompanied by robust expression of a variety of angiogenic factors, including *Pecam1, Tie1, Tek, Angpt1, Angpt2, Fgf2, Vegfa, Vegfc,* and *Figf*. The association of angiogenic factor expression with development of the vascular network is compelling, however, we cannot at this time ascribe a specific role to any single or group of factors in the process of endothelial proliferation and vascular remodeling in the prostate.

We observed a dramatic increase in endothelial proliferation in response to bacterial-induced prostatic inflammation. Endothelial proliferation was increased 16-fold 3 days after bacterial inoculation and decreased to baseline 5 days post-inoculation. Vascular density was also increased. The magnitude of the vascular response to bacterial-induced inflammation was assessed by comparing it to the angiogenic activity in the adolescent (P15) and the normal adult prostate. We selected the P15 for comparison because P15 is a period of robust ductal morphogenesis [39]. These studies revealed that endothelial proliferation was 6-

fold higher at P15 than in the adult, but the relative increase in proliferation was even higher in the inflamed prostate. The increase in endothelial proliferation 3 days post-infection occurs concomitant with a marked increase in epithelial proliferation as previously reported [33, 40].

Angiogenesis is a critical step during inflammation in response to tissue injury and is tightly mediated by a variety of angiogenic factors. The resulting new vessels are essential to provide oxygen in wounded area and facilitate tissue regeneration. Previous studies have shown that airway inflammation induced by *Mycoplasma pulmonis* infection in C3H/HeN mice increased angiogenesis as evidenced by increased endothelial cell proliferation beginning as early as 1 day following infection [16]. The proliferative index of endothelial cells peaked at 5 days, and sharply declined at Day 9 post-infection but remained higher than uninfected control. This angiogenic response to airway inflammation was accompanied by numerous vascular modeling including enlargement of existing vessels, endothelial cell enlargement and increased vessel density.

We found mRNA expression of a majority of angiogenic factors examined to be decreased in the prostate after bacterial infection. This finding stands at odds with the robust endothelial proliferation that accompanies the inflammatory response. It is, to our knowledge, without precedent in the literature. One possible explanation is that inflammation/injury induces the release of previously

synthesized angiogenic factors. An alternative explanation is that endothelial proliferation during bacterial-induced inflammation may not be mediated by the angiogenic factors examined in this study but instead by other factors produced following bacterial-infection. We have previously shown that IL-1 is highly expressed in prostatic inflammation and is required for the epithelial hyperplasia that occurs in response to bacterial-induced inflammation [40]. IL-1 has been demonstrated to be pro-angiogenic and might contribute to the angiogenic response observed. Previous studies have suggested that IL-1 can elicit production of both classical pro-angiogenic factors and inflammatory cytokines such as IL-8, TNFα, HGF, TGFβ, and COX2 that possess angiogenic activity [40-49].

Despite the extensive focus in studying the pathogenesis of BPH, the role of angiogenesis and the angiogenic factors in BPH is poorly studied. Previous studies have showed that microvascularity was increased in BPH [9]. However, subsequent studies to characterize the pro-angiogenic factor expression in BPH tissues are controversial. Studies by Jackson et al [50] have shown 100% cases of BPH were stained positive for VEGFA. Stefanou and colleagues [51] have reported that VEGFA were expressed in 81.25% of BPH samples examined. In contrast, another studies have found that 83% of BPH cases were negative for VEGFA [52]. Thus, it is unclear whether the classical pro-angiogenic factors are important in regulating angiogenesis in BPH due to these inconsistent findings.

Intriguingly, previous studies have shown that inflammatory factors including IL-1, IL-8, TGFβ were capable to mediate angiogenesis in addition to their typical inflammatory functions and more importantly, these factors were highly expressed in some cases of BPH tissues with inflammation [40-57]. Given that angiogenesis is a typical vascular response to inflammation and prostatic inflammation is a common feature in BPH, it is tempting to speculate that prostatic inflammation in BPH induces vascular remodeling through the angiogenic effects of the inflammatory cytokines. The findings in our studies support this concept, leading to a hypothesis that angiogenesis in response to prostatic inflammation may be mediated by inflammatory cytokines rather than the classical angiogenic factors. This suggests a mechanism that may explain the inconsistent findings of the correlation between angiogenesis and classical angiogenic factor expression in BPH and provide a new perspective for a possible role of inflammation-induced vascular remodeling and angiogenesis in the pathogenesis of BPH.

CONCLUSIONS

The developing prostate and the inflamed adult prostate both exhibit robust endothelial proliferation. However, the endothelial proliferation associated with inflammation is characterized by a decrease in pro-angiogenic factor mRNA expression suggesting that it is not a recapitulation of normal vascular development but a process initiated and regulated by a different set of regulatory

factors.

ACKNOWLEDGEMENTS

This work was supported by NIH R01DK0757, T32 ES007015 from the National Institute of Environmental Health Sciences (NIEHS), NIH, and Herman I. Shapiro Distinguished Graduate Fellowship from UW-Madison School of Medicine and Public Health. Its contents are solely the responsibility of the authors and do not necessarily represent the official views of the funders. The authors also greatly appreciate the help from M. Shahriar Salamat, M.D., Ph.D. with his knowledge in pathology and Chee Paul Lin for providing statistical analysis.

TABLE I. Primer Sequences (5' to 3') Used for RT-PCR Analysis

Mediator	Forward Sequence	Reverse Sequence
Pecam1	GTCAGAGTCTTCCTTGCCCC	CTGTTTGGCCTTGGCTTTCC
Pdgfa	AGTCAGATCCACAGCATCCG	TGGTTAATGGCATGGGACCC
Tie1	GCTGCTCCCCACTCTTTTCT	GACACGCAGGTCAGGAAGAA
Tek (Tie2)	ACCTCTTGTGTCTGATGCCG	CAGTGGATCTTGGTGCTGGT
Angpt1	TTCTTCCAGAACACGACGGG	AAGAGAAATCCGGCTCCACG
Angpt2	CATAGCAGCCCCTTTCCACA	GACTGCAGTGCCTTTGGTTG
Angpt4	GGTAATGTGGCCAGAGAGCA	TCCCAGTCATGCAGTTCCAC
Fgf2	GAGAAGAGCGACCCACACG	CAGCCGTCCATCTTCCTTCA
Vegfa	ACTTCTGAGGGGCCTAGGAG	AGGTGGGGTAAGGAGAGGAC
Vegfb	GTGCCTCTGAGCATGGAACT	ACATTCCAGGCCATCGTCAG
Vegfc	CAGCCCACCTCAATACCAG	CTCACGTGGCATGCATTGAG
Figf (Vegfd)	CCCATCGCTCCACCAGATTT	CGCATGTCTCTCTAGGGCTG
Gapdh	AGAACATCATCCCTGCATCC	CACATTGGGGGTAGGAACAC

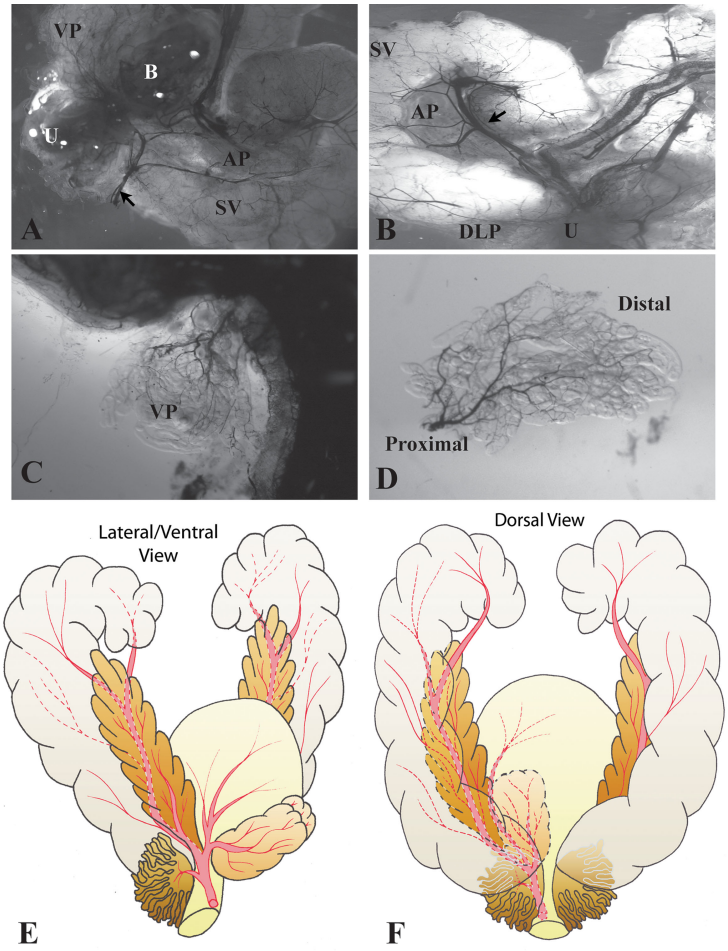

Fig. 1. Visualization of the prostatic vascular anatomy by intracardiac perfusion of India ink. **A.** Low magnification brightfield image of the ventral and lateral side of adult male mouse urogenital tract. The blood vessels were filled with black India ink. Black arrow indicates the main artery supplying the male urogenital tract. Note that left lobe of the ventral prostate was removed to visualize the vessels near the neck of the bladder. **B.** Low magnification brightfield image of the dorsal side of adult mouse male urogenital tract. Black arrow indicates the main artery supplying the seminal vesicle and anterior prostate. **C** and **D.** Images of ventral prostate showing that the vessels supplying the lobe enter close to the urethra and arborize distally. U, urethra; VP, ventral prostate; DLP, dorsalateral prostate; AP, anterior prostate; SV, seminal vesicle; B, bladder. **E** and **F.** Schematic illustrations of the vascular anatomy of the adult male mouse urogenital tract. E. A lateral and ventral view. F. A dorsal view. The main artery on the ventral aspect of the bladder runs laterally onto each side of the male urethra and branches into three vessels near the neck of the bladder: the ventral branch supplies the bladder and the ventral prostate; the central branch supplies the seminal vesicle and the anterior prostate; the dorsal branch supplies the dorsolateral prostate.

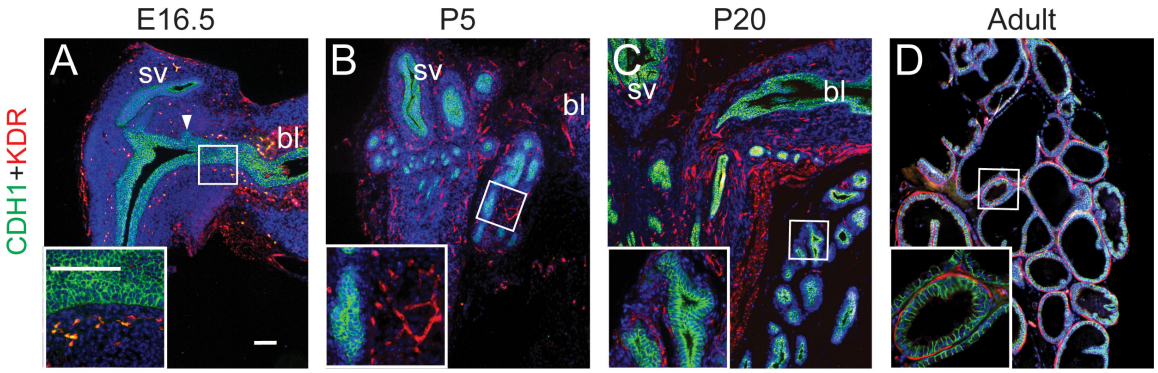

Fig. 2. Immunostaining for CDH1 (Green), KDR (Red) and DAPI (Blue) in the E16.5 UGS **(A)**, P5 ventral prostate **(B)**, P20 ventral prostate **(C)**, adult ventral prostate **(D)**. bl, bladder; sv, seminal vesicle. In panel A, arrowheads indicate prostatic bud. Scale bars in panel A and inset correspond to 100 μm. Note that there is abundant auto-fluorescence of the red blood cells shown as yellow in the E16.5 UGS.

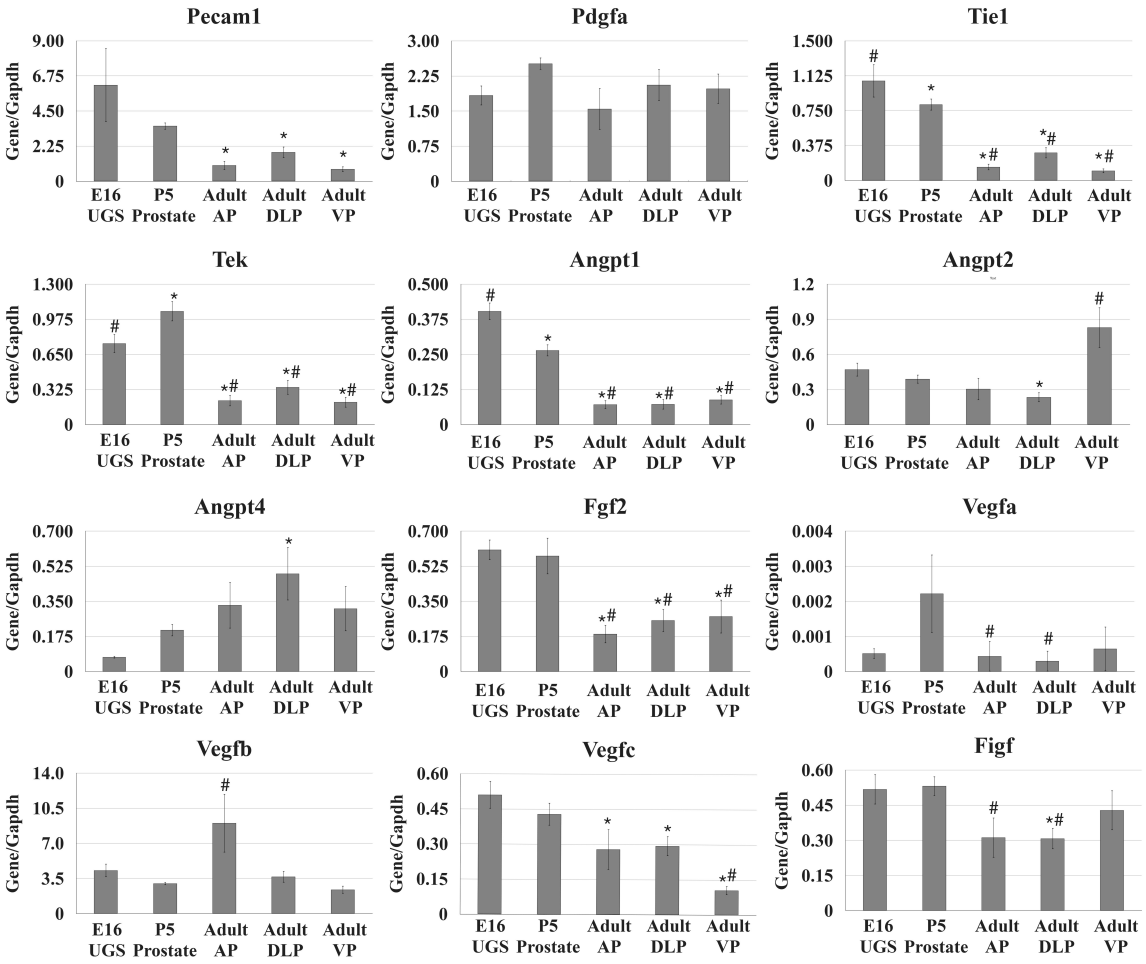

Fig. 3. qRT-PCR analysis for the angiogenic factors in the E16 male UGS, P5 prostate, and the AP, DLP, VP of the adult. The data are presented as the mean ± SEM. * Indicates a P-value < 0.05 compared to E16 UGS by two-sample t-test. # Indicates a P-value < 0.05 compared to P5 prostate by two-sample t-test. UGS, urogenital sinus; AP, anterior prostate; DLP, dorsolateral prostate; VP, ventral prostate.

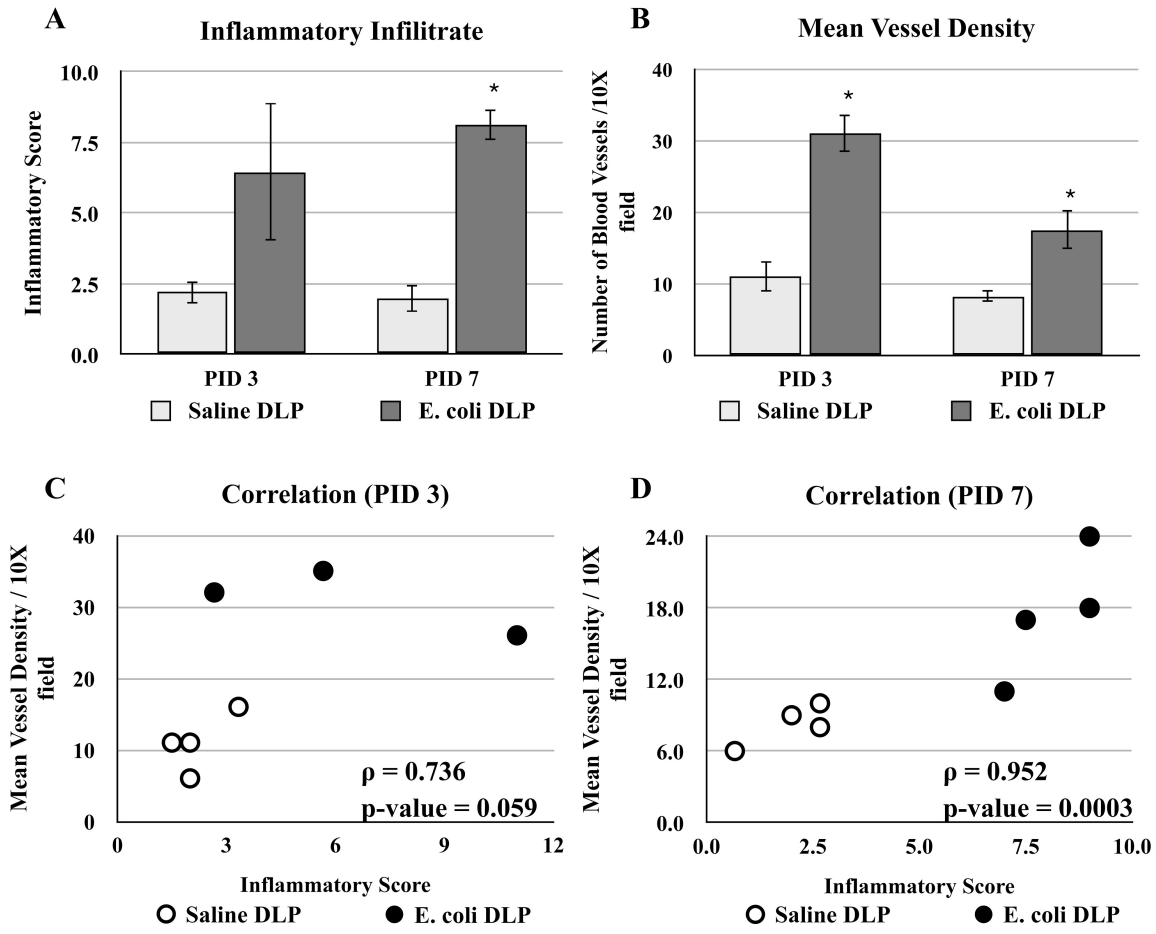

Fig. 4. Vascular response to bacterial-induced acute inflammation. **A.** Comparisons of the inflammatory infiltrate in the DLP of the saline and *E. coli* infected adult male mice at Day 3 and 7 post-instillation (n = 4 each time point). **B.** Comparisons of the mean blood vessel density in the DLP of the saline and *E. coli* infected adult male mice at Day 3 and 7 post-instillation (n = 4 each time point). The data are presented as the mean ± SEM. * Indicates P-value < 0.05 compared to saline by two-sample t-test. **C** and **D.** Spearman correlation analysis of the relationship between inflammation and mean blood vessel density in the DLP of the saline and *E.coli* infected adult male mice at Day 3 (C) and 7 (D) post-instillation. PID, post instillation day.

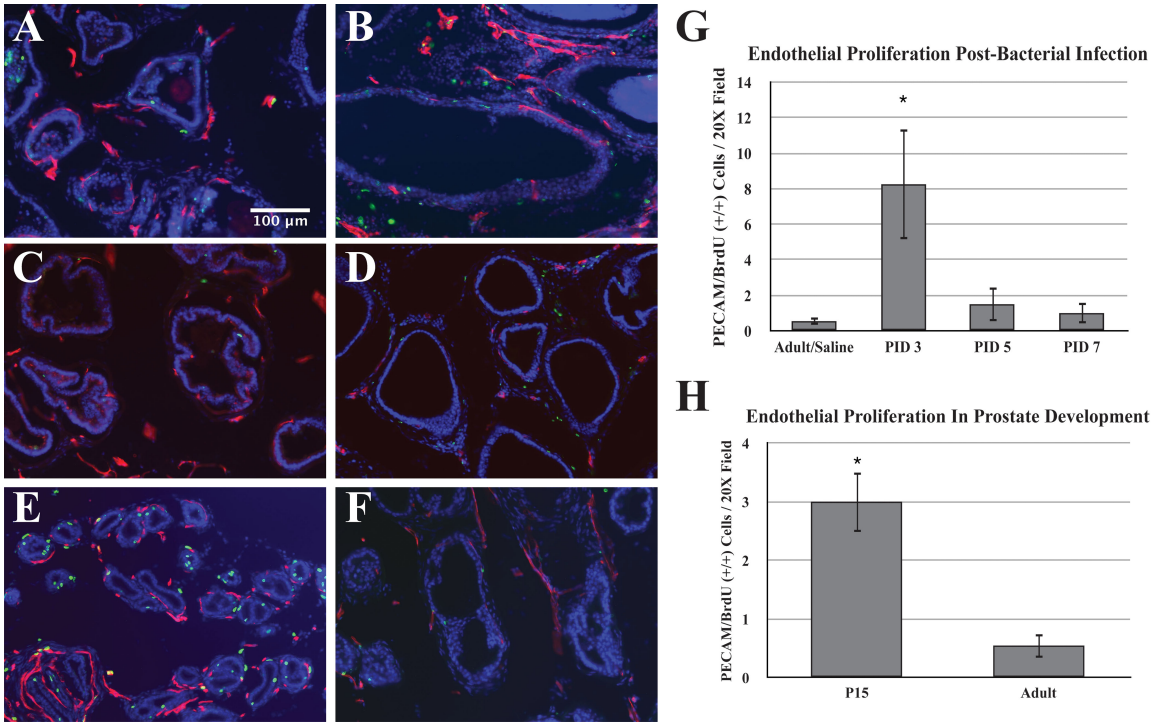

Fig. 5. A-F. Immunostaining for BrdU (Green), PECAM (Red) and DAPI (Blue) in the adult prostate of saline-instilled control **(**A**)**, 3 days post-bacterial inoculation **(**B**)**, 5 days post-bacterial inoculation **(**C**)**, 7 days post-bacterial inoculation (D), postnatal day 15 (E) and adult (F) prostate. Scale bar 100 μm**. G.** Comparisons of the endothelial proliferation determined by double positive PECAM/BrdU (+/+) cells per 20X field in the prostate after saline instillation (n = 5) and Day 3, 5, 7 post-bacterial inoculation (n = 4 each time point). The data are presented as the mean ± SEM. * Indicates P-value < 0.05 compared to saline by two-sample t-test. **H.** Comparison of endothelial proliferation determined by double positive PECAM/BrdU cells per 20X field in the prostate of postnatal Day 15 (n = 6) and adult (n = 6) male mice. The data are presented as the mean ± SEM. * Indicates a P-value < 0.05 compared to adult by two-sample t-test. PID, post instillation day.

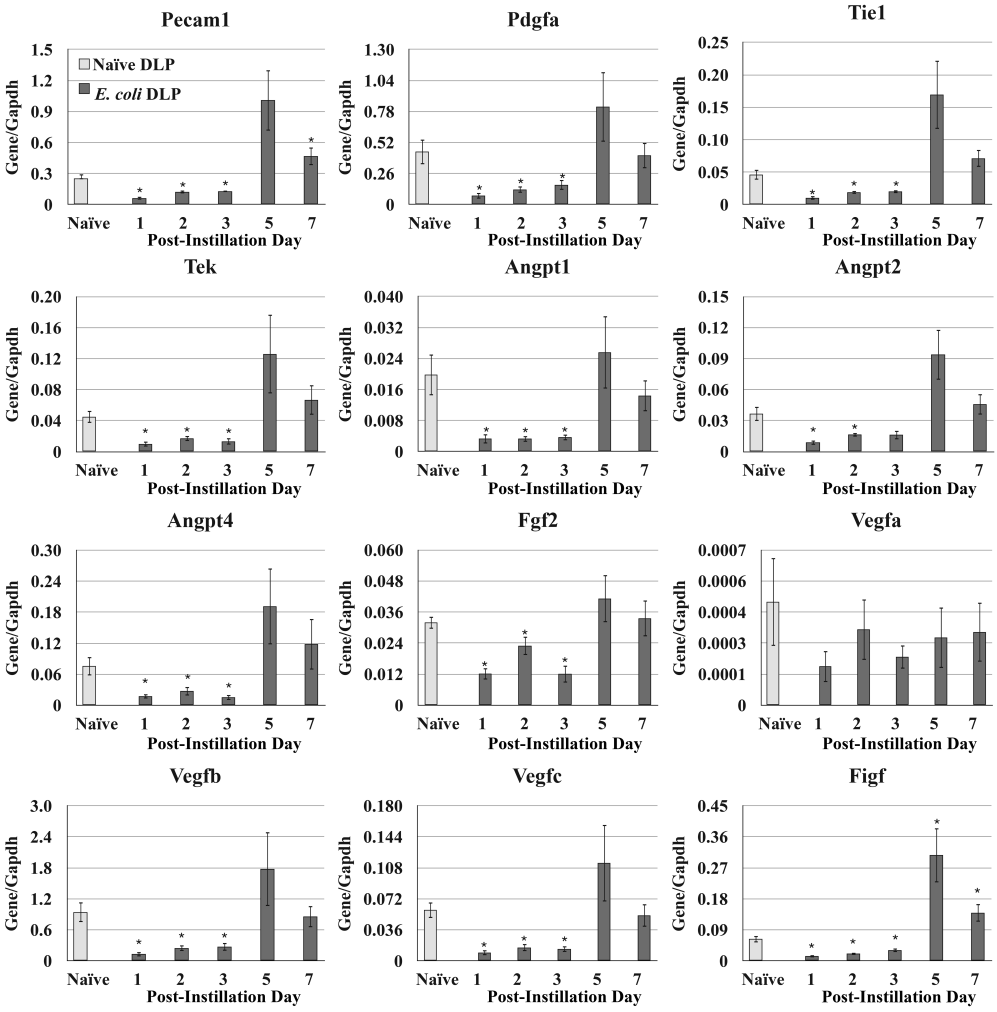

Fig. 6. qRT-PCR for the angiogenic factors in the DLP of the naïve and *E. coli* infected adult male mice at Day 1, 2, 3, 5, and 7 after instillation. The data are presented as the mean ± SEM. * Indicates P-value < 0.05 compared to naïve by two-sample t-test. PID, post instillation day.

REFERENCES

1. Lekas E, Johansoon M, Widmark A, Bergh A, Damber JE. Decrement of blood flow precedes the involution of the ventral prostate in the rat after castration. Urol Res, 1997. 25(5): p. 309-14.

2. Shabisgh A, Tanji N, D'Agati V, Burchardt M, Rubin M, Goluboff ET, Heitjan D, Kiss A, Buttyan R. Early effects of castration on the vascular system of the rat ventral prostate gland. Endocrinology, 1999. 140(4): p. 1920-6.

3. Shabsigh A, Chang DT, Heitjan DF, Kiss A, Olsson CA, Puchner PJ, Buttyan R. Rapid reduction in blood flow to the rat ventral prostate gland after castration: preliminary evidence that androgens influence prostate size by regulating blood flow to the prostate gland and prostatic endothelial cell survival. Prostate, 1998. 36(3): p. 201-6.

4. Franck-Lissbrant I, Häggström S, Damber JE, Bergh A. Testosterone stimulates angiogenesis and vascular regrowth in the ventral prostate in castrated adult rats. Endocrinology, 1998. 139(2): p. 451-6.

5. Lekas E, Engstrand C, Bergh A, Damber JE. Transient ischemia induces apoptosis in the ventral prostate of the rat. Urol Res, 1999. 27(3): p. 174-9.

6. Kozlowski R, Kershen RT, Siroky MB, Krane RJ, Azadzoi KM. Chronic ischemia alters prostate structure and reactivity in rabbits. J Urol, 2001. 165(3): p. 1019-26.

7. Shibata Y, Kashiwagi B, Arai S, Fukabori Y, Suzuki K, Honma S, Yamanaka H. Direct regulation of prostate blood flow by vascular endothelial growth factor and its participation in the androgenic regulation of prostate blood flow in vivo. Endocrinology, 2004. 145(10): p. 4507-12.

8. Bigler SA, Deering RE, Brawer MK. Comparison of microscopic vascularity in benign and malignant prostate tissue. Hum Pathol, 1993. 24(2): p. 220-6.

9. Deering RE, Bigler SA, Brown M, Brawer MK. Microvascularity in benign prostatic hyperplasia. Prostate, 1995. 26(3): p. 111-5.

10. Berger AP, Deibl M, Leonhartsberger N, Bektic J, Horninger W, Fritsche G, Steiner H, Pelzer AE, Bartsch G, Frauscher F. Vascular damage as a risk factor for benign prostatic hyperplasia and erectile dysfunction. BJU Int, 2005. 96(7): p. 1073-8.

11. Berger AP, Horninger W, Bektic J, Pelzer A, Spranger R, Bartsch G, Frauscher F. *V*ascular resistance in the prostate evaluated by colour Doppler ultrasonography: is benign prostatic hyperplasia a vascular disease? BJU Int, 2006. 98(3): p. 587-90.

12. Shabsigh A, Tanji N, D'Agati V, Burchardt T. Burchardt M, Hayek O, Shabisgh R, Buttyan R. Vascular anatomy of the rat ventral prostate. Anat Rec, 1999. 256(4) p . 403-11.

13. Li J, Chen J, Kirsner R. Pathophysiology of acute wound healing. Clin Dermatol, 2007. 25(1): p. 9-18.

14. Li J, Zhang YP, Kirsner RS. Angiogenesis in wound repair: angiogenic growth factors and the extracellular matrix. Microsc Res Tech, 2003. 60(1): p. 107-14.

15. Diegelmann RF, Evans MC. Wound healing: an overview of acute, fibrotic and delayed healing. Front Biosci, 2004. 9: p. 283-9.

16. Ezaki T, Baluk P, Thurston G. La Barbara A, Woo C, McDonald DM. Time course of endothelial cell proliferation and microvascular remodeling in chronic inflammation. Am J Pathol, 2001. 158(6): p. 2043-55.

17. Dahlqvist K, Umemoto EY, Brokaw JJ, Dupuis M, McDonald DM. Tissue macrophages associated with angiogenesis in chronic airway inflammation in rats. Am J Respir Cell Mol Biol, 1999. 20(2): p. 237-47.

18. Aurora AB, Baluk P, Zhang D, Sidhu SS, Dolganov GM, Basbaum C, McDonald DM, Killeen N. Immune complex-dependent remodeling of the airway vasculature in response to a chronic bacterial infection. J Immunol, 2005. 175(10): p. 6319-26.

19. Baluk P, Yao LC, Feng J, Romano T, Jung SS, Schreiter JL, Yan L, Shealy DJ, McDonald DM. TNF-alpha drives remodeling of blood vessels and lymphatics in sustained airway inflammation in mice. J Clin Invest, 2009. 119(10): p. 2954-64.

20. Kwan ML, Gómez AD, Baluk P, Hashizume H, McDonald DM. Airway vasculature after mycoplasma infection: chronic leakiness and selective

hypersensitivity to substance P. Am J Physiol Lung Cell Mol Physiol, 2001. 280(2): p. L286-97.

21. Calabrese F, Kipar A, Lunardi F, Balestro E, Perissinotto E, Rossi E, Nannini N, Marulli G, Stewart JP, Rea F. Herpes virus infection is associated with vascular remodeling and pulmonary hypertension in idiopathic pulmonary fibrosis. PLoS One, 2013. 8(2): p. e55715.
22. Fuxe J, Lashnits E, O'Brien S, Baluk P, Tabruyn SP, Kuhnert F, Kuo C, Thurston G, McDonald DM. Angiopoietin/Tie2 signaling transforms capillaries into venules primed for leukocyte trafficking in airway inflammation. Am J Pathol, 2010. 176(4): p. 2009-18.
23. Robert G, Descazeaud A, Nicolaïew N, Terry S, Sirab N, Vacherot F, Maillé P, Allory Y, de la Taille A. Inflammation in benign prostatic hyperplasia: a 282 patients' immunohistochemical analysis. Prostate, 2009. 69(16): p. 1774-80.
24. Kramer G, Steiner GE, Handisurya A, Stix U, Haitel A, Knerer B, Gessl A, Lee C, Marberger M. Increased expression of lymphocyte-derived cytokines in benign hyperplastic prostate tissue, identification of the producing cell types, and effect of differentially expressed cytokines on stromal cell proliferation. Prostate, 2002. 52(1): p. 43-58.
25. Steiner GE, Stix U, Handisurya A, Willheim M, Haitel A, Reithmayr F, Paikl D, Ecker RC, Hrachowitz K, Kramer G, Lee C, Marberger M. Cytokine expression pattern in benign prostatic hyperplasia infiltrating T cells and

impact of lymphocytic infiltration on cytokine mRNA profile in prostatic tissue. Lab Invest, 2003. 83(8): p. 1131-46.

26. Theyer G, Kramer G, Assmann I, Sherwood E, Preinfalk W, Marberger M, Zechner O, Steiner GE. Phenotypic characterization of infilitrating leukocytes in benign prostatic hyperplasia. Lab Invest, 1992. 66(1): p. 96-107.

27. Berger AP, Deibl M, Halpern EJ, Lechleitner M, Bektic J, Horninger W, Fritsche G, Steiner H, Pelzer A, Bartsch G, Frauscher F. Vascular damage induced by type 2 diabetes mellitus as a risk factor for benign prostatic hyperplasia. Diabetologia, 2005. 48(4): p. 784-9.

28. Berger AP, Bartsch G, Deibl M, Alber H, Pachinger O, Fritsche G, Rantner B, Fraedrich G, Pallwein L, Aigner F, Horninger W, Frauscher F. Atherosclerosis as a risk factor for benign prostatic hyperplasia. BJU Int, 2006. 98(5): p. 1038-42.

29. Michel MC, Mehlburger L, Schumacher H, Bressel HU, Goepel M. Effect of diabetes on lower urinary tract symptoms in patients with benign prostatic hyperplasia. J Urol, 2000. 163(6): p. 1725-9.

30. Bourke JB, Griffin JP. Hypertension, diabetes mellitus, and blood groups in benign prostatic hypertrophy. Br J Urol, 1966. 38(1): p. 18-23.

31. Weisman KM, Larijani GE, Goldstein MR, Goldberg ME. Relationship between benign prostatic hyperplasia and history of coronary artery disease in elderly men. Pharmacotherapy, 2000. 20(4): p. 383-6.

32. Meigs JB, Mohr B, Barry MJ, Collins MM, McKinlay JB. Risk factors for clinical benign prostatic hyperplasia in a community-based population of healthy aging men. J Clin Epidemiol, 2001. 54(9): p. 935-44.

33. Boehm BJ, Colopy SA, Jerde TJ, Loftus CJ, Bushman W. Acute bacterial inflammation of the mouse prostate. Prostate, 2012. 72(3): p. 307-17.

34. Nagy A. Visualizing fetal mouse vasculature by India ink injection. Cold Spring Harb Protoc, 2010. 2010(2): p. pdb prot5371.

35. Hasan MR, Herz J, Hermann DM, Doeppner TR. Intravascular perfusion of carbon black ink allows reliable visualization of cerebral vessels. J Vis Exp 2013; (71): pii: 4374. doi: 10.3791/4374.

36. Abler LL, Keil KP, Mehta V, Joshi PS, Schmit CT, Vezina CM. A high-resolution molecular atlas of the fetal mouse lower urogenital tract. Dev Dyn, 2011. 240(10): p. 2364-77.

37. Ferrara N. Role of vascular endothelial growth factor in regulation of physiological angiogenesis. Am J Physiol Cell Physiol, 2001. 280(6): p. C1358-66.

38. Bouïs D, Kusumanto Y, Meijer C, Mulder NH, Hospers GA. A review on pro- and anti-angiogenic factors as targets of clinical intervention. Pharmacological Research, 2006. 53: p. 89-103.

39. Sugimura Y, Cunha GR, Donjacour AA. Morphogenesis of ductal networks in the mouse prostate. Biol Reprod, 1986. 34(5): p. 961-71

40. Jerde, TJ, Bushman W. IL-1 induces IGF-dependent epithelial proliferation in prostate development and reactive hyperplasia. Sci Signal, 2009. 2(86): ra49.

41. Doll, JA, Reiher FK, Crawford SE, Pins MR, Campbell SC, Bouck NP. Thrombospondin-1, vascular endothelial growth factor and fibroblast growth factor-2 are key functional regulators of angiogenesis in the prostate. Prostate, 2001. 49(4): p. 293-305.

42. Voronov E, Shouval DS, Krelin Y, Cagnano E, Benharroch D, Iwakura Y, Dinare;;o CA, Apte RN. IL-1 is required for tumor invasiveness and angiogenesis. Proc Natl Acad Sci USA, 2003. 100(5): p. 2645-50.

43. Bar D, Apte RN, Voronov E, Dinarello CA, Cohen S. A continuous delivery system of IL-1 receptor antagonist reduces angiogenesis and inhibits tumor development. FASEB J, 2004. 18(1): p. 161-3.

44. Saijo Y, Tanaka M, Miki M, Usui K, Suzuki T, Maemondo M, Hong X, Tazawa R, Kikuchi T, Matsushima K, Nukiwa T. Proinflammatory cytokine IL-1 beta promotes tumor growth of Lewis lung carcinoma by induction of angiogenic factors: in vivo analysis of tumor-stromal interaction. J Immunol, 2002. 169(1): p. 469-75.

45. Carmi Y, Voronov E, Dotan S, Lahat N Rahat MA, Fogel M, Huszar M, White MR, Dinarello CA, Apte RN. The role of macrophage-derived IL-1 in induction and maintenance of angiogenesis. J Immunol, 2009. 183(&): p. 4705-14.

46. Bussolino F, Di Renzo MF, Ziche M, Bocchietto E, Olivero M, Naldini L, Gaudino G, Tamagnone L, Coffer A, Comoglio PM. Hepatocyte growth factor is a potent angiogenic factor which stimulates endothelial cell motility and growth. J Cell Biol, 1992. 119(3): p. 629-41.

47. Kuwano T, Nakao S, Yamamoto H, Tsuneyoshi M, Yamamoto T, Kuwano M, Ono M. Cyclooxygenase 2 is a key enzyme for inflammatory cytokine-induced angiogenesis. FASEB J, 2004. 18(2): p. 300-10.

48. Koch AE, Polverini PJ, Kunkel SL, Harlow LA, DiPietro LA, Elner VM, Elner SG, Strieter RM. Interleukin-8 as a marcophage-derived mediator of angiogenesis. Science, 1992. 258 (5089): p. 1798-1801.

49. Torisu H, Ono M, Kiryu H, Furue M, Ohmoto Y, Nakayama J, Nishioka Y, Sone S, Kuwano M. Macrophage infiltration correlates with tumor stage and angiogenesis in human malignant melanoma- possible involvement of TNFalpha and IL-1alpha. Int J Cancer, 2000. 85(2): p. 182-8.

50. Jackson MW, Bentel JM, Tilley WD. Vascular endothelial growth factor (VEGF) expression in prostate cancer and benign prostatic hyperplasia. J Urol, 1997. 157(6): p. 2323-8.

51. Stefanou D, Batistatou A, Kamina S, Arkoumani E, Papachristou J, Agnantis NJ. Expression of vascular endothelial growth factor (VEGF) and association with microvessel density in benign prostatic hyperplasia and prostate cancer. In Vivo, 2004. 18(2): p. 155-60.

52. Gyftopoulos K, Vourda K, Sakellaropoulos G, Perimenis P, Athanasopoulos A, Papadaki E. The angiogenic switch for vascular endothelial growth factor-A and cyclooxygenase-2 in prostate carcinoma: correlation with microvessel density, androgen receptor content and Gleason grade. Urol Int, 2011. 87(4): p. 464-9.

53. Mori H, Maki M, Oishi K, Jaye M, Igarashi K, Yoshida O, Hatanaka M. Increased expression of genes for basic fibroblast growth factor and transforming growth factor type beta 2 in human benign prostatic hyperplasia. Prostate, 1990. 16(1): p. 71-80.

54. Schauer IG, Ressier SJ, Tuxhorn JA, Dang TD, Rowley DR. Elevated epithelial expression of interleukin-8 correlates with myofibroblast reactive stroma in benign prostatic hyperplasia. Urology, 2008. 72(1): p. 205-13.

55. König JE, Senge T, Allhoff EP, König W. Analysis of the inflammatory network in benign prostatic hyperplasia. Prostate, 2004. 58(2): p. 121-9.

56. Djonov V, Ball RK, Graf S, Mottaz AE, Arnold AM, Flanders K, Studer UE, Merz VW. Transforming growth factor-beta 3 is expressed in nondividing basal epithelial cells in normal human prostate and benign prostatic hyperplasia, and is no longer detectable in prostate carcinoma. Prostate, 1997. 31(2): p. 103-9.

57. Timme TL, Yang G, Truong LD, Kadmon D, Park SH, Thompson TC. Transforming growth factor-beta localization during mouse prostate

morphogenesis and in prostatic growth abnormalities. World J Urol, 1995. 13(6): p. 324-8.

CHAPTER THREE

This manuscript was published in *PLoS One* 2014;9(6):e100770.

Contributions of authors: L.W. designed and performed research experiments and prepared the manuscript. P.R.H. assisted in hydroxyproline assay by HPLC, data analysis and manuscript preparation. W.B. supervised studies and assisted in manuscript preparation.

Prostatic inflammation induces fibrosis in a mouse model of chronic bacterial infection

Letitia Wong, Paul R. Hutson, Wade Bushman

ABSTRACT

Inflammation of the prostate is strongly correlated with development of lower urinary tract symptoms and several studies have implicated prostatic fibrosis in the pathogenesis of bladder outlet obstruction. It has been postulated that inflammation induces prostatic fibrosis but this relationship has never been tested. Here, we characterized the fibrotic response to inflammation in a mouse model of chronic bacterial-induced prostatic inflammation. Transurethral instillation of the uropathogenic *E. coli* into C3H/HeOuJ male mice induced persistent prostatic inflammation followed by a significant increase in collagen deposition and hydroxyproline content. This fibrotic response to inflammation was accompanied with an increase in collagen synthesis determined by the incorporation of ^{3}H-hydroxyproline and mRNA expression of several collagen remodeling-associated genes, including *Col1a1, Col1a2, Col3a1, Mmp2, Mmp9*, and *Lox*. Correlation analysis revealed a positive correlation of inflammation severity with collagen deposition and immunohistochemical staining revealed that CD45+VIM+ fibrocytes were abundant in inflamed prostates at the time point coinciding with increased collagen synthesis. Furthermore, flow cytometric analysis demonstrated an increased percentage of these CD45+VIM+ fibrocytes

among collagen type I expressing cells. These data show – for the first time – that chronic prostatic inflammation induces collagen deposition and implicates fibrocytes in the fibrotic process.

INTRODUCTION

Prostatic inflammation is a common finding in the adult prostate. It is more prevalent in men with benign prostatic hyperplasia (BPH) and lower urinary tract symptoms (LUTS) and the degree of prostatic inflammation correlates with severity and progression of symptoms [1,2]. The mechanisms by which prostatic inflammation contributes to LUTS are a current focus of investigation. Several studies have suggested a correlation of prostatic fibrosis with increased urethral resistance and LUTS [3,4]. Considering that prostatic inflammation and fibrosis are both associated with LUTS in men, it is postulated that prostatic inflammation contributes to the development and progression of BPH/LUTS by inducing prostatic fibrosis.

Inflammation has long been associated with fibrosis in other tissues but evidence for this in the prostate is only inferential. A recent study by Cantiello and colleagues, for example, showed that human prostate samples with evidence of inflammation had a significantly greater collagen content than those without inflammation [5]. However, a causal relationship between inflammation and fibrosis of the prostate has never been established. The purpose of this study

was to examine directly whether inflammation causes fibrosis in a previously described mouse model of bacterial-induced prostatic inflammation [6,7]. While there are significant species-specific differences in the anatomy, cellular and extracellular matrix compositions in the stroma of the mouse and human prostate [8,9], the stromal-epithelial interactions are highly conserved between them [10] and the inflammatory responses to bacterial infection in the mouse prostate, in particular, appears to recapitulate the immunologic features of inflammation in the human prostate [7,11-15]. We therefore expect our studies to provide insight into the causal relationship of inflammation and prostate fibrosis that are relevant to fibrosis of the human prostate.

Using a previously described model of bacterial-induced prostatic inflammation (6) we correlated prostatic inflammation with changes in collagen content using histological and biochemical quantitative methods at different time points after bacterial infection. We analyzed parameters related to inflammation and fibrosis including rates of collagen synthesis, the identity of collagen-producing cells, inflammatory infiltrate subtypes, and the changes in the mRNA expression of collagen remodeling-associated genes. Our observations validate the hypothesis that chronic inflammation induces prostatic fibrosis and describes, for the first time, the role of fibrocytes in the generation of prostatic fibrosis.

RESULTS

Chronic Prostatic Inflammation Induced by Bacterial Infection

Inbred C3H/HeOuJ male mice were instilled transurethrally with either sterile PBS or uropathogenic *E. coli 1677* as described previously [7]. This strain of mouse has previously been shown to remain infected and inflamed for at least 3 months post-inoculation [6]. Histopathological analysis was performed on the ventral prostate (VP), dorsolateral prostate (DLP), and anterior prostate (AP) of saline instilled and *E. coli* infected animals 2, 7, and 28 days post-inoculation. Saline instilled controls showed little or no inflammation whereas all lobes of the *E. coli* infected prostates displayed widespread mild-to-severe inflammation (Figure 1A-R). Significant inflammation was observed as early as on day 2 post-infection in the DLP and AP but not until day 7 in the VP. At 28 days post-inoculation, there was persistent inflammation in all three lobes (Figure 1S-U).

Collagen Deposition In Response to Chronic Inflammation

Picrosirius red staining for collagen content was performed on adjacent serial tissue sections of the H&E stained slides from saline instilled and *E. coli* infected male mice 2, 7, and 28 days post-instillation (Figure 2A-R). As shown in Figure 2S-U, quantitation of the staining showed no significant difference in collagen content of any lobe between saline instilled and *E. coli* infected animals on day 2 post-instillation. On day 7 post-instillation, a significant increase was observed in the AP of the infected mice. On day 28 post-instillation, all three prostatic lobes

from infected mice showed a significant increase in collagen content. Increased collagen deposition on day 28 post-infection (Figure 2F, L, R) appeared to associate with the sites of inflammation as shown in the H&E images (Figure 1F, L, R). Hydroxyproline is a specific and unique amino acid found in collagen that can be used to measure collagen content. To validate the results obtained with picrosirius red staining, we quantitated hydroxyproline content by HPLC 2, 7, 14, 21, and 28 days post-instillation. Naïve animals and saline instilled animals 28 days post-instillation showed no significant difference in hydroxyproline content (Figure S1), confirming that instillation alone had no impact on collagen deposition. In agreement with the picrosirius red staining, no significant change in hydroxyproline content was observed 2 days post-instillation (Figure 3A). Hydroxyproline content was significantly increased on day 7 post-infection and remained increased until 28 days post-infection. We interpret our data as showing that chronic prostatic inflammation induces a significant and sustained increase in prostatic collagen content.

To determine if the increase in collagen content in chronic bacterial-induced prostatic inflammation is due to increased collagen synthesis, we measured the incorporation of ^{3}H-hydroxyproline. Animals transurethrally either instilled with saline or infected with *E. coli* were i.p. injected with ^{3}H-proline 0, 5, 12, 19, 26 days post-instillation and were sacrificed 48 hours later. ^{3}H-hydroxyproline content was significantly increased in the infected prostates when assayed at 7

and 14 days post-infection as compared to saline controls. There was no significant difference when assayed at 21 and 28 days post-infection (Figure 3B). These findings reveal increased collagen synthesis during early phase of inflammation is responsible for the measured increase in collagen content associated with chronic inflammation.

Correlation Between Inflammation And Collagen Deposition

To evaluate the relationship between prostatic inflammation and collagen deposition, we correlated inflammation score determined from H&E images with collagen content determined from adjacent sections stained with picrosirius red for the VP, DLP, AP of saline instilled and *E. coli* infected animals 2, 7, and 28 days post-instillation (Table 1). On day 2 post-instillation, there was no correlation between the degree of inflammation and collagen content. At 7 days post-instillation the inflammation score was significantly and directly correlated with collagen content only in the AP. At 28 days post-instillation all three prostatic lobes showed a significant positive correlation between inflammation and collagen content.

Collagen Remodeling-Associated Gene Expression in the Inflamed Prostate

We analyzed mRNA expression pattern of collagen remodeling-associated genes in the DLP (Figure 4) of saline instilled and *E. coli* infected mice 7 and 28 days post-instillation. Robust changes in expression of several genes was evident 7

days post-infection; expression of *Col1a1, Col1a2, Col3a1, Mmp2, Mmp9* and *Lox* was significantly increased while expression of *Timp3* was significantly decreased. No significant changes were observed in the expression of *Col4a1, Col6a1, Col6a2, Mmp7 and Mmp13* (Figure 4, Figure S2). In striking contrast, we observed no differences in expression of any collagen remodeling-associated genes except *Timp3* 28 days post-instillation. Thus, the time course of increased expression of collagen remodeling-associated genes seems to parallel active collagen synthesis as determined by measurement of ^{3}H-hydroxyproline incorporation.

Characterization of Inflammatory Infiltrates

The inflammatory infiltrates present in the VP, DLP, and AP were characterized 28 days after bacterial inoculation. CD3+ T cells (Figure 5A), CD20+ B cells (Figure 5B) and F4/80+ macrophages (Figure 5C) were the predominant inflammatory cells found in all three *E. coli* infected prostatic lobes. A relatively small but significant number of neutrophils were also present (Figure 5D). To determine the cell type responsible for collagen synthesis associated with inflammation we performed immunohistochemical costaining 7 days post-instillation, a time point that corresponds to the peak of ^{3}H-hydroxyproline incorporation in the inflamed prostate. Staining for vimentin and α-smooth muscle actin surprisingly showed no evidence of VIM+αSMA+ myofibroblasts in either the saline instilled or *E. coli* infected prostates (Figure S3). In contrast,

staining for vimentin and CD45 showed abundant number of CD45+VIM+ fibrocytes in the *E. coli* infected prostates while only minimal number of fibrocytes was detected in the saline instilled prostates (Figure 6A-B). To determine if these fibrocytes are involved in collagen synthesis we performed staining for prolyl 4-hydroxylase (P4H), a key enzyme involved in collagen synthesis that catalyzes the conversion of proline to hydroxyproline before collagen secretion. Triple immunohistochemical staining for vimentin, CD45 and P4H in the *E. coli* infected prostates demonstrated P4H expression in a subpopulation of CD45+VIM+ fibrocytes (Figure 6C-D). Further assessment of prostatic cells isolated from saline instilled and *E. coli* infected mice using flow cytometry demonstrated that CD45+VIM+ fibrocytes are present within collagen type I (COL1) positive cells. Consistent with our immunohistochemical finding, there was a 6-fold increase in the percentage of CD45+VIM+ fibrocytes enriched in COL1 expressing cell population from the *E. coli* infected prostates (Figure 7). This observation strongly suggests fibrocytes as collagen-producing cells in chronic bacterial-induced prostatic inflammation.

DISCUSSION

The collagens are a major group of extracellular matrix proteins. To date, 28 types of collagen have been identified in vertebrates and are grouped into subclasses based on their structural characteristics. The majority of collagen subtypes form fibrils. Others are network-forming collagens, transmembrane

collagens or collagens associated with fibrils [16]. As a group, they play an important role in maintaining structural integrity of various tissues and organs. They are best known to provide tensile strength to the tissues but also have significant roles in tissue scaffolding, cell migration, cell adhesion, morphogenesis and tissue repair [17-19]. The collagen content of the extracellular matrix of the tissues is a function of collagen synthesis and degradation. Dysregulation of collagen turnover resulting in excess collagen accumulation (fibrosis) can disrupt organ structure and function [20-23] and fibrosis is associated with the development and progression of disease in many different organs, including the lung, liver, intestine and heart [24-31].

Collagen remodeling and deposition is cardinal feature of the response to injury and is necessary to restore mechanical strength and function of the injured tissue [17,32]. Immune regulation is critical to prevent excess collagen deposition [33-35]. When inflammation fails to resolve – typically because of persistent tissue injury – a pathologic wound healing response occurs that can produce fibrosis. Fibrosis is generally characterized by an accumulation of fibrogenic cells and excessive deposition of extracellular matrix components [36]. A mouse model of bleomycin-induced lung injury and inflammation showed that repeated injury was accompanied by a loss of normal tissue architecture, a persistent increase in collagen deposition, increased collagen synthesis and increased number of myofibroblasts [37]. The fibrotic change in lung inflammation was associated

with reduced total lung capacity, increased dynamic resistance and decreased dynamic compliance [38]. Subsequent studies showed that a variety of inflammatory cytokines and chemokines including TGFβ, CXCL6, IL-1, IL-5, IL-6, IL-17 modulate collagen deposition and the fibrotic effects of lung inflammation [39-44].

We observed significant collagen deposition with chronic inflammation induced by bacterial infection. Inflammation present on day 2 post-inoculation is characterized by an acute inflammatory infiltrate composed of polymorphonuclear cells and macrophages [7]. At later time points, the inflammation is characterized by a chronic inflammatory infiltrate composed predominantly of T cells, B cells and macrophages. Our quantitative studies revealed that collagen deposition occurs primarily in the early stage of chronic inflammation. Collagen accumulation was associated with the sites of inflammation and we observed a significant positive correlation between collagen content and the severity of inflammation. The observed spatial and temporal association between inflammation and collagen accumulation supports the concept that excessive collagen deposition is a response to chronic inflammation.

We found that collagen deposition in chronic bacterial prostatic inflammation was associated with an increase in *de novo* collagen synthesis and collagen

remodeling-associated gene expression early in the chronic inflammatory phase. Incorporation of ^{3}H-hydroxyproline was significantly increased at 7 and 14 days post-inoculation and then decreased to baseline. Elevated collagen synthesis was accompanied by increased expression of collagens (*Col1a1, Col1a2, Col3a1),* crosslinking enzyme lysyl oxidase (*Lox),* and matrix metalloproteinases (*Mmp2, Mmp9)* and decreased expression of the tissue inhibitor of metalloproteinases (*Timp3)*. These factors coordinately regulate the processes of collagen synthesis, degradation and stabilization. Collagen I and III are the predominant fibrillar types of collagens upregulated in fibrotic conditions associated with inflammation. The increase in expression of these collagen subtypes in our study occurred in parallel with increased collagen deposition, suggesting that collagen synthesis, partly due to enhanced transcriptional level, contributes to collagen accumulation in persistent prostatic inflammation. In addition to increased collagen synthesis, stabilization of collagen fibrillar structures through formation of collagen cross-links by LOXs renders collagen to be less susceptible to degradation mediated by collagenases and therefore could further contribute to its accumulation [45]. Conversely, MMPs, whose proteolytic activity is inhibited by TIMPs, cleave and remodel extracellular matrix components as well as release and activate proinflammatory and profibrotic cytokines, constituting a microenvironment favoring fibrogenic process [46].

Fibroblasts/myofibroblasts are traditionally considered as the main sources of extracellular matrix components in tissue repair and inflammation [47]. However, there is a growing body of research supporting the involvement of a unique population of bone marrow derived inflammatory fibroblast-like cells called fibrocytes in the development of fibrosis in chronic inflammatory diseases, including pulmonary fibrosis [48-52], autoimmune disorders [53,54], asthma [55,56], and chronic kidney disease [57,58]. Fibrocytes are collagen-producing cells that have been classically identified based on their distinctive expression of the common leukocytic surface marker CD45, the hematopoietic stem cell marker CD34 and the fibroblastic markers collagen I, vimentin, and/or prolyl 4-hydroxylase [59,60]. An increased number of fibrocytes has been reported in the circulation and the lungs of patients with fibrotic interstitial lung disease as compared to that in healthy subjects [50-52]. In the mouse model of bleomycin-induced pulmonary fibrosis, the intrapulmonary recruitment of fibrocytes was dramatically increased and correlated with increased collagen deposition in the lungs [49]. Inhibition of fibrocyte infiltration to the lungs of bleomycin-treated mice significantly reduced lung fibrosis, suggesting that fibrocytes could directly contribute to the pathogenesis of fibrosis.

Our data suggests that fibrocytes but not myofibroblasts are a key feature of the fibrotic response to bacterial-induced prostatic inflammation. Whereas immunostaining for vimentin and αSMA showed no evidence of VIM+αSMA+

myofibroblasts in the infected prostates, immunostaining for CD45, vimentin, and prolyl 4-hydroxylase revealed that the *E. coli* infected prostates had abundant CD45+VIM+ fibrocytes of which a subpopulation also expressed prolyl 4-hydroxylase, a key enzyme essential for collagen synthesis. Flow cytometric analysis further demonstrated that CD45+VIM+ fibrocytes are a subpopulation of collagen type I expressing cells in the prostates and there was a significant increase in the percentage of CD45+VIM+ fibrocytes in COL1+ cells post-infection. The appearance of these CD45+VIM+ fibrocytes in the prostates following 7 days of bacterial infection was temporally associated with enhanced collagen synthesis and increased collagen deposition and suggests, therefore, that CD45+VIM+ fibrocytes have a significant if not primary role in prostatic fibrosis. It is noteworthy that a recent study documented the presence of a cell population phenotypically consistent with fibrocytes in the prostate of human patients with LUTS [61]. However, these authors did not characterize the role of this specific cell population in BPH/LUTS. Therefore, to our knowledge, the present study is the first report in the literature to describe fibrocytes in prostatic inflammation and fibrosis.

There is accumulating evidence for the contribution of increased collagen deposition and fibrosis to the pathogenesis of BPH/LUTS [3-5,62]; however, the underlying cause of increased collagen deposition in this common aging-related disease has not been elucidated. Experimental studies have observed a

potential link between inflammation and extracellular matrix alterations in the prostate in both *in vitro* and *in vivo* studies. Barron and colleagues have shown that a transgenic mouse model constructed with constitutively active *Tgfb1* in prostate epithelium exhibited an age-dependent inflammation concomitant with the increase in collagen deposition in the prostates [63]. Another study by Gharaee-Kermani, et al. has demonstrated that treatment of primary human prostate stromal fibroblasts isolated from BPH patients with inflammatory factors such as TGFβ1, CXCL5, CXCL8, CXCL12 induced their collagen expression [61]. Recently, there are several retrospective studies of BPH/LUTS specimens reporting a positive relationship between the degree of chronic inflammation and prostatic fibrosis [4,5]. Although these studies suggested that prostatic inflammation might play a role in promoting the fibrotic changes in BPH/LUTS, this has never been directly verified. Our results support this hypothesis that prostatic chronic inflammation induces collagen deposition and, for the first time, suggest a key role for fibrocytes in inflammation-associated prostatic fibrosis.

MATERIALS AND METHODS

Study Approval

This study was carried out in strict accordance with the recommendations in the Guide for the Care and Use of Laboratory Animals of the National Institutes of Health. All animal studies were approved by the Institutional Animal Care and Use Committee at the University of Wisconsin-Madison (M02448). All surgery

was performed under isoflurane anesthesia and all sacrifice was performed under isoflurane anesthesia immediately followed by cervical dislocation. All efforts were made to minimize animal suffering.

Transurethral Instillation

Transurethral instillation was performed as previously described [7]. 8 week old C3H/HeOuJ male mice (Jackson Laboratories) were anesthetized with isoflurane and catheterized with a lubricated sterile polyethylene catheter per urethra. Inoculation was performed by a single transurethral instillation of uropathogenic *E. coli* 1677 (2 x10^6 CFU/ml) or sterile PBS in a volume of 200 µl.

Animals were sacrificed 2, 7, 14, 21, and 28 days post-instillation. The paired prostatic lobes (VP, DLP, AP) were bisected separately and were used for RNA isolation, hydroxyproline assay, and/or histology. The whole mouse prostates were collected and used for measuring incorporation of ^{3}H-hydroxyproline to determine collagen synthesis. Four to thirteen mice per time point and per treatment were analyzed for histology. Four to seven mice per time point and per treatment were used for gene expression analysis. Four to eight mice per time point and per treatment were used for hydroxyproline assay. Four to seven mice per time point and per treatment were used for determination of collagen synthesis. Four to six mice per treatment were used for FACS analysis.

Quantitation of Inflammatory Degree

Inflammatory Grading

Tissues were fixed in 10% formalin, imbedded in paraffin and serially sectioned at 6μm. Standard H&E staining was performed for histology. Using our previously established scoring system [7], the severity of inflammation was graded in at least 3 random 10X fields of H&E sections from each prostatic lobe. Data are presented as the mean inflammation score ± standard error of the mean (SEM).

Characterization of Inflammatory Infiltrates

Neutrophils were identified as polymorphonuclear leukocytes and counted on 20X fields of H&E stained slides. T-lymphocytes, B-lymphocytes, and macrophages were counted by using immunohistochemistry for specific cell surface markers as previously described [7]. 6μm formalin-fixed paraffin-embedded sections were used. Antigen retrieval was performed by boiling in citrate buffer solution (pH 6.0) for 10 minutes and blocking for nonspecific background was achieved by using 10% donkey serum and 1% BSA in PBS for 1 hour at room temperature. Slides were incubated with primary antibodies in blocking buffer at 4°C overnight and secondary antibodies for one hour at room temperature in dark. Sections were counterstained with Hoechst 33258 at 4μg/ml in PBS, coverslipped with anti-fade media and imaged. Primary antibodies included rabbit polyclonal anti-CD3 (1:100, DAKO A0452), goat

polyclonal anti-CD20 (1:50, Santa cruz sc-7735), and rat monoclonal anti-F4/80 (1:50, eBioscience 14-4801-85). Secondary antibodies included donkey anti-rabbit IgG-Alexa 594 conjugated antibody (1:200, Invitrogen), donkey anti-goat IgG-Alexa 488 conjugated antibody (1:100, Invitrogen), and donkey anti-rat IgG-Alexa 594 conjugated antibody (1:50, Invitrogen), respectively. Data are presented as the mean number of cells ± SEM.

Quantitation of Collagen Content

Picrosirius Red Staining

Adjacent serial tissues sections of H&E stained slides were used for picrosirius red staining. The staining was performed by incubating slides in 0.1% sirius red in saturated aqueous solution of picric acid for one hour at room temperature. Images were taken by digital camera using NIS Element software under a Nikon Eclipse 80i polarized light microscope. The settings of the software and microscope remained unchanged throughout the observation for the purpose of quantitation and comparisons. The color staining that shows up under polarizing microscope corresponds to the birefringence of collagen fibers [64]. Quantitation of the staining for collagen content was then determined by using NIH Image J. Briefly, the images were converted from RBG to 8-bit gray scale and the intensity of the three color channels was summed into one image. The images were manually thresholded to define the collagen staining and a constant value of the threshold was set for all the images analyzed. The region of interest (prostatic

tissues) was manually outlined to analyze the area that was stained for collagen. Large blood vessels and nerve fiber bundles in the prostate were eliminated in the quantitation. Data are presented as the mean percentage of collagen area ± SEM.

Hydroxyproline Assay for Collagen Content by HPLC

Mouse prostate tissues were harvested, snap frozen in liquid nitrogen, and stored at -80°C until further analysis. The procedure was performed as previously described with some modifications [65]. The tissues were thawed on ice and weighed. Each tissue sample was homogenized in 2ml of 12N HCl with a motorized homogenizer in a clean glass tube. 75µl of 20mM sacrosine (reagent grade) as internal standard was mixed in the homogenate. Then, the glass tubes containing the tissue homogenate were tightly capped to prevent evaporation and were incubated in a 110°C heating block for 18 hours. The hydrolysates were allowed to cool to room temperature, neutralized with 2ml of 12N NaOH and 1ml of borate buffer (0.7M boric acid in water, pH 9.5 with NaOH), and were adjusted to a pH 9.5 with NaOH and HCl. Aliquots of 500µl of the sample solution were used for subsequent derivatization process. Some samples were run in duplicate or triplicate for intra-day reaction consistency and these same samples were run on the next day for inter-day reaction consistency. Hydroxyproline (reagent grade) standards of 0.3125, 0.625, 1.25, 2.5, 5, 10, 20mM with 7.5mM L-proline (reagent grade) in water were prepared. 200µl of

each hydroxyproline standard was mixed with 75µl of 20mM sacrosine, 1.8ml of 12N HCl, 2ml of 12N NaOH and 1ml of borate buffer. The solutions were then adjusted to pH 9.5. Aliquots of 500µl of the hydroxyproline standard solution were used for subsequent derivatization process.

Aliquots (500µl) of tissue homogenate or hydroxyproline standard were added with 700µl of borate buffer. The following procedures were performed in dark. The solutions were mixed with 100µl of OPA solution (50mg *o*-phthalaldehyde dissolved in 1ml acetonitrile and 26µl of reagent grade β-mercaptoethanol) by vortexing and allowed to react at room temperature for 1 minute. The solution was then mixed with 100µl of iodoacetamide solution (140mg/ml of iodoacetamide in acetonitrile) by vortexing and reacted at room temperature for 1 minute. 600µl of 5mM FMOC-Cl in acetone was subsequently added, mixed by vortexing and reacted at room temperature for 1 minute. The solutions were then washed three times with 3ml of ethyl ether by vortexing for 30 seconds. The organic layer was discarded each time. 50µl of the aqueous phase was injected into the HPLC. A total of 3 injections were run for each reacted sample or standard. Sample injections were made every 25 minutes without an intervening wash. The isocratic mobile phase was prepared by combining 650ml of 3% glacial acetic acid that was adjusted to pH 4.3 with sodium acetate (reagent grade) with 350ml of acetonitrile, followed by vacuum filtration for degassing. All reagents used were ACS or HPLC grade unless stated otherwise.

The HPLC instrumentation and spectrofluorometer was set up as previously described [65]. The HPLC instrumentation included a Shimadzu LC-10AD HPLC pump, SIL-10A auto injector and system controller. A McPherson Model FL-750 spectrofluorometer was used with the high-sensitivity module, an excitation wavelength of 265nm and without an emission cut-off filter. Separation was achieved by using a Lichrosphere 5 RP18e 250 mm x 4.60 mm, 5µm column. The mobile phase was pumped at a constant rate of 0.75ml/min.

The coefficients of variation for intra-day reaction consistency were less than 4.5% and for inter-day reaction consistency were less than 10.2%. The height ratio of the internal standard (sarcosine) and hydroxyproline peak was calculated for each sample and standard. The exact amount of hydroxyproline standards in µg injected into the HPLC was determined by calculating the total dilution made from the original concentration prepared. The standard curve of hydroxproline standards showed linear regression with R^2=0.998. The amount of hydroxyproline in µg presented in the prostate samples was calculated from the peak height ratio of hydroxyproline and internal standard peak into the linear regression equation obtained from the hydroxyproline standard curve. Data are presented as mean hydroxyproline (µg)/prostate weight (mg) ± SEM.

Collagen Synthesis by Incorporation of ^{3}H-hydroxyproline

The animals instilled transurethrally with either sterile PBS or uropathogenic *E. coli* 1677 were i.p. injected with 15μCi of L-[3,4-^{3}H]-proline (specific activity 50 Ci/mmol, ARC, Inc.) on day 0, 5, 12, 19, 26 post-instillation. For day 0 post-instillation, animals were injected 2-3 hours after bacterial inoculation. Prostates were harvested 48 hours after ^{3}H-proline injection, snap frozen in liquid nitrogen, and stored at -80°C until further analysis. The tissue samples were thawed on ice and weighed. The extraction procedure of hydroxyproline has previously been described in detail [66]. Briefly, each tissue sample was placed in a clean glass tube, homogenized in 2ml 12N HCl with a motorized homogenizer and was heated at 110°C for 18 hours. The hydrolysates were then allowed to cool to room temperature and neutralized with 2ml of 12N KOH and 1ml of 1M boric acid in water. The samples were then adjusted to pH 8.7 with KOH and HCl. Aliquots of 2ml of the sample solution were used for subsequent reaction. First, each sample was reacted with 4ml of 0.2M chloramine T-solution in methoxyethanol at room temperature for 20 minutes. 2.4ml of 3.6M sodium thiosulfate in water was then added followed by saturation with 1.5g KCl. The solutions were then washed 3X with 9ml of toluene by vigorously shaking for 5 minutes each. Organic layer was discarded each time. The samples were heated in boiling water for 30 minutes and then allowed to cool down on ice for 10 minutes. Then, 7ml of toluene was added into each sample and mixed by vigorously shaking for 10 minutes. The organic layer that contained hydroxyproline was then removed and mixed with 7ml of liquid scintillation cocktail (Fisher, SX25-5) in a 20ml liquid

scintillation vial. Counts per minute (cpm) were measured with a Beckman LS 6000TA liquid scintillation counter. Data are presented as mean ^{3}H-hydroxyproline cpm/mg prostate ± SEM.

Immunohistochemical Staining

Immunohistochemical costaining for vimentin, CD45 and P4H was used to assess the presence of fibrocyte in the prostate and the expression of prolyl 4-hydroxylase in fibrocyte. 6μm sections of formalin-fixed paraffin-embedded tissues were dewaxed and rehydrated by passing them through xylene 3X for 5 minutes each, 100% methanol 3X for 5 minutes each, and then running tap water for 10 minutes. The slides were submerged in boiling citrate buffer solution (pH 6.0) for 10 minutes for antigen retrieval, and blocked for nonspecific background by using 10% donkey serum and 1% BSA in PBS for 1 hour at room temperature. Slides were then washed three times with PBS+0.025% Tween 20 (PBST) for 5 minutes. Primary antibodies including rabbit monoclonal anti-vimentin (1:100, Abcam ab92547), rat monoclonal anti-CD45 (1:50, Abcam ab25386), and goat polyclonal anti-P4H (1:50, Abcam ab59497) were added in the blocking solution. The slides were incubated with primary antibodies at 4°C overnight followed by three washes with PBST for 5 minutes each. The slides were then incubated with the secondary antibodies in blocking solution for 1 hour at room temperature in the dark. Secondary antibodies included donkey anti-rabbit IgG-Alexa 594 conjugated antibody (1:100, Invitrogen), donkey anti-rat-

Alexa 488 conjugated antibody (1:100, Invitrogen), and donkey anti-goat-Alexa 647 conjugated antibody (1:200, Invitrogen). Following incubation with secondary antibodies the slides were rinsed three times with PBST for 5 minutes. Nuclei staining was performed by incubating slides with Hoechst 33258 at 4μg/ml in PBST at room temperature for 10 minutes. The slides were then washed 3X with PBST and 2X with distilled water for 5 minutes each. The slides were mounted with anti-fade media, a coverslip and imaged. Images were taken by a digital camera using NIS Element software under Nikon Eclipse Ti-E fluorescent microscope.

Fluorescence Activated Cell Sorting (FACS) Analysis for Collagen Producing Fibrocytes

Prostatic tissues were minced, digested with 1X collagenase/hyaluronidase at 37°C for 3 hours, 0.25% trypsin on ice for 1 hour and 5U/ml dispase at room temperature for 2 minutes. Cells were passed through a 22-gauge needle and then a 100-μm cell strainer to produce a single cell suspension. Cells were resuspended into 100μl 2% FBS/DMEM/F12, incubated with mouse Fc Block (1μg/sample, BD Pharmingen #553142) at 4°C for 15 minutes and washed. Each sample was then divided into 5 aliquots: (a) unstained control, (b) CD45 only control, (c) Vimentin only control, (d) collagen type I only control, and (e) CD45, Vimentin, collagen type I sample. Cells were stained with APC labeled rat anti-mouse CD45 (1:20, BD Pharmingen #559864) at 4°C for 30 minutes in dark,

washed, fixed and permeabilized with BD Cytofix/Cytoperm (BD Pharmingen #554714) at 4°C for 20 minutes. Cells were then stained with PE labeled rabbit anti-mouse Vimentin (1:20, Cell Signaling Technology #12020) and rabbit anti-mouse collagen type I (1:100, Rockland Immunochemical) conjugated with Alexa Fluor 488 using Zenon Rabbit IgG Labeling Kits (Invitrogen #Z-25302) at 4°C for 30 minutes in dark and washed. A three-color analysis of stained cells was performed on a flow cytometer (BD Biosciences FACSCalibur) using Cellquest software and data analysis was subsequently performed using FlowJo software. Unstained and single antibody-stained cells were used as controls. The gate parameters were set based on the findings in controls.

RNA Isolation and Semi-Quantitative Real-Time PCR

RNA from the tissues was extracted using RNeasy Micro Kit (Qiagen, Inc.) and converted to cDNA as previously described [7]. Semi-quantitative RT-PCR was performed with cDNA samples to quantitate gene expression levels. The forward and reverse primers of *Col1a1, Col1a2, Col3a1, Mmp2, Mmp7, Mmp9, Mmp13, Timp3,* and *Lox* were designed using the NCBI mouse nucleotide database, the mouse genomic BLAST database and the Primer-3 program. The sequences of the primers used are shown in Table S1. RT-PCR cycle reactions were detected with SYBR green (Roche) and run on a BioRad Real-Time CFX with run conditions of 95°C for 10 minutes, followed by 50 cycles of 95°C for 15 seconds

and 60°C for 1 minute. Gene expression levels were normalized to the housekeeping gene *Gapdh*.

Statistical Analysis

Each end point of interest (inflammation score, collagen area, hydroxyproline content per prostate weight, collagen synthesis measurement, quantitation of inflammatory cell subtypes and fibrocytes, collagen remodeling-associated gene expressions) was evaluated between saline instilled and *E. coli* infected animals at various time points. We employed a two-sample t-test or Wilcoxon rank-sum test to compare the group difference as appropriate. To explore the relationship between collagen area and inflammation score for each prostatic lobe, Spearman's rank correlation coefficient (ρ) was calculated. All analyses were conducted using SAS 9.2 (SAS Institute, Cary NC) software. A P-value < 0.05 was considered statistically significant in two-tailed statistical tests.

ACKNOWNLEDGEMENTS

The authors greatly thank Dr. William Ricke's laboratory (UW-Madison) for providing polarizing microscopy, Chee Paul Lin (UW-Madison) for providing statistical analysis, the W.M. Keck Laboratory for Biological Imaging for providing fluorescent imaging services (UW-Madison), and the UWCCC Flow Cytometry laboratory (UW-Madison) for providing service and expertise in flow cytometry analysis.

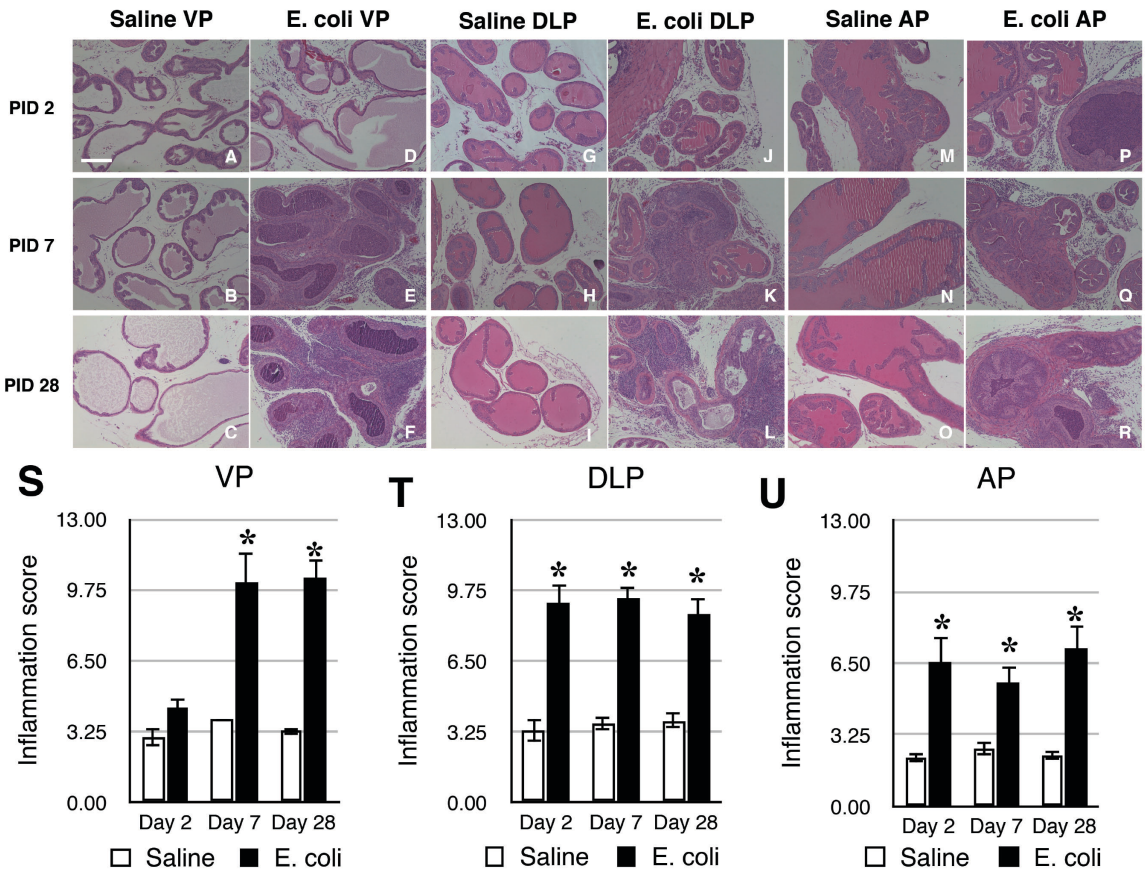

Figure 1. Prostatic inflammation induced by bacterial infection. A-R. Representative H&E stained sections of the VP **(A-F)**, DLP **(G-L)**, and AP **(M-R)** from saline instilled and *E. coli* infected C3H/HeOuJ male mice 2, 7, 28 days post-instillation. Scale bar 200μm in panel A. **S-U.** Comparisons of the degree of inflammation in the VP **(S)**, DLP **(T)** and AP **(U)** of saline instilled and *E. coli* infected C3H/HeOuJ male mice 2, 7, 28 days post-instillation (n = 4-13 per treatment per time point). Data are presented as the mean inflammation score ± SEM. * indicates a P-value < 0.05 compared to saline control by two-sample t-test. Ventral prostate (VP); Dorsolateral prostate (DLP); Anterior prostate (AP).

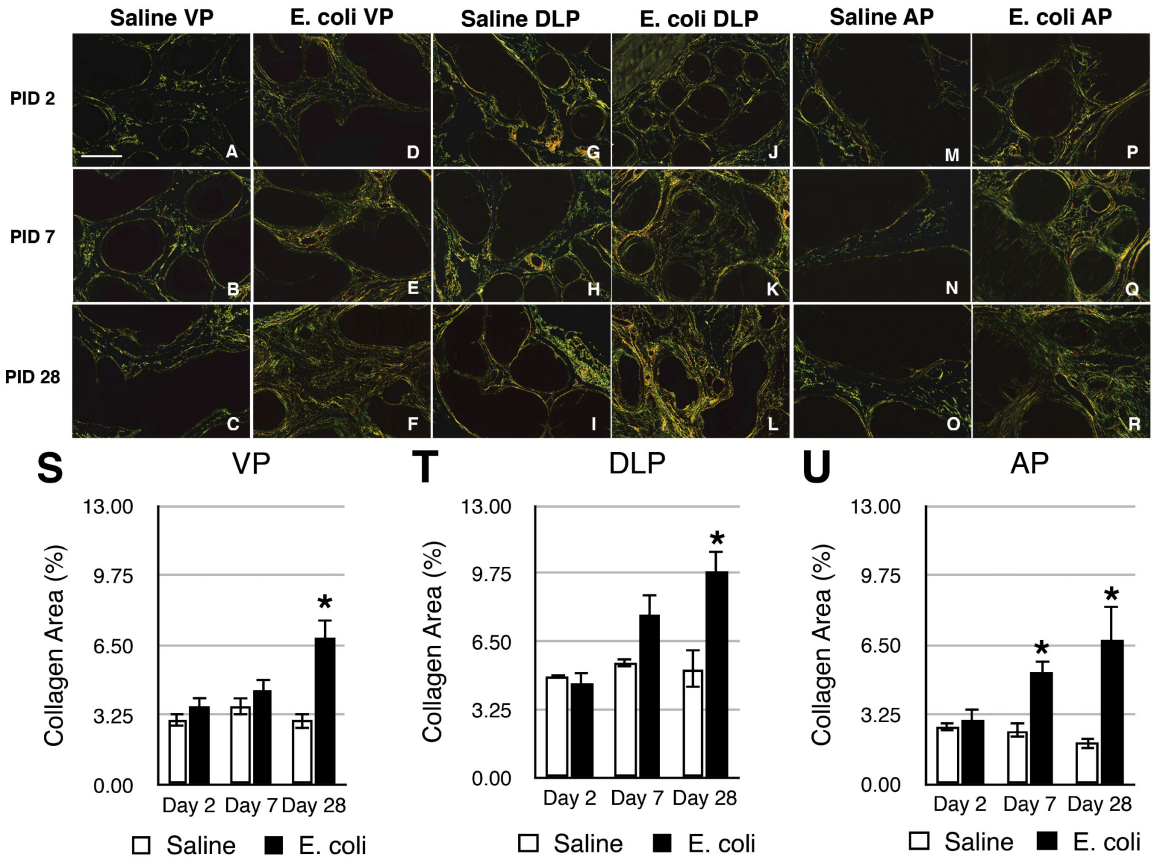

Figure 2. Collagen deposition is increased in response to chronic bacterial-induced prostatic inflammation. A-R. Representative picrosirius red stained sections of the VP **(A-F)**, DLP **(G-L)**, and AP **(M-R)** from saline instilled and *E. coli* infected C3H/HeOuJ male mice 2, 7, 28 days post-instillation. Scale bar 200μm in panel A. **S-U.** Comparisons of the collagen content determined by the percentage of picrosirius red stained area in the VP **(S)**, DLP **(T)** and AP **(U)** of saline instilled and *E. coli* infected C3H/HeOuJ male mice 2, 7, 28 days post-instillation (n = 4-13 per treatment per time point). Data are presented as the mean percentage of collagen area ± SEM. * indicates a P-value < 0.05 compared to saline control by two-sample t-test. Ventral prostate (VP); Dorsolateral prostate (DLP); Anterior prostate (AP).

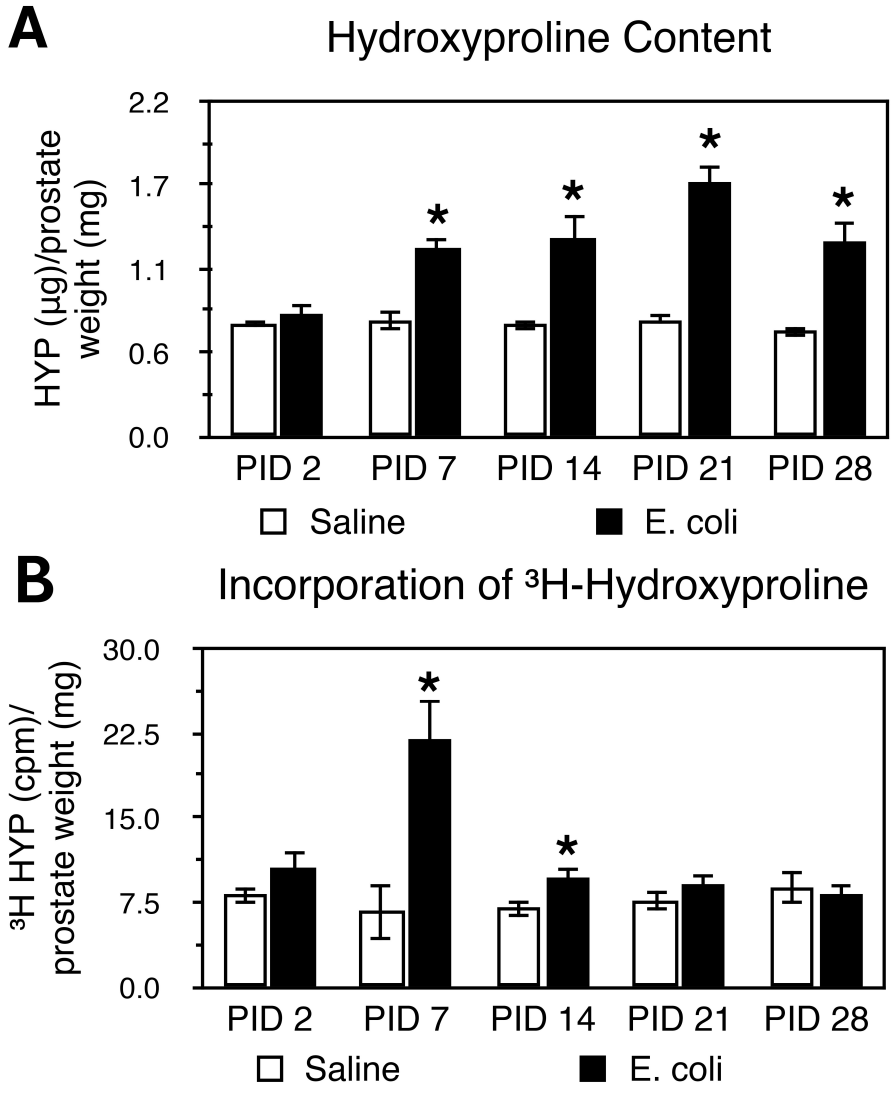

Figure 3. Hydroxyproline content and collagen synthesis are increased in bacterial-induced prostatic inflammation. A. Hydroxyproline content in saline instilled and *E. coli* infected prostates 2, 7, 14, 21, 28 days post-instillation (n = 4-8 per treatment per time point). Data are presented as mean hydroxyproline (µg)/prostate weight (mg) ± SEM. **B.** ^{3}H-hydroxyproline incorporation in saline instilled and *E. coli* infected prostates 2, 7, 14, 21, 28 days post-instillation (n = 4-7 per treatment per time point). Data are presented as mean cpm/mg prostate ± SEM. * indicates a P-value < 0.05 compared to saline control by two-sample t-test. Post-Instillation Day (PID); Hydroxyproline (HYP).

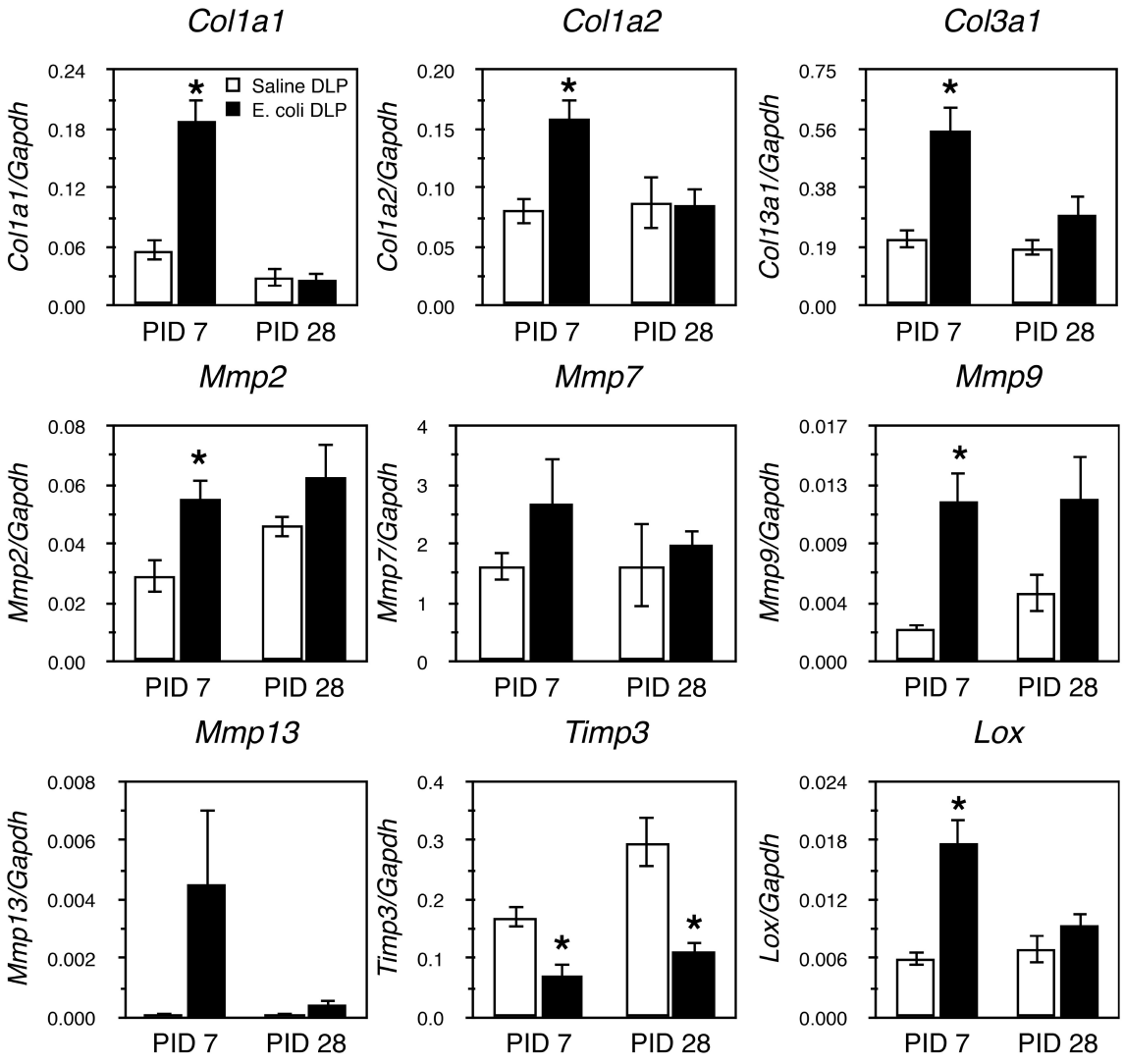

Figure 4. Changes in collagen remodeling-associated gene expressions during bacterial-induced prostatic inflammation. qRT-PCR for collagen remodeling-associated genes in the DLP of saline instilled and *E. coli* infected animals 7 and 28 days post-instillation (n = 4-7 per treatment per time point). Data are presented as mean gene expression ± SEM. Gene expression levels were normalized to the housekeeping gene *Gapdh.* * indicates a P-value < 0.05 compared to saline control by two-sample t-test. Post-Instillation Day (PID); Dorsolateral prostate (DLP).

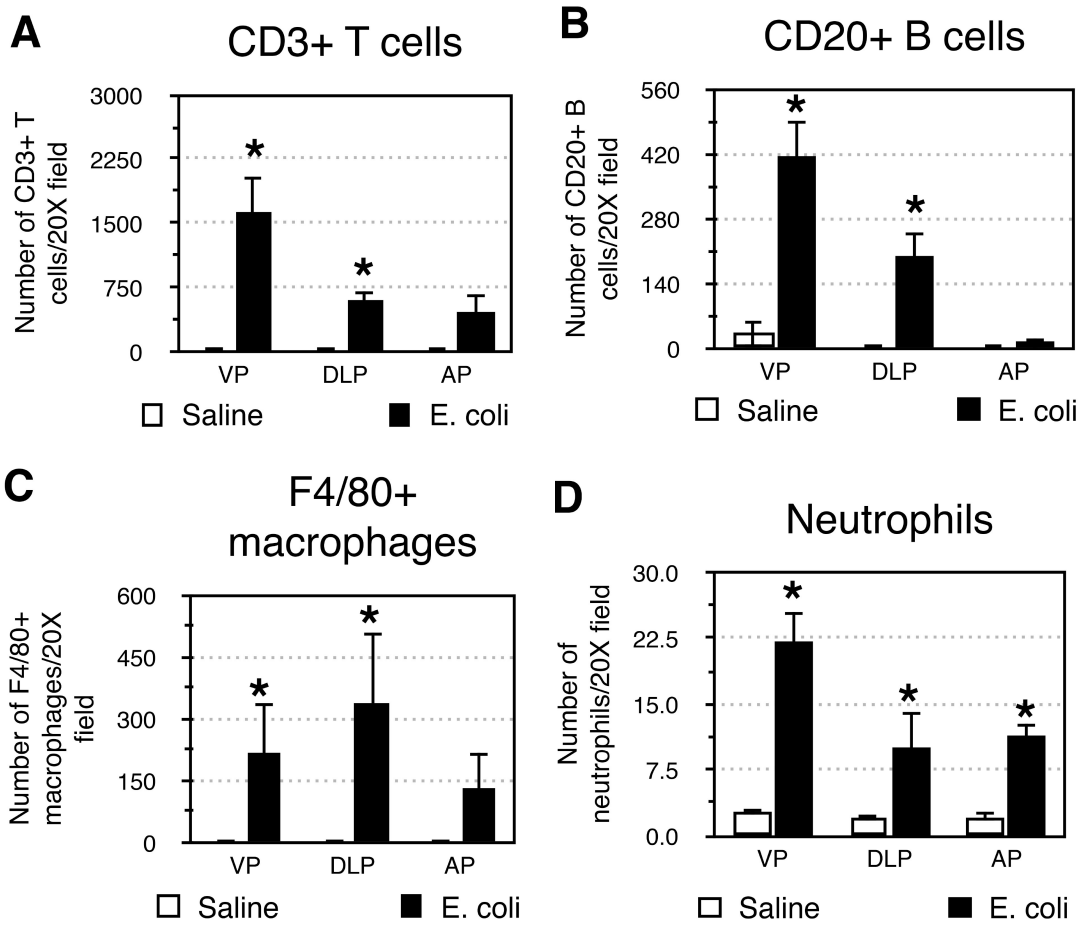

Figure 5. Characterization of inflammatory infiltrate in the inflamed prostate. Comparisons of the number of CD3+ T cells **(A)**, CD20+ B cells **(B)**, F4/80+ macrophages **(C)**, and neutrophils **(D)** in the VP, DLP, and AP from saline instilled and *E. coli* infected mice 28 days post-instillation. n = 4 per group. Data are presented as the mean number of cells per 20X field. * indicates a P-value < 0.05 compared to saline control by Wilcoxon rank-sum test. Ventral prostate (VP); Dorsolateral prostate (DLP); Anterior prostate (AP).

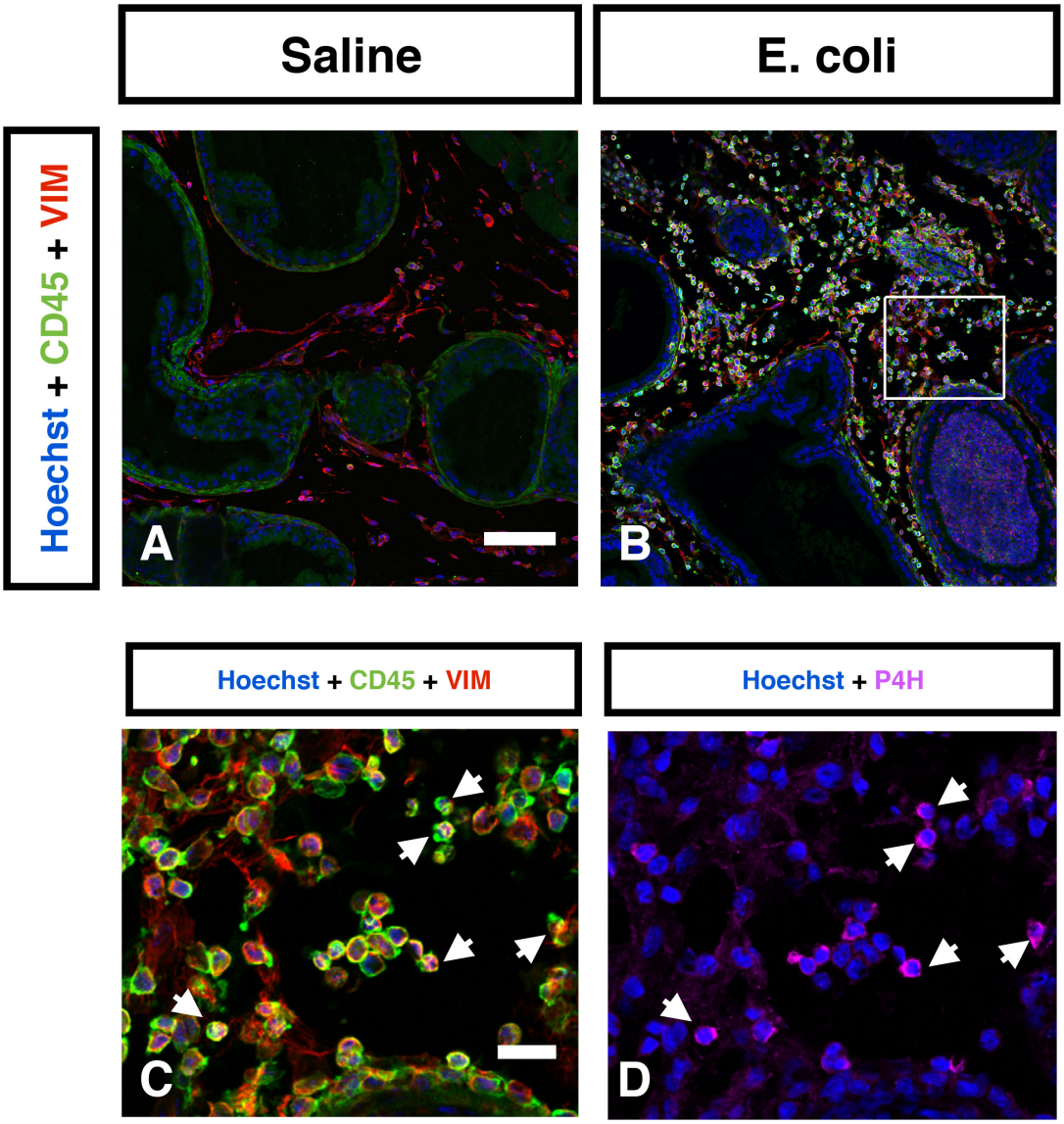

Figure 6. Identification of collagen-producing cells in the inflamed prostate. Representative IHC images of CD45 (Green) and vimentin (Red) in the saline instilled **(A)** and *E. coli* infected **(B)** prostates 7 days post-instillation. n = 4-6 per group. Hoechst nuclear staining is shown in blue. Scale bar 100 μm in panel A. **C.** High magnification inset (box in panel B) shows abundant number of CD45+VIM+ fibrocytes in the *E. coli* infected prostate. Scale bar 20μm in panel C. **D.** Immunostaining for prolyl 4-hydroxylase (Magneta) in the same field as panel C. White arrows indicate localization of prolyl 4-hydroxylase to CD45+VIM+ fibrocytes. Vimentin (VIM); prolyl 4-hydroxylase (P4H).

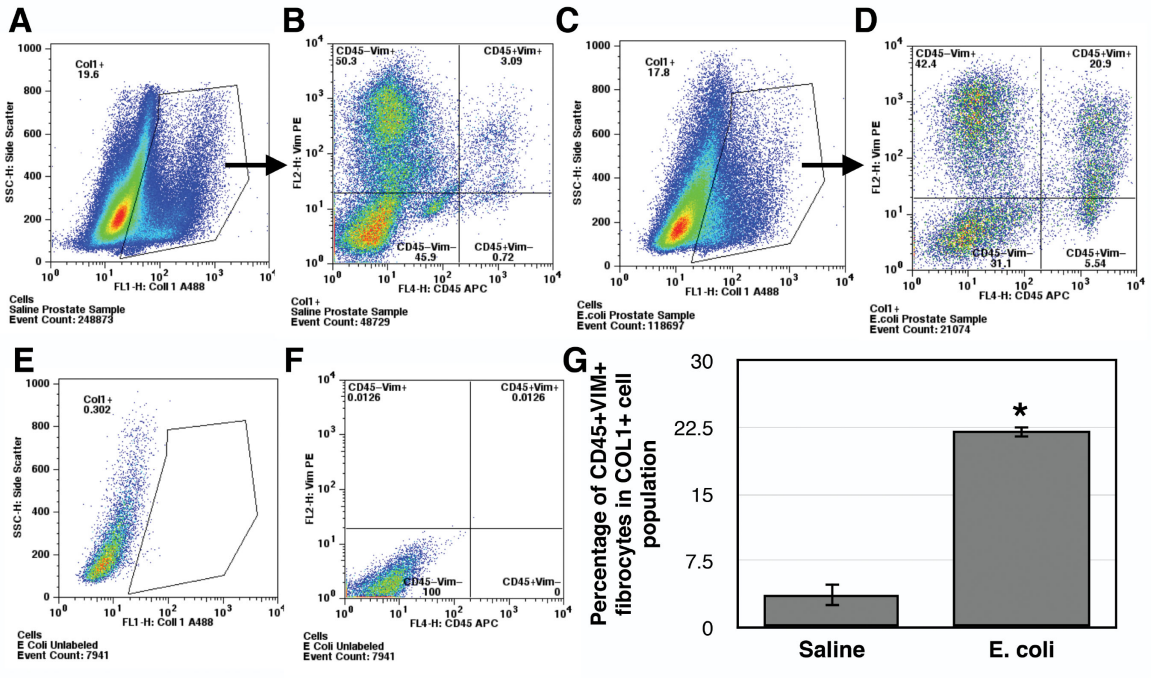

Figure 7. CD45+VIM+ fibrocytes are enriched in the population of COL1+ cells in the inflamed prostate. Representative flow cytometric analyses of freshly isolated prostatic cells from saline instilled **(A-B)** and *E. coli* infected **(C-D)** prostates 7 days post-instillation triple stained for the expression of COL1, CD45 and vimentin. The cells were gated for COL1 expression (A and C) and subsequently COL1 positive cells were analyzed for CD45 and vimentin expression (B and D) based on unstained controls. Representative flow cytometric analyses of unstained prostatic cells control with gate parameter for COL1 were shown in **E** and vimentin/CD45 in **F**. **G.** Comparison of the percentage of CD45+VIM+ fibrocytes in COL1 expressing cell population from the prostates of saline instilled and *E. coli* infected mice. Data are presented as mean percentage ± SEM. Prostatic tissue cells were pooled from 4-6 mice per group and total 3 independent experiments were performed. * indicates a P-value < 0.05 compared to saline control by two-sample t-test.

Table 1. Correlation between inflammation and collagen deposition in the VP, DLP, and AP from saline instilled and *E. coli* infected mice (n = 4-13 per treatment per time point)

	VP		DLP		AP	
	ρ	P-value	ρ	P-value	ρ	P-value
PID 2	0.54	0.11	-0.26	0.47	0.13	0.72
PID 7	0.06	0.86	0.30	0.43	0.89	0.0005
PID 28	0.65	0.0013	0.58	0.0056	0.71	0.0004

ρ: Spearman's rank correlation coefficient; VP: Ventral prostate; DLP: Dorsolateral prostate, AP: anterior prostate

SUPPORTING INFORMATION

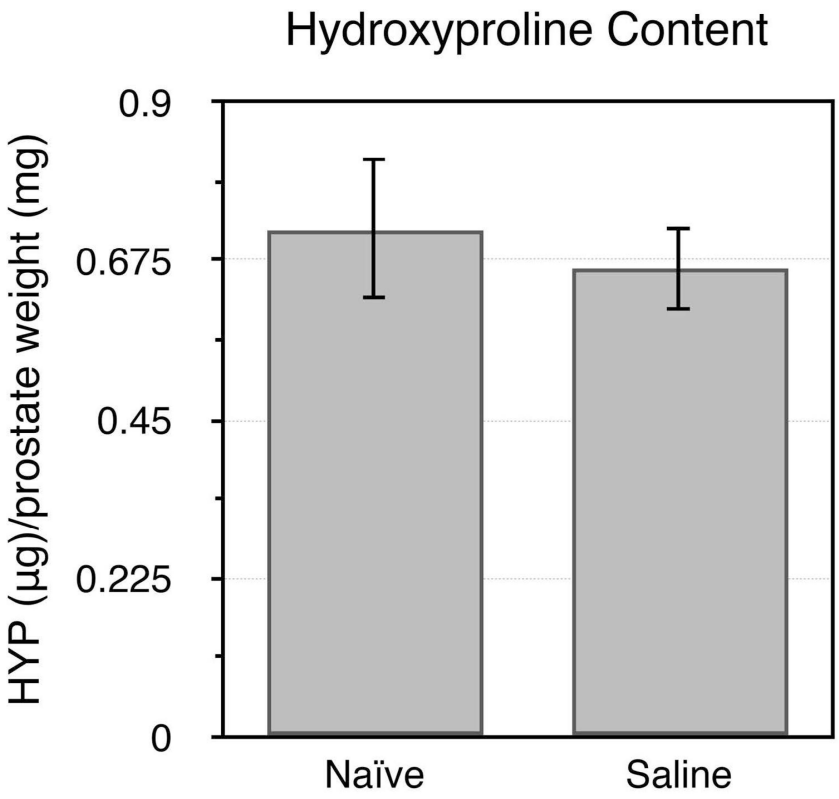

Figure S1. No significant difference in collagen content of the prostate was observed between saline-instilled and naïve controls. Hydroxyproline content of prostate tissues from age-matched naïve C3H/HeOuJ male mice and saline-instilled C3H/HeOuJ mice 28 days post-instillation. n = 8 for naïve group, n = 9 for saline-instilled group. Data are presented as hydroxyproline (µg)/prostate weight (mg) ± SEM. Comparison of the hydroxyproline content between the two groups was performed by two-sample t-test. Hydroxyproline (HYP).

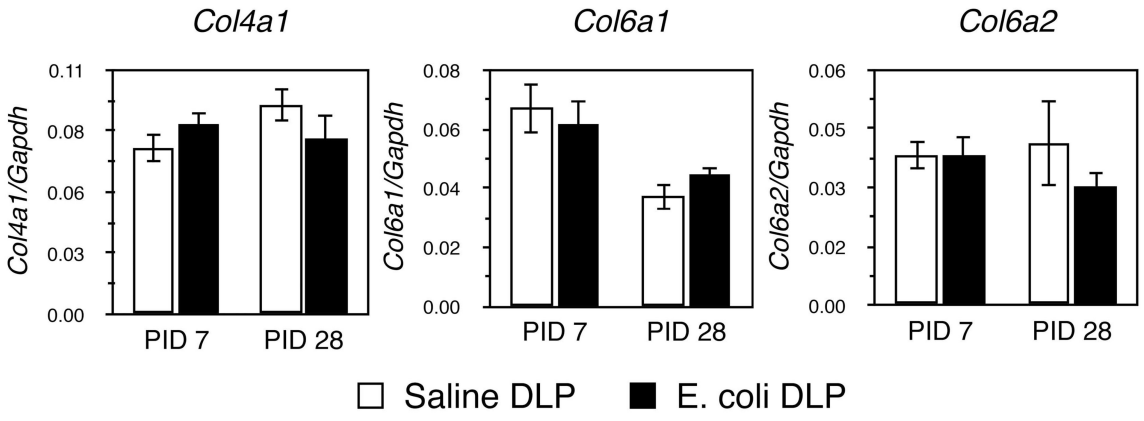

Figure S2. **Collagen subtype gene expressions in bacterial-induced prostatic inflammation.** qRT-PCR for *Col4a1, Col6a1,* and *Col6a*2 in the DLP from saline instilled and *E. coli* infected animals 7 and 28 days post-instillation. n = 4-7 per treatment per time point. Data are presented as mean gene expression ± SEM. Gene expression levels were normalized to the housekeeping gene *Gapdh.* Comparisons of the gene expressions between saline instilled and *E. coli* infected animals were performed by two-sample t-test. Post-Instillation Day (PID); Dorsolateral prostate (DLP).

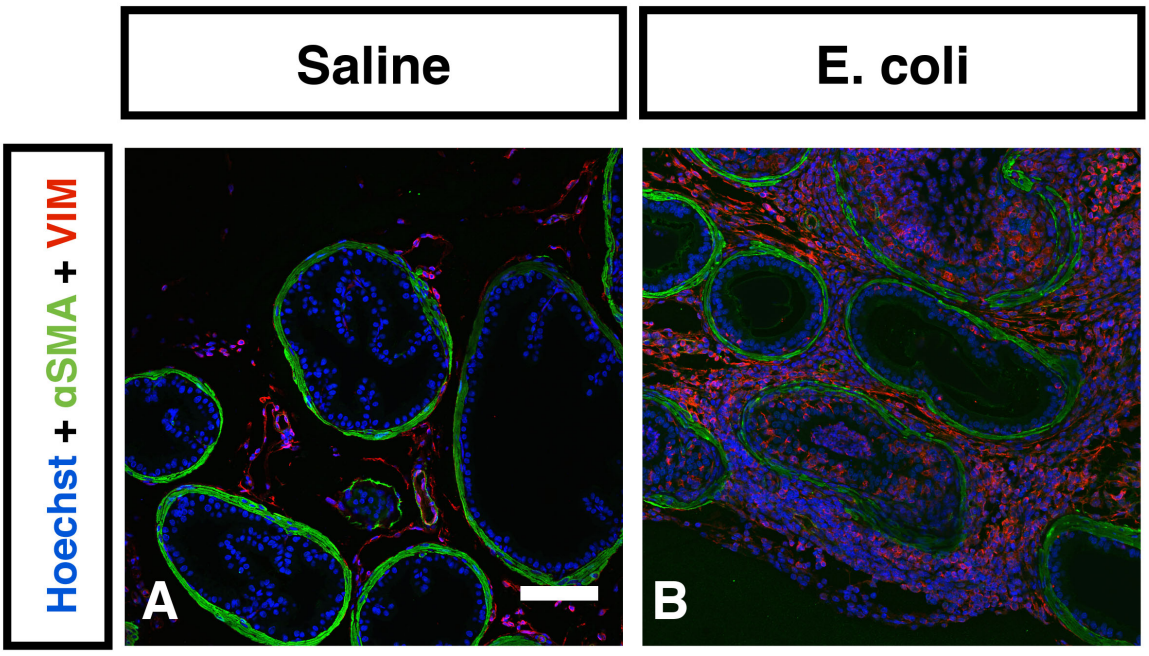

Figure S3. αSMA+VIM+ myofibroblast accumulation is not evident in bacterial-induced prostatic inflammation. Immunohistochemical staining for αSMA (Green), vimentin (Red), and Hoechst (blue) in the saline instilled **(A)** and *E. coli* infected **(B)** prostates 7 days post-instillation. Scale bar 100 μm in panel A. Urogenital sinus obtained from an 18-day-old mouse embryo was used as a positive control for αSMA+VIM+ myofibroblasts (data not shown). Vimentin (VIM); α-smooth muscle actin (αSMA).

Table S1. Primer Sequences (5'-3') Used for RT-PCR Analysis

Gene	Forward Sequence	Reverse Sequence
Col1a1	CCCCAAAAGCCAAAAATATG	TTTTGGTCACGTTCAGTTGG
Col1a2	ACACCCTGACACCTGTTGTG	ACAAGTGGTGCGAATGTTCA
Col3a1	CAACCAGTGCAAGTGACCAA	TGACCTGTATTGGGTGGTTG
Mmp2	TCCGCGTAAAGTATGGGAAC	ATCACTGCGACCAGTGTCTG
Mmp7	AGCTATGCAGCTCACCCTGT	GAGCCTGTTCCCACTGATGT
Mmp9	CATTCGCGTGGATAAGGAGT	TCACACGCCAGAAGAATTTG
Mmp13	AGTTGACAGGCTCCGAGAAA	GGCACTCCACATCTTGGTTT
Timp3	TTGGGTACCCTGGCTATCAG	TTGCTGATGCTCTTGTCTGG
Lox	TTCTTCTGCTGCGTGACAAC	AAACCAGCTTGGAACCAGTG
Gapdh	AGAACATCATCCCTGCATCC	CACATTGGGGGTAGGAACAC

REFERENCES

1. Nickel JC, Roehrborn CG, O'Leary MP, Bostwick DG, Somerville MC, et al. (2008) The relationship between prostate inflammation and lower urinary tract symptoms: examination of baseline data from the REDUCE trial. Eur Urol 54: 1379-1384.

2. Roehrborn CG (2006) Definition of at-risk patients: baseline variables. BJU Int 97 Suppl 2: 7-11; discussion 21-12.

3. Bercovich E, Barabino G, Pirozzi-Farina F, Deriu M (1999) A multivariate analysis of lower urinary tract ageing and urinary symptoms: the role of fibrosis. Arch Ital Urol Androl 71: 287-292.

4. Ma J, Gharaee-Kermani M, Kunju L, Hollingsworth JM, Adler J, et al. (2012) Prostatic fibrosis is associated with lower urinary tract symptoms. J Urol 188: 1375-1381.

5. Cantiello F, Cicione A, Salonia A, Autorino R, Tucci L, et al. (2013) Periurethral fibrosis secondary to prostatic inflammation causing lower urinary tract symptoms: a prospective cohort study. Urology 81: 1018-1023.

6. Elkahwaji JE, Zhong W, Hopkins WJ, Bushman W (2007) Chronic bacterial infection and inflammation incite reactive hyperplasia in a mouse model of chronic prostatitis. Prostate 67: 14-21.

7. Boehm BJ, Colopy SA, Jerde TJ, Loftus CJ, Bushman W (2012) Acute bacterial inflammation of the mouse prostate. Prostate 72: 307-317.

8. Marker PC, Donjacour AA, Dahiya R, Cunha GR (2003) Hormonal, cellular, and molecular control of prostatic development. Dev Biol 253: 165-174.

9. Shappell SB, Thomas GV, Roberts RL, Herbert R, Ittmann MM, et al. (2004) Prostate pathology of genetically engineered mice: definitions and classification. The consensus report from the Bar Harbor meeting of the Mouse Models of Human Cancer Consortium Prostate Pathology Committee. Cancer Res 64: 2270-2305.

10. Cunha GR, Sekkingstad M, Meloy BA (1983) Heterospecific induction of prostatic development in tissue recombinants prepared with mouse, rat, rabbit and human tissues. Differentiation 24: 174-180.

11. Kramer G, Mitteregger D, Marberger M (2007) Is benign prostatic hyperplasia (BPH) an immune inflammatory disease? Eur Urol 51: 1202-1216.

12. Steiner GE, Stix U, Handisurya A, Willheim M, Haitel A, et al. (2003) Cytokine expression pattern in benign prostatic hyperplasia infiltrating T cells and impact of lymphocytic infiltration on cytokine mRNA profile in prostatic tissue. Lab Invest 83: 1131-1146.

13. Robert G, Descazeaud A, Nicolaiew N, Terry S, Sirab N, et al. (2009) Inflammation in benign prostatic hyperplasia: a 282 patients' immunohistochemical analysis. Prostate 69: 1774-1780.

14. Shinohara DB, Vaghasia AM, Yu SH, Mak TN, Bruggemann H, et al. (2013) A mouse model of chronic prostatic inflammation using a human prostate

cancer-derived isolate of Propionibacterium acnes. Prostate 73: 1007-1015.

15. De Marzo AM, Marchi VL, Epstein JI, Nelson WG (1999) Proliferative inflammatory atrophy of the prostate: implications for prostatic carcinogenesis. Am J Pathol 155: 1985-1992.
16. Gordon MK, Hahn RA (2010) Collagens. Cell Tissue Res 339: 247-257.
17. Frantz C, Stewart KM, Weaver VM (2010) The extracellular matrix at a glance. J Cell Sci 123: 4195-4200.
18. Kadler KE, Baldock C, Bella J, Boot-Handford RP (2007) Collagens at a glance. J Cell Sci 120: 1955-1958.
19. Rodés J (2007) Textbook of hepatology from basic science to clinical practice. 3rd ed. Malden, Mass.: Blackwell.
20. Thickett DR, Poole AR, Millar AB (2001) The balance between collagen synthesis and degradation in diffuse lung disease. Sarcoidosis Vasc Diffuse Lung Dis 18: 27-33.
21. Armstrong L, Thickett DR, Mansell JP, Ionescu M, Hoyle E, et al. (1999) Changes in collagen turnover in early acute respiratory distress syndrome. Am J Respir Crit Care Med 160: 1910-1915.
22. Garcia-Bolao I, Lopez B, Macias A, Gavira JJ, Azcarate P, et al. (2008) Impact of collagen type I turnover on the long-term response to cardiac resynchronization therapy. Eur Heart J 29: 898-906.

23. Selman M, Montano M, Ramos C, Chapela R (1986) Concentration, biosynthesis and degradation of collagen in idiopathic pulmonary fibrosis. Thorax 41: 355-359.

24. Pardo A, Selman M (2002) Idiopathic pulmonary fibrosis: new insights in its pathogenesis. Int J Biochem Cell Biol 34: 1534-1538.

25. Selman M, King TE, Pardo A, American Thoracic S, European Respiratory S, et al. (2001) Idiopathic pulmonary fibrosis: prevailing and evolving hypotheses about its pathogenesis and implications for therapy. Ann Intern Med 134: 136-151.

26. Farrell GC, Larter CZ (2006) Nonalcoholic fatty liver disease: from steatosis to cirrhosis. Hepatology 43: S99-S112.

27. Adams LA, Lymp JF, St Sauver J, Sanderson SO, Lindor KD, et al. (2005) The natural history of nonalcoholic fatty liver disease: a population-based cohort study. Gastroenterology 129: 113-121.

28. Rieder F, Fiocchi C (2009) Intestinal fibrosis in IBD--a dynamic, multifactorial process. Nat Rev Gastroenterol Hepatol 6: 228-235.

29. Fiocchi C (1998) Inflammatory bowel disease: etiology and pathogenesis. Gastroenterology 115: 182-205.

30. Querejeta R, Lopez B, Gonzalez A, Sanchez E, Larman M, et al. (2004) Increased collagen type I synthesis in patients with heart failure of hypertensive origin: relation to myocardial fibrosis. Circulation 110: 1263-1268.

31. McLenachan JM, Dargie HJ (1990) Ventricular arrhythmias in hypertensive left ventricular hypertrophy. Relationship to coronary artery disease, left ventricular dysfunction, and myocardial fibrosis. Am J Hypertens 3: 735-740.

32. Broughton G, 2nd, Janis JE, Attinger CE (2006) The basic science of wound healing. Plast Reconstr Surg 117: 12S-34S.

33. Borthwick LA, Wynn TA, Fisher AJ (2013) Cytokine mediated tissue fibrosis. Biochim Biophys Acta 1832: 1049-1060.

34. Atamas SP (2002) Complex cytokine regulation of tissue fibrosis. Life Sci 72: 631-643.

35. Ueha S, Shand FH, Matsushima K (2012) Cellular and molecular mechanisms of chronic inflammation-associated organ fibrosis. Front Immunol 3: 71.

36. Wight TN, Potter-Perigo S (2011) The extracellular matrix: an active or passive player in fibrosis? Am J Physiol Gastrointest Liver Physiol 301: G950-955.

37. Rydell-Tormanen K, Andreasson K, Hesselstrand R, Risteli J, Heinegard D, et al. (2012) Extracellular matrix alterations and acute inflammation; developing in parallel during early induction of pulmonary fibrosis. Lab Invest 92: 917-925.

38. Lv XX, Wang XX, Li K, Wang ZY, Li Z, et al. (2013) Rupatadine protects against pulmonary fibrosis by attenuating PAF-mediated senescence in rodents. PLoS One 8: e68631.

39. Besnard AG, Struyf S, Guabiraba R, Fauconnier L, Rouxel N, et al. (2013) CXCL6 antibody neutralization prevents lung inflammation and fibrosis in mice in the bleomycin model. J Leukoc Biol 94: 1317-1323.

40. Kang HR, Cho SJ, Lee CG, Homer RJ, Elias JA (2007) Transforming growth factor (TGF)-beta1 stimulates pulmonary fibrosis and inflammation via a Bax-dependent, bid-activated pathway that involves matrix metalloproteinase-12. J Biol Chem 282: 7723-7732.

41. Gharaee-Kermani M, McGarry B, Lukacs N, Huffnagle G, Egan RW, et al. (1998) The role of IL-5 in bleomycin-induced pulmonary fibrosis. J Leukoc Biol 64: 657-666.

42. Degryse AL, Tanjore H, Xu XC, Polosukhin VV, Jones BR, et al. (2011) TGFbeta signaling in lung epithelium regulates bleomycin-induced alveolar injury and fibroblast recruitment. Am J Physiol Lung Cell Mol Physiol 300: L887-897.

43. Saito F, Tasaka S, Inoue K, Miyamoto K, Nakano Y, et al. (2008) Role of interleukin-6 in bleomycin-induced lung inflammatory changes in mice. Am J Respir Cell Mol Biol 38: 566-571.

44. Wilson MS, Madala SK, Ramalingam TR, Gochuico BR, Rosas IO, et al. (2010) Bleomycin and IL-1beta-mediated pulmonary fibrosis is IL-17A dependent. J Exp Med 207: 535-552.

45. Vater CA, Harris ED, Jr., Siegel RC (1979) Native cross-links in collagen fibrils induce resistance to human synovial collagenase. Biochem J 181: 639-645.

46. Lagente V, Manoury B, Nenan S, Le Quement C, Martin-Chouly C, et al. (2005) Role of matrix metalloproteinases in the development of airway inflammation and remodeling. Braz J Med Biol Res 38: 1521-1530.

47. Hinz B (2007) Formation and function of the myofibroblast during tissue repair. J Invest Dermatol 127: 526-537.

48. Hashimoto N, Jin H, Liu T, Chensue SW, Phan SH (2004) Bone marrow-derived progenitor cells in pulmonary fibrosis. J Clin Invest 113: 243-252.

49. Phillips RJ, Burdick MD, Hong K, Lutz MA, Murray LA, et al. (2004) Circulating fibrocytes traffic to the lungs in response to CXCL12 and mediate fibrosis. J Clin Invest 114: 438-446.

50. Peng X, Mathai SK, Murray LA, Russell T, Reilkoff R, et al. (2011) Local apoptosis promotes collagen production by monocyte-derived cells in transforming growth factor beta1-induced lung fibrosis. Fibrogenesis Tissue Repair 4: 12.

51. Mehrad B, Burdick MD, Zisman DA, Keane MP, Belperio JA, et al. (2007) Circulating peripheral blood fibrocytes in human fibrotic interstitial lung disease. Biochem Biophys Res Commun 353: 104-108.

52. Andersson-Sjoland A, de Alba CG, Nihlberg K, Becerril C, Ramirez R, et al. (2008) Fibrocytes are a potential source of lung fibroblasts in idiopathic pulmonary fibrosis. Int J Biochem Cell Biol 40: 2129-2140.

53. Galligan CL, Siminovitch KA, Keystone EC, Bykerk V, Perez OD, et al. (2010) Fibrocyte activation in rheumatoid arthritis. Rheumatology (Oxford) 49: 640-651.

54. Galligan CL, Fish EN (2012) Circulating fibrocytes contribute to the pathogenesis of collagen antibody-induced arthritis. Arthritis Rheum 64: 3583-3593.

55. Schmidt M, Sun G, Stacey MA, Mori L, Mattoli S (2003) Identification of circulating fibrocytes as precursors of bronchial myofibroblasts in asthma. J Immunol 171: 380-389.

56. Wang CH, Huang CD, Lin HC, Lee KY, Lin SM, et al. (2008) Increased circulating fibrocytes in asthma with chronic airflow obstruction. Am J Respir Crit Care Med 178: 583-591.

57. Sakai N, Furuichi K, Shinozaki Y, Yamauchi H, Toyama T, et al. (2010) Fibrocytes are involved in the pathogenesis of human chronic kidney disease. Hum Pathol 41: 672-678.

58. Sakai N, Wada T, Yokoyama H, Lipp M, Ueha S, et al. (2006) Secondary lymphoid tissue chemokine (SLC/CCL21)/CCR7 signaling regulates fibrocytes in renal fibrosis. Proc Natl Acad Sci U S A 103: 14098-14103.

59. Bucala R, Spiegel LA, Chesney J, Hogan M, Cerami A (1994) Circulating fibrocytes define a new leukocyte subpopulation that mediates tissue repair. Mol Med 1: 71-81.

60. Pilling D, Fan T, Huang D, Kaul B, Gomer RH (2009) Identification of markers that distinguish monocyte-derived fibrocytes from monocytes, macrophages, and fibroblasts. PLoS One 4: e7475.

61. Gharaee-Kermani M, Kasina S, Moore BB, Thomas D, Mehra R, et al. (2012) CXC-type chemokines promote myofibroblast phenoconversion and prostatic fibrosis. PLoS One 7: e49278.

62. Morrison C, Thornhill J, Gaffney E (2000) The connective tissue framework in the normal prostate, BPH and prostate cancer: analysis by scanning electron microscopy after cellular digestion. Urol Res 28: 304-307.

63. Barron DA, Strand DW, Ressler SJ, Dang TD, Hayward SW, et al. (2010) TGF-beta1 induces an age-dependent inflammation of nerve ganglia and fibroplasia in the prostate gland stroma of a novel transgenic mouse. PLoS One 5: e13751.

64. Junqueira LC, Bignolas G, Brentani RR (1979) Picrosirius staining plus polarization microscopy, a specific method for collagen detection in tissue sections. Histochem J 11: 447-455.

65. Hutson PR, Crawford ME, Sorkness RL (2003) Liquid chromatographic determination of hydroxyproline in tissue samples. J Chromatogr B Analyt Technol Biomed Life Sci 791: 427-430.

66. McAnulty RJ (2005) Methods for measuring hydroxyproline and estimating in vivo rates of collagen synthesis and degradation. Methods Mol Med 117: 189-207.

CHAPTER FOUR

This manuscript was submitted to *The Prostate* on July 8, 2014.

Contributions of authors: L.W. designed and performed research experiments and prepared manuscript. P.R.H. performed kinetic analysis and assisted in hydroxyproline assay by HPLC and manuscript preparation. W.B. supervised studies and assisted in manuscript preparation.

Resolution of chronic bacterial-induced prostatic inflammation reverses established fibrosis

Letitia Wong, Paul R. Hutson, Wade Bushman

ABSTRACT

BACKGROUND. Prostatic inflammation has been suggested to contribute to the etiology of lower urinary tract symptoms by inducing fibrosis. We previously used a well-characterized mouse model of bacterial-induced prostate inflammation to demonstrate that chronic prostatic inflammation induces collagen deposition. Here, we examined stability of the newly synthesized collagen in bacterial-induced prostatic inflammation and the reversibility of fibrosis after resolution of infection and inflammation.

METHODS. Uropathogenic *E. coli* 1677 was instilled transurethrally into adult C3H/HeOuJ male mice to induce chronic prostatic inflammation. Collagen was labeled by ^{3}H-proline administration for 28 days post-inoculation and ^{3}H-hydroxyproline incorporation measured to determine stability of the newly synthesized collagen. Inflammation score was graded using a previously established system and total collagen content was measured by picrosirius red staining quantitation and hydroxyproline content. Resolution of inflammation and reversal of collagen deposition was assessed after treatment with antibiotic enrofloxacin for two weeks on day 28 post-inoculation followed by an eight-week recovery period.

RESULTS. Decay analysis of incorporated ^{3}H-hydroxyproline revealed the half-life of newly synthesized collagen to be significantly shorter in infected/inflamed prostates than in controls. Treatment with antibiotic enrofloxacin completely eradicated bacterial infection and allowed resolution of inflammation. This was followed by marked attenuation of collagen content and correlation analysis verified a positive association between the resolution of inflammation and the reversal of collagen deposition.

CONCLUSIONS. These data demonstrate, for the first time, that inflammation-induced prostatic fibrosis is a reversible process.

INTRODUCTION

Prostatic inflammation is frequently present in aging men. It has been suggested to be a major etiological factor for benign prostatic hyperplasia (BPH) and lower urinary tract symptoms (LUTS) as there is accumulating evidence showing that the degree of inflammation was correlated with symptom severity and disease progression of BPH/LUTS [1,2]. However, the underlying mechanism for this association remains to be established. Several studies have shown that prostatic fibrosis is strongly associated with impaired urethral function and LUTS severity [3,4]. This led to the hypothesis that prostatic inflammation contributes to the pathogenesis of BPH/LUTS by inducing prostatic fibrosis and impairing opening of the bladder neck – prostate complex during voiding. Using a previously described mouse model of bacterial-induced prostatic inflammation [5], we

recently characterized the fibrotic response to inflammation in the prostate [6]. Our findings demonstrated that chronic prostatic inflammation results in a significant increase in prostate collagen content, strongly supporting a role for inflammation in prostatic fibrosis.

Given that inflammation-induced prostatic fibrosis could be a major contributing factor in the development and progression of BPH/LUTS, it is imperative to determine whether the injured prostate has the capacity to resolve and remodel the established fibrosis induced by inflammation. In this study, we extended our work to investigate the reversibility of fibrosis induced by inflammation. We first measured the stability of the newly synthesized collagen to examine whether collagen induced in prostate inflammation undergoes remodeling and degradation. We then used antibiotic treatment to induce resolution of bacterial-induced inflammation and measured reversal of the associated fibrosis over an eight-week recovery period. Our findings demonstrate, for the first time, that prostatic fibrosis induced by chronic inflammation is at least partly reversible.

MATERIALS AND METHODS

Transurethral Instillation

Transurethral instillation was performed as previously described [5]. 8-week old C3H/HeOuJ male mice (Jackson Laboratories, Bar Harbor, Maine) were anesthetized with isoflurane and catheterized with a lubricated sterile

polyethylene catheter per urethra. Inoculation was performed by a single transurethral instillation of uropathogenic *E. coli* 1677 (2 x10^6 CFU/ml) or sterile PBS in a volume of 200µl.

Antibiotic Treatment

At day 28 post-instillation some animals were treated with 1ml of 100mg/ml enrofloxacin (Baytril® 100, Bayer Corp., Pittsburgh, PA) per 450 ml drinking water for two weeks. Fresh water with enrofloxacin was replaced every 3-4 days. Other animals received sham treatment (regular drinking water). After two weeks of treatment, all animals received regular drinking water. Animals were sacrificed either immediately or 8 weeks after the end of enrofloxacin/sham treatment. The prostatic lobes (ventral prostate, dorsolateral prostate, anterior prostate) were harvested separately and were used for bacterial culture and histology. The whole mouse prostates were collected and used for hydroxyproline assay and measuring the incorporation of ^{3}H-hydroxyproline to determine collagen stability. Four to six mice per treatment group were analyzed for histology. Four mice per treatment group were used for bacterial counts. Four to five mice per treatment group were used for hydroxyproline assay. Three to eight mice per time point per treatment group were used for collagen stability measurement.

Bacterial Counts

Each prostatic lobe was collected separately, weighed and homogenized in 400µl of sterile cold PBS. The homogenate was serially diluted to 1:100 and 1:1000 and plated onto Levine EMB agar at 37°C for 24 hours. Each dilution was plated in duplicate. Prostatic bacterial titers are presented as the mean colony-forming units (CFUs) $x10^3$/prostate weight (mg) ± standard error of the mean (SEM).

Quantitation of Inflammatory Degree

Tissues were fixed in 10% formalin, imbedded in paraffin and serially sectioned at 6µm. Standard H&E staining was performed for histology. Using our previously established scoring system [5], the severity of inflammation was graded in at least 3 random 10X fields of H&E sections from each prostatic lobe. Data are presented as the mean inflammation score ± SEM.

Quantitation of Collagen Content

Picrosirius Red Staining

Adjacent tissues sections of H&E stained slides were used for picrosirius red staining. The staining was performed by incubating slides in 0.1% sirius red in saturated aqueous solution of picric acid for one hour at room temperature. Images were taken by digital camera using NIS Element software under a Nikon Eclipse 80i polarized light microscope. The settings of the software and microscope remained unchanged throughout the observation for the purpose of quantitation and comparisons. The color staining that shows up under polarizing

microscope corresponds to the birefringence of collagen fibers [7]. Quantitation of the staining for collagen content was then determined by using NIH Image J. Briefly, the images were converted from RBG to 8-bit gray scale and the intensity of the three color channels was summed into one image. The images were manually thresholded to define the collagen staining and a constant value of the threshold was set for all the images analyzed. The region of interest (prostatic tissues) was manually outlined to analyze the area that was stained for collagen. Large blood vessels and nerve fiber bundles in the prostate were eliminated in the quantitation. Data are presented as the mean percentage of collagen area ± SEM.

Hydroxyproline Assay for Collagen Content by High-Performance Liquid Chromatography (HPLC)

Mouse prostate tissues were harvested, snap frozen in liquid nitrogen, and stored at -80°C until further analysis. The procedure was performed as previously described with some modifications [8]. The tissues were thawed on ice and weighed. Each tissue sample was homogenized in 2ml of 12N HCl with a motorized homogenizer in a clean glass tube. 75µl of 20mM sacrosine (reagent grade) as internal standard was mixed in the homogenate. Then, the glass tubes containing the tissue homogenate were tightly capped to prevent evaporation and were incubated in a 110°C heating block for 18 hours. The hydrolysates were allowed to cool to room temperature, neutralized with 2ml of

12N NaOH and 1ml of borate buffer (0.7M boric acid in water, pH 9.5 with NaOH), and were adjusted to a pH 9.5 with NaOH and HCl. Aliquots of 500µl of the sample solution were used for subsequent derivatization process. Some samples were run in duplicate or triplicate for intra-day reaction consistency and these same samples were run on the next day for inter-day reaction consistency. Hydroxyproline (reagent grade) standards of 0.3125, 0.625, 1.25, 2.5, 5, 10, 20mM with 7.5mM L-proline (reagent grade) in water were prepared. 200µl of each hydroxyproline standard was mixed with 75µl of 20mM sacrosine, 1.8ml of 12N HCl, 2ml of 12N NaOH and 1ml of borate buffer. The solutions were then adjusted to pH 9.5. Aliquots of 500µl of the hydroxyproline standard solution were used for subsequent derivatization process.

Aliquots (500µl) of tissue homogenate or hydroxyproline standard were added with 700µl of borate buffer. The following procedures were performed in dark. The solutions were mixed with 100µl of OPA solution (50mg *o*-phthalaldehyde dissolved in 1ml acetonitrile and 26µl of reagent grade β-mercaptoethanol) by vortexing and allowed to react at room temperature for 1 minute. The solution was then mixed with 100µl of iodoacetamide solution (140mg/ml of iodoacetamide in acetonitrile) by vortexing and reacted at room temperature for 1 minute. 600µl of 5mM FMOC-Cl in acetone was subsequently added, mixed by vortexing and reacted at room temperature for 1 minute. The solutions were then washed three times with 3ml of ethyl ether by vortexing for 30 seconds each.

The organic layer was discarded each time. 50µl of the aqueous phase was injected into the HPLC. A total of 3 injections were run for each reacted sample or standard. Sample injections were made every 25 minutes without an intervening wash. The isocratic mobile phase was prepared by combining 650ml of 3% glacial acetic acid that was adjusted to pH 4.3 with sodium acetate (reagent grade) with 350ml of acetonitrile, followed by vacuum filtration for degassing. All reagents used were ACS or HPLC grade unless stated otherwise.

The HPLC instrumentation and spectrofluorometer was set up as previously described [8]. The HPLC instrumentation included a Shimadzu LC-10AD HPLC pump, SIL-10A auto injector and system controller. A McPherson Model FL-750 spectrofluorometer was used with the high-sensitivity module, an excitation wavelength of 265ηm and without an emission cut-off filter. Separation was achieved by using a Lichrosphere 5 RP18e 250 mm x 4.60 mm, 5µm column. The mobile phase was pumped at a constant rate of 0.75ml/min.

The coefficients of variation for intra-day reaction consistency were less than 2.2% and for inter-day reaction consistency were less than 11%. The height ratio of the internal standard (sarcosine) and hydroxyproline peak was calculated for each sample and standard. The exact amount of hydroxyproline standards in µg injected into the HPLC was determined by calculating the total dilution made from the original concentration prepared. The standard curve of hydroxyproline

standards showed linear regression with $R^2 = 0.995$. The amount of hydroxyproline in µg presented in the prostate samples was calculated from the peak height ratio of hydroxyproline and internal standard peak into the linear regression equation obtained from the hydroxyproline standard curve. Data are presented as mean hydroxyproline (µg)/prostate weight (mg) ± SEM.

Collagen Stability Measured by The Incorporation of ^{3}H-hydroxyproline

Animals instilled transurethrally with either sterile PBS or uropathogenic *E. coli* 1677 were injected intraperitoneally with 15µCi of L-[3,4-^{3}H] proline (specific activity 50-60 Ci/mmol, ARC, Inc.) every two days for 28 days. Animals were sacrificed on day 1, 4, 8, 15, 22, 29, 36, 57, 78, 113 after the last injection of ^{3}H-proline. The whole prostate was harvested, snap frozen in liquid nitrogen and stored at -80°C until further analysis. The extraction procedure of hydroxyproline has previously been described in detail.[9] Briefly, each tissue sample was placed in a clean glass tube, homogenized in 2ml 12N HCl with a motorized homogenizer and was heated at 110°C for 18 hours. The hydrolysates were then allowed to cool to room temperature and neutralized with 2ml of 12N KOH and 1ml of 1M boric acid in water. The samples were then adjusted to pH 8.7 with KOH and HCl. Aliquots of 2ml of the sample solution were used for subsequent reaction. First, each sample was reacted with 4ml of 0.2M chloramine T-solution in methoxyethanol at room temperature for 20 minutes. 2.4ml of 3.6M sodium thiosulfate in water was then added followed by saturation

with 1.5g KCl. The solutions were then washed 3X with 9ml of toluene by vigorously shaking for 5 minutes each. Organic layer was discarded each time. The samples were heated in boiling water for 30 minutes and then allowed to cool down on ice for 10 minutes. Then, 7ml of toluene was added into each sample and mixed by vigorously shaking for 10 minutes. The organic layer that contained hydroxyproline was then removed and mixed with 7ml of liquid scintillation cocktail (Fisher, SX25-5) in a 20ml liquid scintillation vial. Counts per minute (cpm) were measured with a Beckman LS 6000TA liquid scintillation counter. Decay curves were graphed individually for saline instilled and *E.* coli infected prostates by fitting a non-linear regression line through individual data points. The non-linear regression equation is $y = y_0 / (1 + y_0 k x)$, where y is remaining ^{3}H-hydroxyproline radioactivity (cpm)/prostate, y_0 and k are fitting parameters, x is time (days). The graphs are plotted as the natural log of cpm versus time after the last injection of ^{3}H-proline. The half-life ($t_{½}$) is calculated using the following equation $t_{½} = 1/(y_0 k)$ obtained from the non-linear regression line.

Statistical Analysis

Inflammation score, collagen area, hydroxyproline content per prostate weight were compared between untreated saline instilled, antibiotic treated saline instilled, untreated *E. coli* infected, and antibiotic treated *E. coli* infected animals. ANOVA (analysis of variance) was employed, followed by a Fisher's protected

LSD (Least Significant Difference) test for pair-wise comparisons of different groups. Prior to ANOVA, Levene's test was used to verify the homoscedasticity assumption. The relationship between inflammation score and collagen area for each prostatic lobe in different groups of animals was assessed via Spearman's rank correlation. All analysis was conducted using SAS 9.2 (SAS Institute, Cary NC) software. A P-value < 0.05 was considered statistically significant in two-tailed statistical tests.

Study Approval

All animal studies were approved by the Institutional Animal Care and Use Committee at the University of Wisconsin-Madison.

RESULTS

Collagen Stability In Chronic Bacterial-induced Prostatic Inflammation

Our previous work demonstrated that collagen deposition was significantly increased in bacterial-induced prostatic inflammation and this increase was associated with enhanced collagen synthesis as determined by ^{3}H-hydroxyproline incorporation and mRNA expression of collagen genes [6]. Here, we measured the stability of the newly synthesized collagen in saline and *E. coli* instilled prostates using a direct *in vivo* radiolabeling method. Inbred C3H/HeOuJ mice instilled transurethrally either with sterile saline or *E. coli* were i.p. injected with ^{3}H-proline every 2 days for 28 days, a timeframe within which collagen

synthesis and content were significantly elevated and peaked post-infection [6]. The radioactivity of ^{3}H-hydroxyproline in the prostates 1, 4, 8, 15, 22, 29, 36, 57, 78, 113 days after the last ^{3}H-proline labeling was measured and decay curves generated from these data **(Figure 1A and B)**. We noted a greater ^{3}H-hydroxyproline content in the infected prostates 1 day after the last labeling. This reflects increased *de novo* collagen synthesis in prostatic inflammation as previously demonstrated [6]. A rapid decrease in ^{3}H-hydroxyproline content was observed in the first 36 days and the level reached a plateau after 57 days in both groups. The decline in total radioactivity with time signifies disappearance of labeled collagen from the prostate. As determined from the decay curves, the half-life of collagen in the saline instilled prostates was 18.6 days whereas the collagen synthesized in the *E. coli* infected prostates had a half-life of 13.7 days. Our findings revealed that the newly synthesized collagen in chronic prostatic inflammation is relatively less stable and tends to undergo rapid degradative remodeling.

Resolution of Chronic Bacterial-Induced Prostatic Inflammation After Antibiotic Treatment

To ascertain the reversibility of fibrosis, we used antibiotic treatment to resolve infection and inflammation and examined the effect on collagen content. Saline instilled and *E. coli* infected mice were treated with or without enrofloxacin for two weeks on day 28 post-inoculation. We first performed bacterial cultures of each

individual prostatic lobe to evaluate the effectiveness of the antibiotic treatment **(Table I)**. Significant bacterial infection was present in all three prostatic lobes from sham-treated *E. coli* infected animals whereas no bacteria were cultured from any infected prostatic lobe after treatment with enrofloxacin. Prostatic tissues from saline instilled mice with and without antibiotic treatment were both culture negative. Histopathological analysis was performed in the ventral prostate (VP) **(Figure 2A-B, G-H, M)**, dorsolateral prostate (DLP) **(Figure 2C-D, I-J, N)**, and anterior prostate (AP) **(Figure 2E-F, K-L, O)** of sham, and enrofloxacin-treated saline instilled and *E. coli* infected animals after a recovery period of 8 weeks. Saline instilled animals with and without antibiotic treatment had no or minimal prostatic inflammation. All three prostatic lobes from sham-treated *E. coli* infected animals showed evidence of widespread severe inflammation whereas enrofloxacin-treated infected prostates exhibited very mild inflammation with a restoration of the normal prostatic ductal architecture similar to saline instilled controls. These findings demonstrate resolution of chronic bacterial-induced prostatic inflammation after complete elimination of infection with antibiotic treatment.

Reversibility of Excess Collagen Deposition Induced in Response to Chronic Bacterial Prostatic Inflammation

Picrosirius red staining for collagen content was performed on adjacent serial tissue sections of the H&E stained slides from saline instilled and *E. coli* infected

male mice with and without antibiotic treatment **(Figure 3A-L)**. As shown in Figure 3M-O, quantitation of the staining showed that there was no significant difference in collagen content of any prostatic lobe between saline instilled animals with and without antibiotic treatment, indicating that treatment with enrofloxacin alone had no effect on collagen deposition in the prostate. A significant increase in collagen deposition was observed in all lobes of sham-treated *E. coli* infected animals. In striking contrast, collagen content in all three prostatic lobes from enrofloxacin-treated *E. coli* infected animals decreased to levels comparable to saline instilled controls. To validate the quantitative result of the picrosirius red staining, hydroxyproline content measured by HPLC was performed **(Figure 4)**. In accordance with the picrosirius red staining, a substantial increase in hydroxyproline content was observed in the prostates of sham-treated *E. coli* infected animals. On the other hand, hydroxyproline content in the prostates of enrofloxacin-treated *E. coli* infected animals was significantly decreased. However, unlike the result obtained from the picrosirius red staining, the reduction of hydroxyproline content in the prostates of enrofloxacin-treated infected animals did not completely reach the baseline level.

To evaluate the relationship between inflammation and reversal of fibrosis, we correlated the inflammation score determined from the H&E images with collagen content measured from the adjacent picrosirius red stained sections for the VP **(Figure 5A)**, DLP **(Figure 5B)**, and AP **(Figure 5C)** of saline instilled and *E. coli*

infected mice with and without enrofloxacin treatment. A significant positive correlation between inflammation and collagen deposition was shown in all three prostatic lobes. Taken together, our results suggest that collagen deposition induced by chronic bacterial-induced prostatic inflammation is at least partly reversible after resolution of inflammation.

DISCUSSION

Fibrosis resulting from excessive deposition of collagen is traditionally recognized as a progressive irreversible condition and an end stage of inflammatory diseases; however, there is compelling evidence in both animal and human studies to support that the development of fibrosis could potentially be a reversible process when the underlying cause is removed or suppressed in various tissues, including the liver and kidney [10-17]. Collagen degradation has been suggested to be a key mechanism mediating the recovery process of fibrosis through the enzymatic action of collagenases. Studies of a rodent model of liver inflammation and fibrosis have shown that increased collagen deposition in the liver of rats injected repeatedly with hepatotoxin carbon tetrachloride (CCl_4) was spontaneously regressed to control level and the extracellular matrix was remodeled to restore the tissue architecture over time after termination of the toxin injection [12,13]. The recovery phase of fibrosis in this model was associated with decreased mRNA expression of collagenase inhibitors, increased expression of interstitial collagenase and increased collagenase

activity [13,18,19]. Follow-up studies demonstrated that liver fibrosis with an accumulation of collagenase-resistant type I collagen in CCl_4-treated Col1a1$^{r/r}$ mice failed to undergo significant regression and remodeling [20].

Accumulating evidence has suggested that collagen stabilization is the principal mechanism regulating the rate of collagen degradation and thus determines the reversal of fibrosis in pathological conditions [21-25]. The stability of collagen is conferred by the extent of collagen cross-linking [21]. Previous studies of an *in vitro* model system have demonstrated that formation of cross-links in collagen molecules significantly increased the resistance of collagen to collagenase degradation [21]. In support of this, subsequent studies of an *in vivo* model of liver fibrosis have indicated that incomplete resolution of liver fibrosis in rats treated with CCl_4 was accompanied with a substantial amount of matrix crosslinks as compared to the rats undergoing extensive regression of fibrosis [12]. Indeed, the level of cross-links appears to be increased in the livers from patients with irreversible granulomatous liver fibrosis [26,27] and is associated with the degree of reversibility of fibrosis in experimental models [28,29]. Taken together, these studies support the concept that reversibility of fibrosis is determined by the extent of collagen stabilization.

Our data suggests that the stability of newly synthesized collagen was decreased in chronic bacterial prostatic inflammation. Prostatic fibrosis induced by chronic

bacterial inflammation is attributed to a significant increase in *de novo* collagen synthesis as determined by the incorporation of ^{3}H-hydroxyproline [6]. Collagen content increases predominantly between 7 and 14 days post-inoculation. At later time points, collagen content remains elevated but collagen turnover appears homeostatic. Decay analysis of incorporated ^{3}H-hydroxyproline showed that this newly synthesized collagen in prostatic inflammation had a relatively short half-life. Considering that the short-lived ^{3}H-hydroxyproline incorporated in collagen predominantly represents those induced at early time points, our study suggests that collagen produced primarily in early stage of chronic prostatic inflammation undergoes rapid remodeling and is more liable to degradation.

We found that collagen content significantly decreased with resolution of chronic prostatic inflammation. Inflammation was completely resolved after eradication of bacterial infection with antibiotic treatment and an eight-week recovery period. Our quantitative studies revealed that resolution of inflammation and restoration of normal ductal architecture in the prostate was accompanied by marked attenuation of collagen content. These findings were in agreement with our decay study of incorporated ^{3}H-hydroxyproline suggesting that collagen synthesized in chronic prostatic inflammation is susceptible to a rapid degradative remodeling. These findings support the conclusion that inflammation-induced prostatic fibrosis is at least partly reversible when the underlying cause is completely treated and sufficient recovery time is allowed.

It is noteworthy that there was a disparity between the results obtained from picrosirius red staining and hydroxyproline content for measurement of collagen deposition. Picrosirius red staining showed that prostatic fibrosis in antibiotic-treated infected animals was remodeled through the recovery period of 8 weeks to level comparable to saline instilled controls while the reduced hydroxyproline content in these animals was still significantly different from controls. This difference reflects the distinct mechanism of the two quantitative methods. Sirius red is an elongated dye molecule that attaches parallel to collagen by reacting its sulfonic acid groups with the basic groups of collagen molecules [7]. Such interaction enhances the birefringence of the highly oriented collagen fibers in tissue sections that can easily be identified in polarized light [30]. Conversely, the biochemical analysis of hydroxyproline content is based on the general concept that this amino acid is abundant and almost exclusively found in collagen. Thus one possibility is that proteins other than collagen also contain hydroxyproline. Indeed, hydroxyproline is found in elastin, hypoxia inducible factor α, complement protein C1q and other non-collagen proteins with collagenous domains [31]. However, the amount of hydroxyproline in these proteins is much less than that in collagen and thus is likely negligible in collagen-enriched tissues [32]. Another explanation is the presence of collagen fragments by MMP cleavage remaining before complete degradation in the antibiotic-treated infected prostates. Collagen fragments lacks the highly-ordered molecular orientation as found in intact collagen fibers and is expected to lose

the birefringence promoted by Sirius red staining, while hydroxyproline content in collagen fragments can still be detectible. In support of this, previous studies have demonstrated that a pathological condition characterized by collagen degradation resulted in fragmented and damaged collagens that were weakly birefringent when detected by the picrosirius-polarization method [33].

Prostatic inflammation-induced fibrosis has gained increasing attention as a major contributing factor in the pathogenesis of BPH/LUTS. Several epidemiological studies of human BPH/LUTS have provided evidence for the contribution of excessive collagen deposition and fibrosis in the prostate to impaired urethral function and LUTS. Bercovich and colleagues were the first to report an inverse correlation of uroflow with prostatic fibrosis and symptom score in BPH/LUTS patients [34]. A subsequent study by Ma et al. has demonstrated that prostatic tissues from men with moderate/severe LUTS had a greater mechanical stiffness and a significantly higher collagen content than men with no/mild LUTS [3]. Further, Cantiello et al. have shown that collagen content was significantly higher in prostatic tissues with inflammation than those without inflammation [4]. There were also positive correlations between LUTS severity, inflammation degree, and collagen content. Together, these observational analyses lead to the hypothesis that prostatic fibrosis caused by inflammation increases tissue stiffness that compromises the opening of bladder neck – prostate complex during micturition, and subsequently promotes LUTS. Our

recent study of a mouse model of bacterial-induced prostatic inflammation supports this speculation, suggesting a role of chronic inflammation in promoting excessive collagen deposition in the prostate [6]. Therefore, considering that prostatic fibrosis is induced by inflammation and is a potential etiologic factor of BPH/LUTS, it is critical to understand whether the injured/inflamed prostate has the capacity for recovery from the associated established fibrosis. However, the reversibility of fibrosis has never been examined in the prostate. Our present study is the first report demonstrating that collagen induced in chronic prostatic inflammation is more susceptible to degradation and is at least partly reversible when the underlying cause is resolved.

CONCLUSIONS

Collagen deposition induced by chronic prostatic inflammation exhibits a relatively short half-life as compared to the collagen content of the uninflamed prostate. Our findings show that inflammation-induced prostatic fibrosis is at least partly reversible and suggest that fibrosis of the human prostate may be addressed therapeutically by removing the cause of inflammation or suppressing the inflammatory response.

ACKNOWNLEDGEMENTS

This work was supported by NIH R01DK0757, T32 ES007015 from the National Institute of Environmental Health Sciences (NIEHS), NIH, and Herman I. Shapiro

Distinguished Graduate Fellowship from UW-Madison School of Medicine and Public Health. Its contents are solely the responsibility of the authors and do not necessarily represent the official views of the funders. The authors also greatly thank Dr. William Ricke's laboratory (UW-Madison) for providing polarizing microscopy and Chee Paul Lin (UW-Madison) for providing statistical analysis.

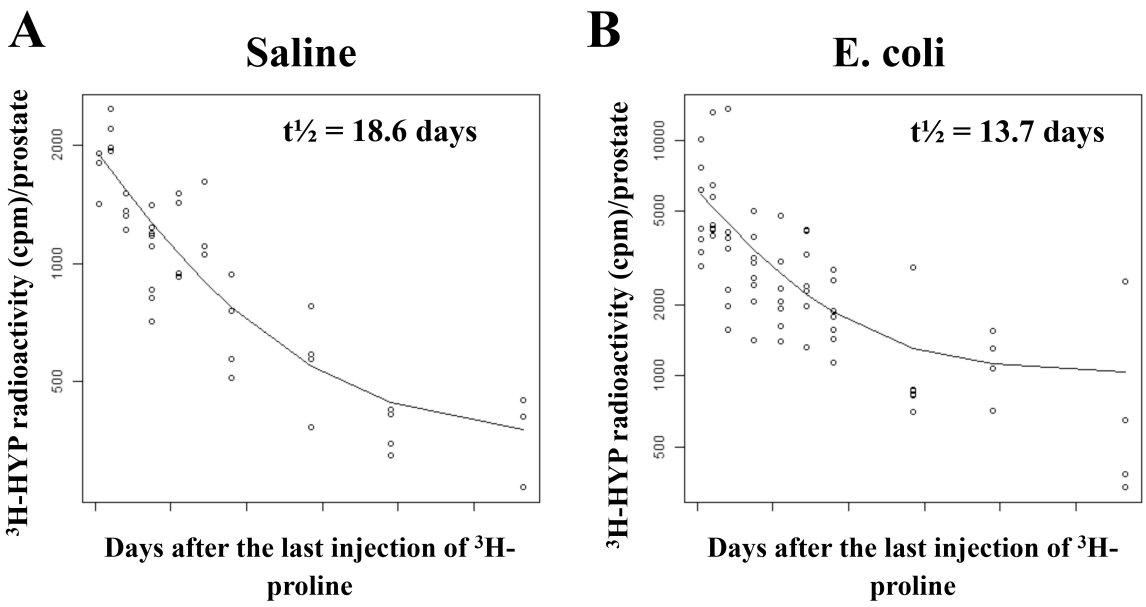

Figure 1. Decay curves of ^{3}H-hydroxyproline radioactivity for collagen stability in the prostates of saline instilled **(A)** and *E. coli* infected **(B)** mice (n = 3-8 per treatment per time point). Each data point represents an individual mouse and the line on each graph represents the nonlinear regression line calculated through the data points. The graphs are plotted as the natural log of cpm/prostate versus time after the last injection of ^{3}H-proline. Hydroxyproline (HYP); Count per minute (cpm); Half-life (t½).

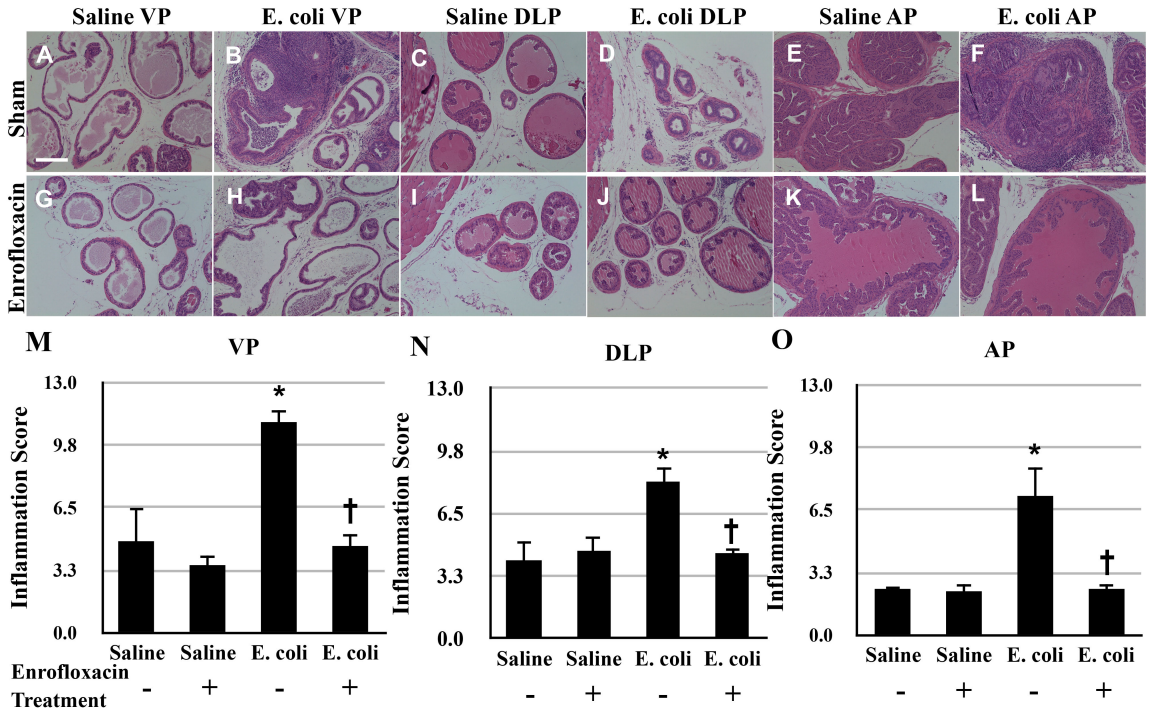

Figure 2. Representative H&E images of the VP **(A-B, G-H)**, DLP **(C-D, I-J)**, and AP **(E-F, K-L)** from saline instilled and *E. coli* infected mice 28 days post-instillation that were treated either with enrofloxacin or sham for another 2 weeks. Scale bar 200μm in panel A. Comparisons of the degree of inflammation in the VP **(M)**, DLP **(N)** and AP **(O)** from saline instilled and *E. coli* infected mice 28 days post-instillation that were treated either with enrofloxacin or sham for another 2 weeks. The animals were harvested 8 weeks after the antibiotic treatment (n = 4-6 per treatment). Data are presented as mean inflammation score ± SEM. * indicates a P-value < 0.05 compared to saline treated with sham. **†** indicates a P-value < 0.05 for *E. coli* treated with enrofloxacin compared to *E. coli* treated with sham. Ventral prostate (VP); Dorsolateral prostate (DLP); Anterior prostate (AP).

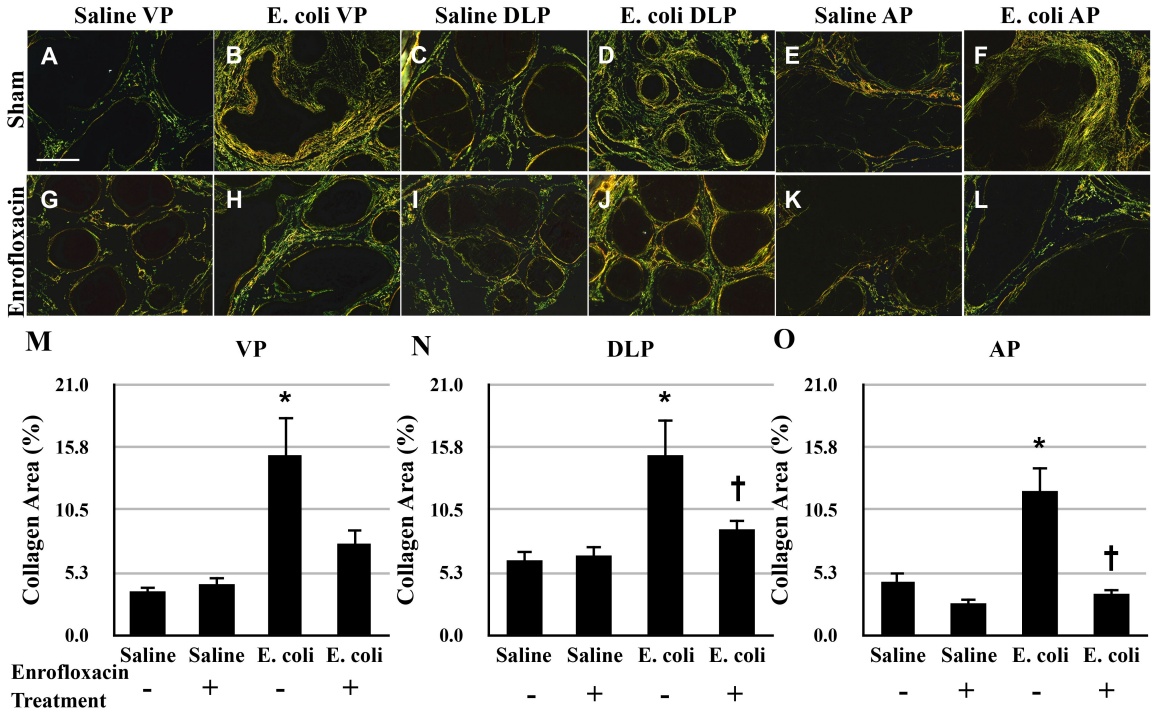

Figure 3. Representative picrosirius red stained sections of the VP **(A-B, G-H)**, DLP **(C-D, I-J)**, and AP **(E-F, K-L)** from saline instilled and *E. coli* infected mice 28 days post-instillation that were treated either with enrofloxacin or sham for another 2 weeks. Scale bar 200μm in panel A. Comparisons of the collagen content determined by the percentage of picrosirius red stained area in the VP **(M)**, DLP **(N)** and AP **(O)** from saline instilled and *E. coli* infected mice 28 days post-instillation that were treated either with enrofloxacin or sham for another 2 weeks. The animals were harvested 8 weeks after the antibiotic treatment (n = 4-6 per treatment). Data are presented as mean percentage of collagen area ± SEM. * indicates a P-value < 0.05 compared to saline treated with sham. **†** indicates a P-value < 0.05 for *E. coli* treated with enrofloxacin compared to *E. coli* treated with sham. Ventral prostate (VP); Dorsolateral prostate (DLP); Anterior prostate (AP).

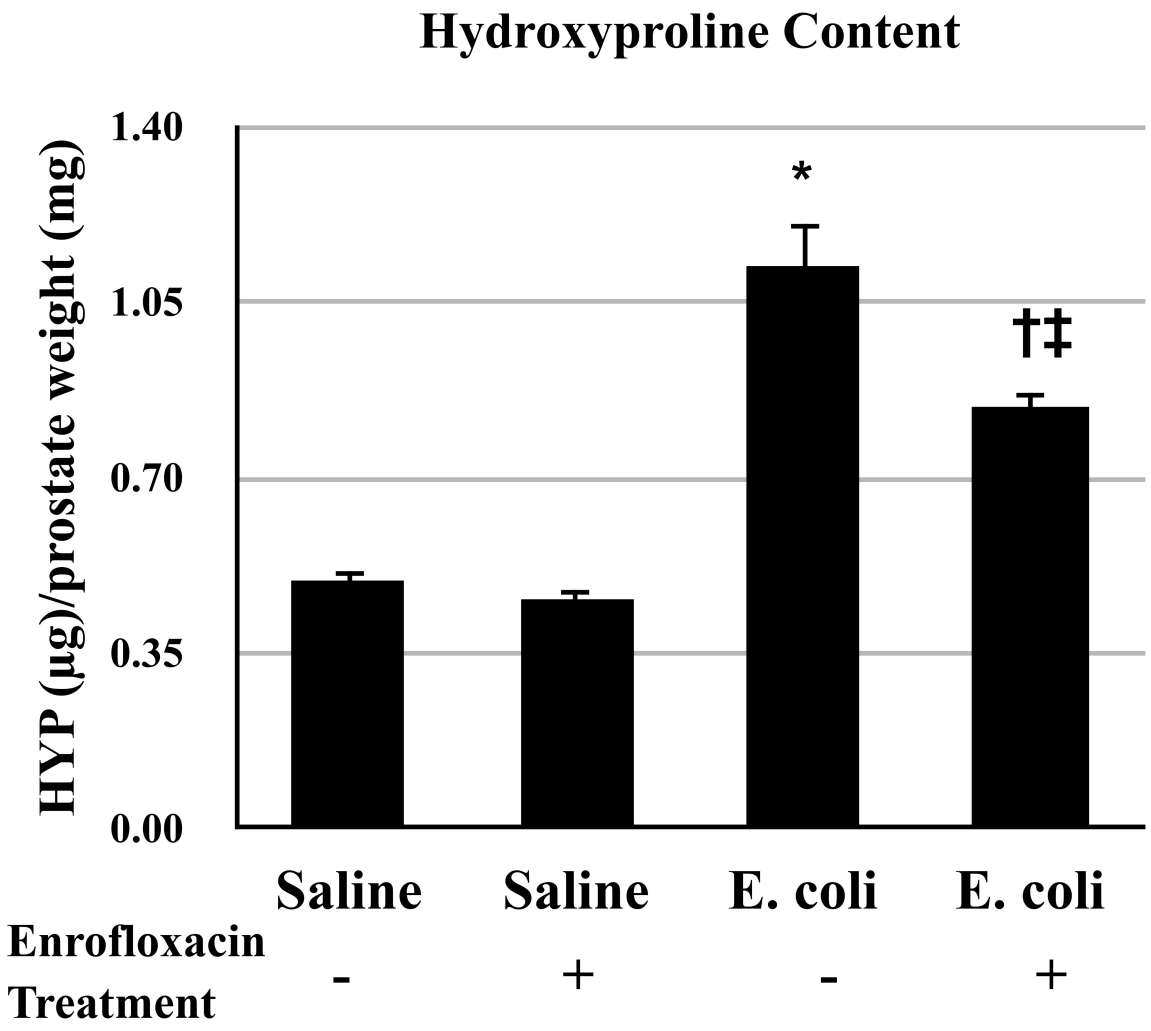

Figure 4. Comparisons of hydroxyproline content in the prostates of saline instilled and *E. coli* infected mice 28 days post-instillation that were treated either with enrofloxacin or sham for another 2 weeks. The animals were harvested 8 weeks after the antibiotic treatment (n = 4-5 per treatment). Data are presented as mean hydroxyproline (µg)/prostate weight (mg) ± SEM. * indicates a P-value < 0.05 compared to saline treated with sham. † indicates a P-value < 0.05 for *E. coli* treated with enrofloxacin compared to *E. coli* treated with sham. ‡ indicates a P-value < 0.05 compared to saline treated with enrofloxacin. Hydroxyproline (HYP).

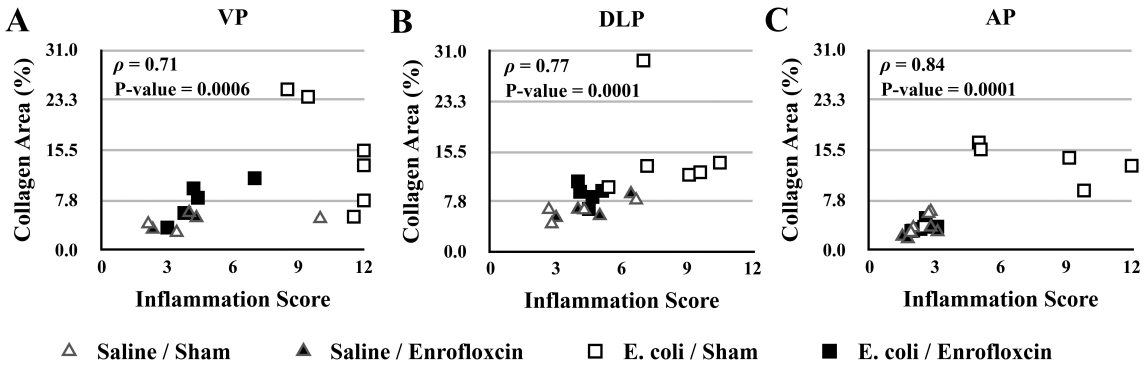

Figure 5. Spearman correlation analysis of the relationship between prostatic inflammation and collagen deposition in the VP **(A)**, DLP **(B)**, and AP **(C)** from saline instilled and *E. coli* infected mice 28 days post-instillation that were treated either with enrofloxacin or sham for another 2 weeks. The animals were harvested 8 weeks after the antibiotic treatment (n = 4-6 per treatment). Ventral prostate (VP); Dorsolateral prostate (DLP); Anterior prostate (AP), Spearman's rank correlation coefficient *(ρ)*.

REFERENCES

1. Robert G, Descazeaud A, Nicolaiew N, Terry S, Sirab N, et al. (2009) Inflammation in benign prostatic hyperplasia: a 282 patients' immunohistochemical analysis. Prostate 69: 1774-1780.

2. Nickel JC, Roehrborn CG, O'Leary MP, Bostwick DG, Somerville MC, et al. (2008) The relationship between prostate inflammation and lower urinary tract symptoms: examination of baseline data from the REDUCE trial. Eur Urol 54: 1379-1384.

3. Ma J, Gharaee-Kermani M, Kunju L, Hollingsworth JM, Adler J, et al. (2012) Prostatic fibrosis is associated with lower urinary tract symptoms. J Urol 188: 1375-1381.

4. Cantiello F, Cicione A, Salonia A, Autorino R, Tucci L, et al. (2013) Periurethral fibrosis secondary to prostatic inflammation causing lower urinary tract symptoms: a prospective cohort study. Urology 81: 1018-1023.

5. Boehm BJ, Colopy SA, Jerde TJ, Loftus CJ, Bushman W (2012) Acute bacterial inflammation of the mouse prostate. Prostate 72: 307-317.

6. Wong L, Hutson PR, Bushman W (2014) Prostatic Inflammation Induces Fibrosis in a Mouse Model of Chronic Bacterial Infection. PLoS One 9: e100770.

7. Junqueira LC, Bignolas G, Brentani RR (1979) Picrosirius staining plus polarization microscopy, a specific method for collagen detection in tissue sections. Histochem J 11: 447-455.

8. Hutson PR, Crawford ME, Sorkness RL (2003) Liquid chromatographic determination of hydroxyproline in tissue samples. J Chromatogr B Analyt Technol Biomed Life Sci 791: 427-430.

9. McAnulty RJ (2005) Methods for measuring hydroxyproline and estimating in vivo rates of collagen synthesis and degradation. Methods Mol Med 117: 189-207.

10. Sohrabpour AA, Mohamadnejad M, Malekzadeh R (2012) Review article: the reversibility of cirrhosis. Aliment Pharmacol Ther 36: 824-832.

11. Pol S, Carnot F, Nalpas B, Lagneau JL, Fontaine H, et al. (2004) Reversibility of hepatitis C virus-related cirrhosis. Hum Pathol 35: 107-112.

12. Issa R, Zhou X, Constandinou CM, Fallowfield J, Millward-Sadler H, et al. (2004) Spontaneous recovery from micronodular cirrhosis: evidence for incomplete resolution associated with matrix cross-linking. Gastroenterology 126: 1795-1808.

13. Iredale JP, Benyon RC, Pickering J, McCullen M, Northrop M, et al. (1998) Mechanisms of spontaneous resolution of rat liver fibrosis. Hepatic stellate cell apoptosis and reduced hepatic expression of metalloproteinase inhibitors. J Clin Invest 102: 538-549.

14. Chatziantoniou C, Dussaule JC (2008) Is kidney injury a reversible process? Curr Opin Nephrol Hypertens 17: 76-81.

15. Zeisberg M, Kalluri R (2008) Reversal of experimental renal fibrosis by BMP7 provides insights into novel therapeutic strategies for chronic kidney disease. Pediatr Nephrol 23: 1395-1398.

16. Adamczak M, Gross ML, Krtil J, Koch A, Tyralla K, et al. (2003) Reversal of glomerulosclerosis after high-dose enalapril treatment in subtotally nephrectomized rats. J Am Soc Nephrol 14: 2833-2842.

17. Boffa JJ, Lu Y, Placier S, Stefanski A, Dussaule JC, et al. (2003) Regression of renal vascular and glomerular fibrosis: role of angiotensin II receptor antagonism and matrix metalloproteinases. J Am Soc Nephrol 14: 1132-1144.

18. Fallowfield JA, Mizuno M, Kendall TJ, Constandinou CM, Benyon RC, et al. (2007) Scar-associated macrophages are a major source of hepatic matrix metalloproteinase-13 and facilitate the resolution of murine hepatic fibrosis. J Immunol 178: 5288-5295.

19. Watanabe T, Niioka M, Hozawa S, Kameyama K, Hayashi T, et al. (2000) Gene expression of interstitial collagenase in both progressive and recovery phase of rat liver fibrosis induced by carbon tetrachloride. J Hepatol 33: 224-235.

20. Issa R, Zhou X, Trim N, Millward-Sadler H, Krane S, et al. (2003) Mutation in collagen-1 that confers resistance to the action of collagenase results in failure of recovery from CCl4-induced liver fibrosis, persistence of

activated hepatic stellate cells, and diminished hepatocyte regeneration. FASEB J 17: 47-49.

21. Vater CA, Harris ED, Jr., Siegel RC (1979) Native cross-links in collagen fibrils induce resistance to human synovial collagenase. Biochem J 181: 639-645.

22. Harris ED, Jr., Farrell ME (1972) Resistance to collagenase: a characteristic of collagen fibrils cross-linked by formaldehyde. Biochim Biophys Acta 278: 133-141.

23. Harris ED, Jr., McCroskery PA (1974) The influence of temperature and fibril stability on degradation of cartilage collagen by rheumatoid synovial collagenase. N Engl J Med 290: 1-6.

24. Hamlin CR, Kohn RR (1971) Evidence for progressive, age-related structural changes in post-mature human collagen. Biochim Biophys Acta 236: 458-467.

25. Hamlin CR, Luschin JH, Kohn RR (1978) Partial characterization of the age-related stabilizing factor of post-mature human collagen--I. By the use of bacterial collagenase. Exp Gerontol 13: 403-414.

26. Ricard-Blum S, Bresson-Hadni S, Guerret S, Grenard P, Volle PJ, et al. (1996) Mechanism of collagen network stabilization in human irreversible granulomatous liver fibrosis. Gastroenterology 111: 172-182.

27. Ricard-Blum S, Bresson-Hadni S, Vuitton DA, Ville G, Grimaud JA (1992) Hydroxypyridinium collagen cross-links in human liver fibrosis: study of alveolar echinococcosis. Hepatology 15: 599-602.

28. Ricard-Blum S, Liance M, Houin R, Grimaud JA, Vuitton DA (1995) Covalent cross-linking of liver collagen by pyridinoline increases in the course of experimental alveolar echinococcosis. Parasite 2: 113-118.

29. Ricard-Blum S, Ville G, Grimaud JA (1992) Pyridinoline, a mature collagen cross-link, in fibrotic livers from Schistosoma mansoni-infected mice. Am J Trop Med Hyg 47: 816-820.

30. Puchtler H, Waldrop FS, Valentine LS (1973) Polarization microscopic studies of connective tissue stained with picro-sirius red FBA. Beitr Pathol 150: 174-187.

31. Gorres KL, Raines RT (2010) Prolyl 4-hydroxylase. Crit Rev Biochem Mol Biol 45: 106-124.

32. Edwards CA, O'Brien WD, Jr. (1980) Modified assay for determination of hydroxyproline in a tissue hydrolyzate. Clin Chim Acta 104: 161-167.

33. Borges LF, Gutierrez PS, Marana HR, Taboga SR (2007) Picrosirius-polarization staining method as an efficient histopathological tool for collagenolysis detection in vesical prolapse lesions. Micron 38: 580-583.

34. Bercovich E, Barabino G, Pirozzi-Farina F, Deriu M (1999) A multivariate analysis of lower urinary tract ageing and urinary symptoms: the role of fibrosis. Arch Ital Urol Androl 71: 287-292.

FUTURE DIRECTIONS

BPH is a significant health burden in elderly men due to its associated LUTS and consequent bladder and renal complications. Although aging and androgen have traditionally been viewed as the major factors for BPH/LUTS, recent observations suggest that prostatic inflammation plays an important role in the initiation and progression of this disease. The mechanism has not been elucidated. Findings from the studies of human BPH samples and animal models have led to the speculation that prostatic inflammation could contribute to BPH/LUTS through a variety of mechanisms, including hyperplasia and proliferation of epithelial and stromal cells, alteration of vascular remodeling and homeostasis, induction of extracellular matrix accumulation, and alteration in nerve sensitization.

We utilized our previously established mouse model of bacterial infection to demonstrate that prostatic inflammation induces significant vascular and fibrotic changes in the mouse prostates. Our findings of the present studies are believed to provide novel perspectives on the inflammatory mechanisms leading to BPH/LUTS as well as clinical implication for the development of therapeutic treatments for inflammation-associated prostatic diseases.

In chapter 2, we described the effects of acute bacterial-induced prostatic inflammation on vasculature. We found that prostatic inflammation caused a significant increase in endothelial proliferation and vascular density. Surprisingly,

RT-PCR analysis revealed that these vascular changes were associated with decreased pro-angiogenic factor expression, including *Pecam1, Pdgfa, Tie1, Tek, Angpt1, Angpt2, Angpt4, Fgf2, Vegfb, Vegfc,* and *Figf.* This result was unexpected because it is in contrast to our study of prostatic development showing vascular formation and endothelial proliferation were accompanied by increased expression of most of these pro-angiogenic factors. Therefore, we propose that endothelial proliferation during prostatic inflammation may not be mediated by the pro-angiogenic factors examined here but rather by other factors induced after injury.

What are the factors mediating angiogenesis in prostatic inflammation?

Several inflammatory factors such as IL-1 were highly expressed in some cases of human BPH samples as well as in the mouse prostates after bacterial infection [1-3]. Inhibition of IL-1 signaling using IL-1R1 knockout mice reduced epithelial reactive hyperplasia in response to prostatic inflammation [4], suggesting that IL-1 signaling is required for inflammatory response to bacterial infection in the prostates. Intriguingly, IL-1 has been shown to induce *in vivo* angiogenesis in mouse tumor xenograft and cornea models [5-8]. Subsequent *in vitro and in vivo* studies have demonstrated that the angiogenic effect of IL-1 was mediated through production of pro-angiogenic factors (eg. VEGFA) and inflammatory factors with angiogenic activity (eg. IL-8, TNFα, COX2, HGF) in both paracrine and autocrine manners [7-11]. Therefore, further studies focusing on the role of

inflammatory pathways, particularly IL-1 signaling, in prostatic angiogenesis are necessary to improve our understanding of the vascular mechanisms of the pathogenesis of BPH/LUTS.

In chapter 3, we demonstrated that chronic prostatic inflammation induces fibrosis in a mouse model of bacterial infection. Picrosirius red staining and hydroxyproline assay showed that collagen deposition was significantly increased in the inflamed prostates. Histopathological examination revealed that accumulation of collagen was associated with the sites of inflammation and correlation analysis showed that the degree of inflammation was positively associated with collagen content. This fibrotic change in inflammation was accompanied with an increase in collagen synthesis determined by the incorporation of ^{3}H-hydroxyproline and mRNA expression of several collagen remodeling-associated genes *(Col1a1, Col1a2, Col3a1, Mmp2, Mmp9,* and *Lox).* At the time point coinciding with increased collagen synthesis, immunostaining showed that CD45+VIM+ fibrocytes were abundant in inflamed prostates and flow cytometric analysis further demonstrated an increased percentage of CD45+VIM+ fibrocytes in collagen type I expressing cells as compared to saline control. These findings indicate that prostatic inflammation induces collagen deposition and also implicate a role for fibrocytes in the generation of prostatic fibrosis.

What are the molecular factors responsible for mediating excess collagen production and deposition in prostatic inflammation?

A variety of inflammatory factors such as TGFβ, IL-1, IL-6 have been shown to be highly expressed in human BPH and experimental mouse model of prostatic inflammation [1-4,12,13]. More important, studies using overexpression and deficiency of certain inflammatory factors in transgenic mouse models have demonstrated that some of them play a critical role in regulating collagen deposition during inflammation and tissue injury/repair in multiple organ systems [14]. However, these have never been studied in the prostate. Thus, studies examining the role of these profibrotic factors in inflammation-induced prostatic fibrosis are warranted.

What is the role of fibrocytes in inflammation-induced prostatic fibrosis?

The contribution of fibrocytes to tissue fibrosis has been suggested in various human fibrosing diseases and experimental models associated with conditions such as skin wounds, pulmonary, hepatic and renal fibrosis [15-20]. Fibrocytes are capable of producing profibrotic factors such as TGFβ and collagen type I, as well as differentiating into myofibroblasts, the key effector cells in fibrogenesis [17,19,21-24]. Immunostaining and flow cytometric analyses have revealed that fibrocytes express chemokine receptors CCR7, CXCR4 and CCR2, allowing them to migrate into the injured tissues in response to chemokines [15,17,22,23,25]. Blockade of CCL21/CCR7 signaling in CCR7-/- mice reduced

fibrocyte infiltration and renal fibrosis after ureteral ligation [15]. Similar findings in studies of experimental pulmonary fibrosis have also been reported when CXCL12/CXCR4 and CCL2/CCR2 pathways were blocked [17,25]. In human with idiopathic pulmonary fibrosis, fibrocytes were detected in the lung tissues [18] and circulation of these patients [26] and an increased number of circulating fibrocytes has been associated with poor prognosis [27]. Recently, studies of LUTS patients have reported that fibrocytes were present predominantly in prostatic tissues with increased collagen content from men with moderate/severe LUTS [28]. This is consistent with the result presented here in chapter 3 that fibrocytes were recruited in inflammation-induced prostatic fibrosis. Future investigations into the role of fibrocytes in collagen deposition, the mechanisms of their prostatic recruitments into the fibrotic areas, and their capability of differentiating into myofibroblasts are critical to elucidate the cellular and molecular mechanisms of fibrosis in the prostate.

In chapter 4, we characterized the reversibility of collagen deposition induced by prostatic inflammation in our previously established mouse model of bacterial-infection. We showed that prostatic inflammation had completely resolved following antibiotic treatment and a recovery period. Resolution of inflammation was associated with a significant reduction in established collagen deposition as determined by picrosirius red staining and hydroxyproline assay, suggesting that prostatic fibrosis is potentially a reversible process when the cause of injury is

removed or treated. We also found that the newly synthesized collagen in inflamed prostates had a shorter half-life and were more susceptible to degradation than that in control. Taken together, we interpret the findings in this study as that the reversal of collagen induced in response to prostatic inflammation is at least partly attributed to increased collagen remodeling and degradation.

What are the factors determining the reversibility of prostatic fibrosis?

Collagen degradation has been suggested to be essential for resolution of fibrosis, however the mechanisms of collagen degradation pathway are not completely understood. MMPs are a group of zinc dependent endopeptidases that are well recognized for their ability to cleave and degrade extracellular matrix (ECM) components [29]. The proteolytic activity of MMPs is tightly regulated by their endogenous inhibitors TIMPs. To date, 28 members have been identified in the MMP family. Because of their primary functions on the ECM, they are implicated to have an important anti-fibrotic role in tissue fibrosis. In a mouse model of CCl_4-induced hepatic fibrosis, RT-PCR analyses have shown that *Mmp13* mRNA expression was reduced during progression phase of fibrosis and was significantly increased in the recovery phase [30,31]. Deletion of *Mmp13* in mice treated with CCl_4 retarded resolution of fibrosis [31]. On the other hand, contradictory results showing a profibrotic effect of MMPs have also been reported in numerous experimental models [32]. Indeed, microarray and

immunostaining analyses revealed that mRNA and protein expression of several MMPs (eg. MMP1, 2, 7, 9, 14) were highly expressed in studies of human fibrotic lung and liver [33,34]. It has been suggested that the profibrotic effect of MMPs is attributed to the ability of MMPs to degrade basement membrane for facilitating fibroblast invasion and reepithelization, and to process and activate growth factors, cytokines, chemokines, and cell surface receptors that subsequently contribute to the process of fibrogenesis [33,35]. Thus, it is apparent that MMPs have complex biological activities in regulating collagen remodeling and degradation during tissue injury/repair and fibrosis. Nonetheless, at this point only a few MMPs have been characterized in the prostate and little is known about their ECM remodeling role in prostatic fibrosis.

Another factor that is involved in the regulation of collagen degradation is collagen cross-linking. In vitro assays have demonstrated that cross-linking increased the stabilization of collagen molecules and rendered the collagen fibers to be less susceptible to MMP1 degradation [36]. Interestingly, in the rodent model of CCl_4-induced liver injury, a prolonged 12-week CCl_4 treatment resulted in an incomplete resolution of established fibrosis and a failure of restoration of normal tissue architecture even after one year of recovery [37]. Further, immunostaining and western blotting have revealed that the failure to undergo complete resolution was associated with the presence of tissue transglutaminase-mediated matrix crosslinks. Thus, it is likely that collagen

crosslinking also has an important role in determining the reversibility of prostatic fibrosis, as we observed an increased mRNA expression of crosslinking enzyme LOX in early inflammation but no change at later time in our bacterial-induced mouse fibrosis model (see Chapter 3, Figure 4). Further investigation in this aspect is anticipated to improve our understanding of the mechanisms mediating and restricting the reversibility of collagen deposition in prostatic inflammation.

Clinical relevance of experimental animal data in human BPH/LUTS

It is hypothesized that prostatic inflammation induces fibrosis resulting in a stiffer tissue that impairs the urethral flexibility and function, and consequently promotes LUTS in men. Although accumulating studies have established a correlation between these parameters [38], this hypothesis has never been directly tested. Our studies using the established mouse model of bacterial infection – for the first time – show that prostatic inflammation induces fibrosis and demonstrate further that prostatic fibrosis is a treatable condition upon resolution of inflammation. These findings provide a novel perspective of the pathobiology of inflammation-associated prostate diseases.

Nevertheless, the mechanisms of how prostatic fibrosis leads to LUTS are not well understood. Thus, a functional study with the aim of evaluating the relationship of prostatic fibrosis with the changes in tissue stiffness, urethral function and voiding dysfunction is required. This should also include the testing

of the reversibility of these parameters after recovery from fibrosis. Further characterization of the cellular and molecular changes underlying this relationship could provide clinically relevant implication in the development and progression of BPH/LUTS.

Moving forward, it is important to note that BPH-related LUTS is a multifactorial disease and this is the major reason that complicates our understanding of the pathophysiology of LUTS. Human and experimental studies have suggested a role for aging, hormonal change, inflammation, obesity, diabetes, cardiovascular disease in LUTS through a variety of mechanisms such as epithelial and stromal hyperplasia, fibrosis, alteration in nerve fiber sensitization and possibly other important yet unknown factors. However, it is still uncertain of how these factors together influence the clinical setting in one individual. This is likely due to the fact that the currently available data are combined with pieces of information from multiple epidemiological studies based on different populations. Thus, efforts to conduct a detailed clinical and histological characterization for each patient in one population are necessary to understand the complex relationships between these factors as well as to incorporate their combined relationship into further studies on the etiology of LUTS.

REFERENCES

1. Boehm BJ, Colopy SA, Jerde TJ, Loftus CJ, Bushman W (2012) Acute bacterial inflammation of the mouse prostate. Prostate 72: 307-317.

2. Castro P, Giri D, Lamb D, Ittmann M (2003) Cellular senescence in the pathogenesis of benign prostatic hyperplasia. Prostate 55: 30-38.

3. Giri D, Ittmann M (2000) Interleukin-1alpha is a paracrine inducer of FGF7, a key epithelial growth factor in benign prostatic hyperplasia. Am J Pathol 157: 249-255.

4. Jerde TJ, Bushman W (2009) IL-1 induces IGF-dependent epithelial proliferation in prostate development and reactive hyperplasia. Sci Signal 2: ra49.

5. Bar D, Apte RN, Voronov E, Dinarello CA, Cohen S (2004) A continuous delivery system of IL-1 receptor antagonist reduces angiogenesis and inhibits tumor development. FASEB J 18: 161-163.

6. Carmi Y, Dotan S, Rider P, Kaplanov I, White MR, et al. (2013) The role of IL-1beta in the early tumor cell-induced angiogenic response. J Immunol 190: 3500-3509.

7. Saijo Y, Tanaka M, Miki M, Usui K, Suzuki T, et al. (2002) Proinflammatory cytokine IL-1 beta promotes tumor growth of Lewis lung carcinoma by induction of angiogenic factors: in vivo analysis of tumor-stromal interaction. J Immunol 169: 469-475.

8. Voronov E, Shouval DS, Krelin Y, Cagnano E, Benharroch D, et al. (2003) IL-1 is required for tumor invasiveness and angiogenesis. Proc Natl Acad Sci U S A 100: 2645-2650.

9. Carmi Y, Voronov E, Dotan S, Lahat N, Rahat MA, et al. (2009) The role of macrophage-derived IL-1 in induction and maintenance of angiogenesis. J Immunol 183: 4705-4714.

10. Kuwano T, Nakao S, Yamamoto H, Tsuneyoshi M, Yamamoto T, et al. (2004) Cyclooxygenase 2 is a key enzyme for inflammatory cytokine-induced angiogenesis. FASEB J 18: 300-310.

11. Torisu H, Ono M, Kiryu H, Furue M, Ohmoto Y, et al. (2000) Macrophage infiltration correlates with tumor stage and angiogenesis in human malignant melanoma: possible involvement of TNFalpha and IL-1alpha. Int J Cancer 85: 182-188.

12. Djonov V, Ball RK, Graf S, Mottaz AE, Arnold AM, et al. (1997) Transforming growth factor-beta 3 is expressed in nondividing basal epithelial cells in normal human prostate and benign prostatic hyperplasia, and is no longer detectable in prostate carcinoma. Prostate 31: 103-109.

13. Royuela M, Ricote M, Parsons MS, Garcia-Tunon I, Paniagua R, et al. (2004) Immunohistochemical analysis of the IL-6 family of cytokines and their receptors in benign, hyperplasic, and malignant human prostate. J Pathol 202: 41-49.

14. Borthwick LA, Wynn TA, Fisher AJ (2013) Cytokine mediated tissue fibrosis. Biochim Biophys Acta 1832: 1049-1060.

15. Sakai N, Wada T, Yokoyama H, Lipp M, Ueha S, et al. (2006) Secondary lymphoid tissue chemokine (SLC/CCL21)/CCR7 signaling regulates fibrocytes in renal fibrosis. Proc Natl Acad Sci U S A 103: 14098-14103.

16. Sakai N, Furuichi K, Shinozaki Y, Yamauchi H, Toyama T, et al. (2010) Fibrocytes are involved in the pathogenesis of human chronic kidney disease. Hum Pathol 41: 672-678.

17. Phillips RJ, Burdick MD, Hong K, Lutz MA, Murray LA, et al. (2004) Circulating fibrocytes traffic to the lungs in response to CXCL12 and mediate fibrosis. J Clin Invest 114: 438-446.

18. Andersson-Sjoland A, de Alba CG, Nihlberg K, Becerril C, Ramirez R, et al. (2008) Fibrocytes are a potential source of lung fibroblasts in idiopathic pulmonary fibrosis. Int J Biochem Cell Biol 40: 2129-2140.

19. Scholten D, Reichart D, Paik YH, Lindert J, Bhattacharya J, et al. (2011) Migration of fibrocytes in fibrogenic liver injury. Am J Pathol 179: 189-198.

20. Bucala R, Spiegel LA, Chesney J, Hogan M, Cerami A (1994) Circulating fibrocytes define a new leukocyte subpopulation that mediates tissue repair. Mol Med 1: 71-81.

21. Chesney J, Metz C, Stavitsky AB, Bacher M, Bucala R (1998) Regulated production of type I collagen and inflammatory cytokines by peripheral blood fibrocytes. J Immunol 160: 419-425.

22. Ekert JE, Murray LA, Das AM, Sheng H, Giles-Komar J, et al. (2011) Chemokine (C-C motif) ligand 2 mediates direct and indirect fibrotic responses in human and murine cultured fibrocytes. Fibrogenesis Tissue Repair 4: 23.

23. Abe R, Donnelly SC, Peng T, Bucala R, Metz CN (2001) Peripheral blood fibrocytes: differentiation pathway and migration to wound sites. J Immunol 166: 7556-7562.

24. Schmidt M, Sun G, Stacey MA, Mori L, Mattoli S (2003) Identification of circulating fibrocytes as precursors of bronchial myofibroblasts in asthma. J Immunol 171: 380-389.

25. Moore BB, Kolodsick JE, Thannickal VJ, Cooke K, Moore TA, et al. (2005) CCR2-mediated recruitment of fibrocytes to the alveolar space after fibrotic injury. Am J Pathol 166: 675-684.

26. Mehrad B, Burdick MD, Zisman DA, Keane MP, Belperio JA, et al. (2007) Circulating peripheral blood fibrocytes in human fibrotic interstitial lung disease. Biochem Biophys Res Commun 353: 104-108.

27. Moeller A, Gilpin SE, Ask K, Cox G, Cook D, et al. (2009) Circulating fibrocytes are an indicator of poor prognosis in idiopathic pulmonary fibrosis. Am J Respir Crit Care Med 179: 588-594.

28. Gharaee-Kermani M, Kasina S, Moore BB, Thomas D, Mehra R, et al. (2012) CXC-type chemokines promote myofibroblast phenoconversion and prostatic fibrosis. PLoS One 7: e49278.

29. Egeblad M, Werb Z (2002) New functions for the matrix metalloproteinases in cancer progression. Nat Rev Cancer 2: 161-174.

30. Watanabe T, Niioka M, Hozawa S, Kameyama K, Hayashi T, et al. (2000) Gene expression of interstitial collagenase in both progressive and recovery phase of rat liver fibrosis induced by carbon tetrachloride. J Hepatol 33: 224-235.

31. Fallowfield JA, Mizuno M, Kendall TJ, Constandinou CM, Benyon RC, et al. (2007) Scar-associated macrophages are a major source of hepatic matrix metalloproteinase-13 and facilitate the resolution of murine hepatic fibrosis. J Immunol 178: 5288-5295.

32. McKleroy W, Lee TH, Atabai K (2013) Always cleave up your mess: targeting collagen degradation to treat tissue fibrosis. Am J Physiol Lung Cell Mol Physiol 304: L709-721.

33. Pardo A, Selman M (2006) Matrix metalloproteases in aberrant fibrotic tissue remodeling. Proc Am Thorac Soc 3: 383-388.

34. Hemmann S, Graf J, Roderfeld M, Roeb E (2007) Expression of MMPs and TIMPs in liver fibrosis - a systematic review with special emphasis on anti-fibrotic strategies. J Hepatol 46: 955-975.

35. McCawley LJ, Matrisian LM (2001) Matrix metalloproteinases: they're not just for matrix anymore! Curr Opin Cell Biol 13: 534-540.

36. van der Slot-Verhoeven AJ, van Dura EA, Attema J, Blauw B, Degroot J, et al. (2005) The type of collagen cross-link determines the reversibility of experimental skin fibrosis. Biochim Biophys Acta 1740: 60-67.

37. Issa R, Zhou X, Constandinou CM, Fallowfield J, Millward-Sadler H, et al. (2004) Spontaneous recovery from micronodular cirrhosis: evidence for incomplete resolution associated with matrix cross-linking. Gastroenterology 126: 1795-1808.

38. Ma J, Gharaee-Kermani M, Kunju L, Hollingsworth JM, Adler J, et al. (2012) Prostatic fibrosis is associated with lower urinary tract symptoms. J Urol 188: 1375-1381.